

EXTREMAL GRAPHICAL MODELING WITH LATENT VARIABLES

SEBASTIAN ENGELKE¹ AND ARMEEN TAEB²

ABSTRACT. Extremal graphical models encode the conditional independence structure of multivariate extremes and provide a powerful tool for quantifying the risk of rare events. Prior work on learning these graphs from data has focused on the setting where all relevant variables are observed. For the popular class of Hüsler–Reiss models, we propose the `eglatent` method, a tractable convex program for learning extremal graphical models in the presence of latent variables. Our approach decomposes the Hüsler–Reiss precision matrix into a sparse component encoding the graphical structure among the observed variables after conditioning on the latent variables, and a low-rank component encoding the effect of a few latent variables on the observed variables. We provide finite-sample guarantees of `eglatent` and show that it consistently recovers the conditional graph as well as the number of latent variables. We highlight the improved performances of our approach on synthetic and real data.

1. INTRODUCTION

Floods, heat waves, and financial crashes illustrate the environmental and economic hazards primarily influenced by rare, yet significant, events. Such catastrophic scenarios often result from the simultaneous occurrence of extreme values across multiple variables (Asadi et al., 2015, Zhou, 2009, Zscheischler and Seneviratne., 2017). To effectively measure and mitigate these disasters, it is essential to understand the dependencies between the various risk factors. From a mathematical perspective, this requires examining the tail dependence between the components of the random vector $X = (X_1, \dots, X_d)$. Extreme value theory provides the theoretical foundation for extrapolations to the distributional tail of the random vector X . Within the multivariate setting, there are two different yet closely related approaches for modeling extremal data. The first method considers component-wise maxima of independent copies of X and leads to the notion of max-stable distributions (de Haan and Resnick, 1977). The second method relies on multivariate Pareto distributions that describe the random vector X conditioned on the event that there is an extreme in one of the coordinates of X (Rootzén and Tajvidi, 2006).

Given the increasing complexity and dimensionality of contemporary data sets, identifying sparse representations for distributions of extreme events is critical for accurate modeling and risk assessment (Engelke and Ivanovs, 2021). Graphical models serve as powerful tools in achieving such sparse representations, offering clear and interpretable models for understanding dependencies among variables (Lauritzen, 1996). However, in the framework of max-stable distributions, Papastathopoulos and Strokorb (2016) highlighted limitations in developing non-trivial graphical models for their densities. On the other hand, multivariate Pareto distributions do not face these limitations. Indeed, Engelke and Hitz (2020) introduced extremal graphical models that factorize according to multivariate Pareto distributions and encode extremal conditional independence relationships, and Segers (2020) showed that extremal trees naturally arise as limits of Markov trees. For the popular Hüsler–Reiss family

¹RESEARCH CENTER FOR STATISTICS, GSEM, UNIVERSITY OF GENEVA, SWITZERLAND

²DEPARTMENT OF STATISTICS, UNIVERSITY OF WASHINGTON, U.S.

E-mail addresses: `sebastian.engelke@unige.ch`, `ataeb@uw.edu`.

Date: April 10, 2024.

(Hüsler and Reiss, 1989), Hentschel et al. (2022) showed that, similarly to the Gaussian case, the sparsity pattern of an extremal graphical model can be read off from a positive semi-definite precision matrix Θ with the all-ones vector in its null space. This precision matrix Θ is derived from a transformation of the variogram matrix Γ that parameterizes a Hüsler–Reiss distribution. Several recent papers have proposed methods to learn the extremal graphical structure from data (Chang and Allen, 2023, Engelke et al., 2022c, Engelke and Volgushev, 2022, Hu et al., 2022, Lederer and Oesting, 2023, Wan and Zhou, 2023).

The study and techniques for modeling extremes have so far concentrated on scenarios where all relevant variables are directly observable. However, in many real-world situations, there exist latent variables that are not observable due to prohibitive costs or other practical constraints. Mathematically, the overall system of variables is then given by $X = (X_O, X_H)$, where X_O are the observed and X_H the latent variables, with $(O, H) = \{1, 2, \dots, d\}$. The importance of accounting for latent factors becomes apparent in the example of a single latent variable $X_H = \{X_c\}$, where the data is generated through the one-factor model

$$X_j = X_c + \varepsilon_j, \quad j \in O.$$

Here, X_c is the common (unobserved) factor influencing all observed variables, and ε_j , $j \in O$, are independent noise terms. Suppose that the exceedances of the random vector X converge in distribution to a multivariate Pareto distribution $Y = (Y_O, Y_H)$; a concrete example where this is satisfied is when X_H is standard exponential and the noise variables are normally distributed, in which case Y has a Hüsler–Reiss distribution, but many other combinations are possible (Engelke et al., 2019). The joint vector Y can be shown to be an extremal graphical model with respect to the star graph on the left-hand side of Figure 1, where the observed variables Y_O are conditionally independent given the latent variable Y_H . However, the sub-model model of Y corresponding to the observed variables, that is, the limiting multivariate Pareto distribution arising from threshold exceedances of X_O , induces, in general, the fully connected extremal graph on the right-hand side of Figure 1, where all the variables are conditionally dependent.

This simple example illustrates that ignoring the effect of latent variables induces confounding dependencies among the observed variables: even for a sparse joint graph of observed and latent variables, any two observed variables are dependent when conditioning on the remaining observed variables. This phenomenon also appears in many real-world applications. In such cases, a latent extremal graphical model with possibly more than one latent variable Y_H serves multiple purposes:

- (i) it obtains the number of latent variables $h = |H|$ that summarize the effect of external phenomena on the observed variables;
- (ii) it identifies the residual graph structure among the observed variables after extracting away the effect of these external factors;
- (iii) it often yields a more sparsely represented and accurate statistical model than a model that ignores the latent variables.

Latent extremal graphical models have only been studied when the graphical structure among the observed and latent variables is a tree, and where the tree structure is assumed to be known (Asenova and Segers, 2023, Röttger et al., 2023b).

1.1. Our contributions. We introduce a general latent Hüsler–Reiss graphical model where the graphical structure among the observed and latent variables as well as the number of latent variables may be arbitrary. Letting $\Theta \in \mathbb{R}^{d \times d}$ be the precision matrix, a key result that we establish is that the marginal precision matrix $\tilde{\Theta} \in \mathbb{R}^{p \times p}$ over the observed variables can be expressed in terms of blocks



FIGURE 1. One-factor graph with one latent variable with four observed variables O_1, \dots, O_4 and one latent variable H (left) and its marginalization on the observed variables (right).

of Θ as

$$\tilde{\Theta} = \Theta_O - \Theta_{OH}\Theta_H^{-1}\Theta_{HO}, \quad \text{where } \Theta = \begin{pmatrix} \Theta_O & \Theta_{OH} \\ \Theta_{HO} & \Theta_H \end{pmatrix}.$$

The representation of Θ resembles the Schur complement in Gaussian latent variable graphical models (Chandrasekaran et al., 2012). However, in the Hüsler–Reiss case, the matrices Θ and $\tilde{\Theta}$ are not invertible since they have the all-one vector in their kernel, and the link between our representation and the Schur complement is therefore non-trivial.

Assuming that the conditional graph among the observed variables is sparse and that there are a few latent variables influencing the observed variables, the marginal precision matrix $\tilde{\Theta}$ is decomposed as the sum of a sparse and a low-rank matrix. The sparse component Θ_O encodes the conditional graphical structure among the observed variables after conditioning on the latent variables and the low-rank component $\Theta_{OH}\Theta_H^{-1}\Theta_{HO}$ encodes the effect of a few latent variables on the observed variables. Using this decomposition, we propose a convex optimization procedure named **eglatent** that estimates each term in the decomposition without knowledge of the underlying graphical structure or the number of latent variables. Under some identifiability assumptions, we provide finite-sample consistency guarantees for our estimator, showing that our procedure recovers the conditional graph and the number of latent variables. Our identifiability conditions assume that the number of latent variables is small (compared to the observed variables) and they affect many observed variables.

Figure 2 highlights the advantage of our method **eglatent** over the existing extremal graph learning method **eglearn** (Engelke et al., 2022c), which does not account for latent variables. In this synthetic example, we generated 5000 approximate observations from an extremal graphical model with $h = 2$ latent variables and a cycle graph among $p = 30$ observed variables, and fitted both methods for different values of the regularization parameters; see Section 5.1.1 for details on the setup. Compared to **eglearn**, our **eglatent** produces a better model fit on validation data and more accurate graph estimates among the observed variables in terms of F -score. Indeed, due to the latent confounding, the marginal graph among the observed variables, encoded by the zero pattern in $\tilde{\Theta}$, is dense, and thus the sparsity that **eglearn** exploits is not appropriate: the best validated **eglearn** model has 283 edges while the true graph has 30 edges. On the other hand, conditional on the latent variables, the conditional graph among the observed variables, encoded by the zero pattern in Θ_O , is sparse, and **eglatent** exploits this structure. Furthermore, **eglatent** estimates the correct number of latent variables and a near-perfect graph among the observed variables for regularization parameters with high validation likelihood. Note that in the left plot, the crosses for **eglearn** mean that the estimated graphical model is disconnected and therefore does not lead to a valid Hüsler–Reiss model. In contrast,

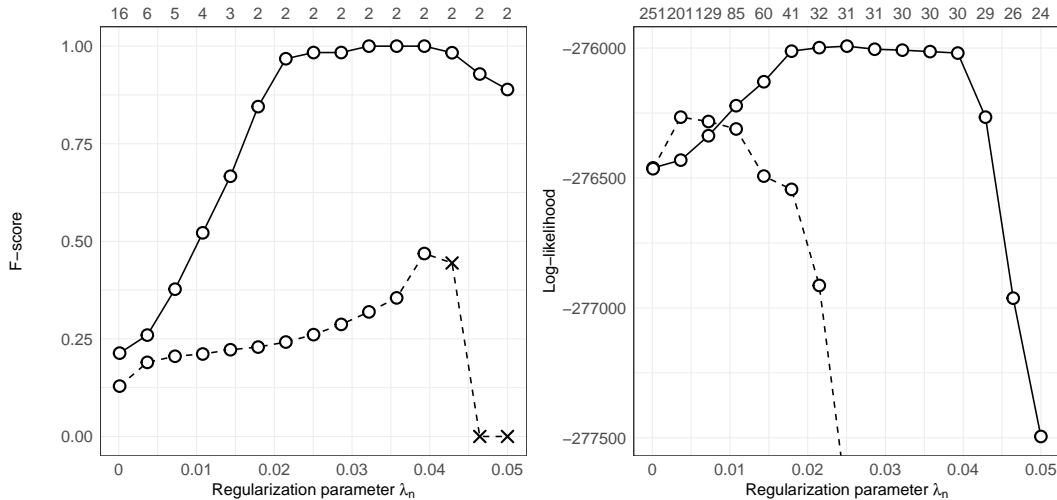


FIGURE 2. Left: F -score of our proposed method **eglatent** (solid line) and **eglearn** (dashed line) as function of the regularization parameter with larger F -scores being better; top axis shows the number of estimated latent variables. Right: the likelihood of the same methods evaluated on a validation data set; the top axis shows the number of estimated edges in the latent model.

eglatent always yields a valid Hüsler–Reiss model. More simulations and an application to large flight delays in the U.S. are presented in Section 5.

The **eglatent** method is implemented in the R package **graphicalExtremes** (Engelke et al., 2022a) and all numerical results and figures can be reproduced using the code on https://github.com/sebastian-engelke/extremal_latent_learning.

1.2. Notation. We denote I_r as an $r \times r$ identity matrix and denote $\mathbf{1}_r$ as the all-ones vector with r coordinates. The collection of $r \times r$ symmetric matrices is denoted by S^r . The following matrix norms are employed throughout this paper: $\|M\|_2$ denotes the spectral norm, or the largest singular value of M ; $\|M\|_\infty$ denotes the largest entry in the magnitude of M ; $\|M\|_*$ denotes the nuclear norm, or the sum of the singular values of M (this reduces to the trace for positive semidefinite matrices); and $\|M\|_1$ denotes the sum of the absolute values of the entries of M . Finally, we will denote $\sigma_{\min}(M)$ as the largest non-zero singular value of M .

2. BACKGROUND

2.1. Multivariate extreme value theory. Multivariate extreme value theory studies asymptotically motivated models for the largest observations of a random vector $X = (X_j : j \in V)$ with index set $V = \{1, \dots, d\}$. Since we concentrate on models for the extremal dependence structure, we assume that the marginal distributions of X have been standardized to standard exponential distributions. In practice, this standardization can be achieved by using the marginal empirical distribution functions; see Section 3.3.1.

A multivariate Pareto distribution models the multivariate tail of the distribution of X . It is defined as the limit in distribution of the conditional exceedances over a high threshold u , that is,

$$(1) \quad Y = \lim_{u \rightarrow \infty} (X - u \mid \max(X_1, \dots, X_d) > u),$$

if the limit exists (Rootzén and Tajvidi, 2006). Here the simple normalization by subtracting u in each component of X is due to the exponential marginals. The random vector X is said to be in

the domain of attraction of the multivariate Pareto distribution Y , which is supported on the space $\mathcal{L} = \{y \in \mathbb{R}^d : \max(y_1, \dots, y_d) > 0\}$. Multivariate Pareto distributions are the only possible limits of threshold exceedances (Rootzén et al., 2018) and therefore a canonical model for extremes. If the convergence in (1) holds, it is easy to see that for any non-empty subset $I \subset V$, the sub-vector $X_I = (X_j : j \in I)$ is itself in the domain of attraction of a $|I|$ -dimensional Pareto distribution, which we call the I th sub-model of Y .

We now introduce the Hüsler–Reiss model, which is the most popular parametric sub-class of multivariate Pareto distributions. It can be seen as the analog of Gaussian distributions in multivariate extreme value theory, a fact, that will become apparent when studying extremal graphical models in the next section.

Definition 1. *A multivariate Pareto distribution $Y = (Y_1, \dots, Y_d)$ is called a Hüsler–Reiss distribution parameterized by the variogram matrix Γ in the space of conditionally negative definite matrices*

$$(2) \quad \mathcal{C}^d = \{\Gamma \in [0, \infty)^{d \times d} : \Gamma = \Gamma^\top, \text{diag}(\Gamma) = \mathbf{0}, \mathbf{v}^\top \Gamma \mathbf{v} < 0 \forall \mathbf{0} \neq \mathbf{v} \perp \mathbf{1}\},$$

if its density has the form

$$(3) \quad f(y; \Gamma) = c_\Gamma \exp \left\{ -\frac{1}{2} (y - \mu_\Gamma)^\top \Theta (y - \mu_\Gamma) - \frac{1}{d} \sum_{i=1}^d y_i \right\}, \quad y \in \mathcal{L},$$

where $c_\Gamma > 0$ is a normalizing constant, $\mu_\Gamma = \Pi(-\Gamma/2)\mathbf{1}_d$, and $\Pi = I_d - \mathbf{1}_d \mathbf{1}_d^\top / d$ is the projection matrix onto the orthogonal complement of the all-ones vector in d -dimensions. The matrix $\Theta = (\Pi(-\Gamma/2)\Pi)^\dagger$ is the positive semi-definite Hüsler–Reiss precision matrix (Hentschel et al., 2022), where A^\dagger is the Moore–Penrose pseudoinverse of a matrix A .

The Hüsler–Reiss distribution is stable under marginalization, in the sense that for $I \subset V$, the Hüsler–Reiss sub-model corresponding to the I th marginal is again Hüsler–Reiss distributed with parameter matrix Γ_I . While the density in (3) resembles the density of a multivariate normal distribution, we note that there are important differences. First, this function would not have finite integral on \mathbb{R}^d because of the second term in the exponential, and the restriction to the subset \mathcal{L} is crucial. Second, the precision matrix Θ is of rank $d - 1$, which complicates theoretical and practical considerations.

An important summary statistic of the dependence structure in multivariate Pareto distributions is the extremal variogram (Engelke and Volgushev, 2022). It takes a similar role as the covariance matrix in the non-extremal world.

Definition 2. *For a multivariate Pareto distribution $Y = (Y_j : j \in V)$ the extremal variogram rooted at node $m \in V$ is defined as the matrix $\Gamma^{(m)}$ with entries*

$$\Gamma_{ij}^{(m)} = \text{Var} \{Y_i - Y_j \mid Y_m > 1\}, \quad i, j \in V,$$

whenever the right-hand side is finite.

If Y follows a Hüsler–Reiss distribution with parameter matrix Γ , it can be checked that the extremal variogram matrices coincide for all $m \in V$, and that they satisfy

$$(4) \quad \Gamma = \Gamma^{(1)} = \dots = \Gamma^{(d)}.$$

We use this fact later to combine empirical estimators of the extremal variograms rooted at the different nodes to obtain a more efficient joint estimator of Γ .

2.2. Extremal graphical models. Conditional independence for multivariate Pareto distributions Y is non-standard since it is defined on the space \mathcal{L} , which is not a product space. Engelke and Hitz (2020) therefore define a new notion of extremal conditional independence using the auxiliary vectors $Y^{(m)}$, for $m \in \{1, \dots, d\}$, defined as Y conditioned on the event that $\{Y_m > 0\}$. For non-empty sub-sets $A, B, C \subset V$, we say that Y_A is conditionally independent of Y_B given Y_C , denoted by $Y_A \perp_e Y_B \mid Y_C$, if for all auxiliary random vectors, we have the corresponding statement in the usual sense, that is,

$$Y_A^{(m)} \perp\!\!\!\perp Y_B^{(m)} \mid Y_C^{(m)} \quad \text{for all } m \in V.$$

It can be shown that requiring the relation above is equivalent to requiring the existence of a single $m \in V$ for which $Y_A^{(m)} \perp\!\!\!\perp Y_B^{(m)} \mid Y_C^{(m)}$ (Engelke et al., 2022b).

Let $\mathcal{G} = (V, E)$ be an undirected graph with nodes $V = \{1, \dots, d\}$ and edge set $E \subset V \times V$. Using the new notion of conditional independence, an extremal graphical model on \mathcal{G} is a multivariate Pareto distribution Y that satisfies the extremal pairwise Markov property on \mathcal{G} , that is,

$$Y_i \perp_e Y_j \mid Y_{V \setminus \{i, j\}} \quad \text{if } (i, j) \notin E.$$

Engelke and Hitz (2020) show that this definition is natural in the sense that it enables a Hammersley–Clifford theorem showing that densities factorize into lower-dimensional terms on the cliques of the graph.

For a multivariate Gaussian distribution with covariance matrix Σ , the conditional dependence relationships, or equivalently the edges in the Gaussian graphical model can be identified from the nonzeros of the precision matrix Σ^{-1} . A similar property holds for extremal graphical models if Y follows a Hüsler–Reiss distribution, where the matrix Θ in Definition 1 plays a key role.

Proposition 1 (Lemma 1 and Proposition 3 of Engelke and Hitz (2020)). *Let $Y \in \mathbb{R}^d$ follow a Hüsler–Reiss distribution with precision matrix Θ . Then,*

$$(5) \quad Y_i \perp_e Y_j \mid Y_{V \setminus \{i, j\}} \Leftrightarrow \Theta_{ij} = 0.$$

A consequence of Proposition 1 is that for a Hüsler–Reiss graphical model on an arbitrary connected graph \mathcal{G} , we can read off the graph structure from the zero pattern of the precision matrix Θ .

Finally, we note that an important property of an extremal graphical model is that if Y possesses a density that factorizes on the graph \mathcal{G} , then \mathcal{G} must *necessarily be connected* (Engelke and Hitz, 2020). The state-of-the-art structure learning methods for extremal data (Engelke et al., 2022c, Wan and Zhou, 2023) can yield disconnected graphs that thus do not always yield a valid distribution (see the example in Figure 1). For a detailed review of recent progress on extremal graphical models, we refer to Engelke et al. (2024). In the next section, we present our approach for structure learning, which can handle latent variables and always yields a valid distribution.

3. LATENT HÜSLER–REISS MODELS AND THE EGLATENT METHOD

3.1. Latent Hüsler–Reiss models. In the illustrative example in the introduction, we presented a Hüsler–Reiss model with a single latent variable and a very simple graphical structure among the observed variables. We next introduce a latent Hüsler–Reiss model with a general extremal graphical structure and any number of latent variables. In what follows, let $X_O \in \mathbb{R}^p$ be the collection of observed variables, $X_H \in \mathbb{R}^h$ be a collection of latent variables, and put $d := p + h$.

Definition 3 (Latent Hüsler–Reiss models). *Suppose that the random vector $X = (X_O, X_H) \in \mathbb{R}^d$, indexed by $V = (O, H)$, is in the domain of attraction of a Hüsler–Reiss distribution $Y \in \mathbb{R}^d$ in the*

sense of (1) with variogram and precision matrices, and corresponding extremal graphical structure

$$\Gamma = \begin{pmatrix} \Gamma_O & \Gamma_{OH} \\ \Gamma_{HO} & \Gamma_H \end{pmatrix}, \quad \Theta = \begin{pmatrix} \Theta_O & \Theta_{OH} \\ \Theta_{HO} & \Theta_H \end{pmatrix}, \quad \text{and} \quad \mathcal{G} = (V, E),$$

respectively. Here $\Theta = (\Pi(-\Gamma/2)\Pi)^+$, Γ_O and Θ_O are $p \times p$ -dimensional symmetric matrices, and $E = \{(i, j) : i, j \in V, i \neq j, \Theta_{ij} \neq 0\}$. We then say that Y is a latent Hüsler–Reiss model, and we note that the observed variables X_O are in the domain of attraction of a Hüsler–Reiss model with variogram Γ_O .

Note that Θ_O and Θ_H in the above definition are positive definite since $\Gamma \in \mathcal{C}^d$; see Definition 1 and Engelke and Hitz (2020, Appendix B). Latent Hüsler–Reiss models have been studied only for very simple graphs, namely tree structures (Asenova et al., 2021, Röttger et al., 2023b) and block graphs (Asenova and Segers, 2023). All of the above methods assume the underlying graph structure among the observed and latent variables and the number of latent variables to be known, which is rarely realistic in practice. To handle more general graphs, we establish the following theorem, which relates the marginal distribution of the observed variables to components of the precision matrix Θ .

Theorem 2. *Let $\tilde{\Pi} = I_p - \mathbf{1}_p \mathbf{1}_p^T / p$ be the projection matrix onto the orthogonal complement of the all-ones vector in p dimensions. Then, the precision matrix $\tilde{\Theta} \in \mathbb{R}^{p \times p}$ of the observed variables of a latent Hüsler–Reiss model with variogram matrix Γ satisfies*

$$(6) \quad \tilde{\Theta} = (\tilde{\Pi}(-\Gamma_O/2)\tilde{\Pi})^+ = \Theta_O - \Theta_{OH}\Theta_H^{-1}\Theta_{HO}.$$

While it is not possible to observe the joint precision matrix Θ or any of its components directly, Theorem 3 provides a useful decomposition of the observable precision matrix $\tilde{\Theta}$ into the difference of two terms, each term involving the components of Θ . By the property in (5), we have for any $i, j \in O$ that

$$Y_i \perp_e Y_j \mid Y_H, Y_{O \setminus \{i, j\}} \Leftrightarrow [\Theta_O]_{i, j} = 0.$$

Thus, the first term Θ_O in decomposition (6) specifies the conditional independencies among the observed variables after conditioning on the latent variables. Moreover, the sparsity pattern of Θ_O encodes the residual graph \mathcal{G}_O among the observed variables after extracting the influence of the latent variables. Here, $\mathcal{G}_O = (O, E_O)$ is a subgraph of \mathcal{G} restricted to the observed variables where $E_O = \{(i, j) \in E, i, j \in O\}$. The second term $\Theta_{OH}\Theta_H^{-1}\Theta_{HO}$ in decomposition (6) serves as a summary of the marginalization of the latent variables Y_H and encodes their effect on the observed variables. The rank of this matrix is equal to the number of latent variables. The overall term $\Theta_O - \Theta_{OH}\Theta_H^{-1}\Theta_{HO}$ is a Schur complement with respect to Θ_H .

As an illustration, consider the extremal graph on the left-hand side of Figure 1. Here, the matrix Θ_O is diagonal. Furthermore, the matrix $\Theta_{OH}\Theta_H^{-1}\Theta_{HO}$ has rank equal to one with all of its entries being nonzero. Note that $\tilde{\Theta}$ generally consists of all nonzero entries and hence the marginal graphical structure among the observed variables on the right-hand side of Figure 1 is fully connected.

3.2. Sparse plus low-rank decomposition. In this paper, we consider a latent Hüsler–Reiss graphical model where the subgraph \mathcal{G}_O among the observed variables is sparse and the number of latent variables is small relative to the number of observed variables, that is, $h \ll p$. This modeling assumption is often natural in real-world applications. For example, Chandrasekaran et al. (2012) and Taeb and Chandrasekaran (2016) showed that a large fraction of the conditional dependencies among stock returns can be explained by a small number of latent variables and interpreted these to be correlated to exchange rate and government expenditures. In a similar spirit, Taeb et al. (2017) demonstrated

that the California reservoir network is sparsely connected after accounting for a few latent factors, and interpreted these latent factors to be highly correlated to environmental variables such as drought level and precipitation.

In the case of extremes, a sparse subgraph \mathcal{G}_0 and the presence of only a few latent variables in the model translate to a latent Hüsler–Reiss model with matrix Θ_O being sparse, the matrix $\Theta_{OH}\Theta_H^{-1}\Theta_{HO}$ being low-rank, and thus the observed precision matrix $\tilde{\Theta}$ being decomposed as a sparse plus low-rank matrix having zero row sums. Notice that the matrix $\tilde{\Theta}$ will generally be dense due to the additional low-rank term $\Theta_{OH}\Theta_H^{-1}\Theta_{HO}$, highlighting how the latent variables induce many confounding dependencies among the observed variables (see Figure 1), and how structure learning procedures that impose sparsity on the precision matrix $\tilde{\Theta}$ will generally not perform well.

In summary, we can cast the problem of learning a latent Hüsler–Reiss graphical model as obtaining a sparse plus low-rank decomposition of the precision matrix $\tilde{\Theta}$ of the observed variables. The sparse component provides the residual graphical structure of the observed variables after accounting for the latent variables, the rank of the low-rank component provides the number of latent variables, and the overall sum provides a compact model of the observed variables that can be used for downstream tasks. In the following section, we propose a convex optimization procedure to accurately estimate each of these components from data.

Remark 1. *In the setting where the observed and latent variables are jointly Gaussian, Chandrasekaran et al. (2012) also models the precision matrix among the observed variables as a sum of a sparse and a low-rank matrix. Analogous to our setting, the sparse component encodes the subgraph of the observed variables and the low-rank component encodes the effect of the latent variables on the observed variables. An important distinguishing feature with our extremal setting however is that in the Gaussian context, the resulting sum is not constrained to have zero row sum. As we describe in Section 3.3, the additional subspace constraint in our extremal setting results in a different estimation procedure and assumptions for statistical consistency.*

3.3. Inference for latent Hüsler–Reiss graphical models. Let $X = (X_O, X_H)$ be a collection of observed and latent variables in the domain of attraction of a latent Hüsler–Reiss graphical model with a sparse subgraph among the observed variables and a small number of latent variables; we will specify the sparsity level and the number of latent variables in our theoretical results. Let Γ^* be the underlying population variogram matrix and Θ^* be the population precision matrix with components Θ_O^* , Θ_{OH}^* and Θ_H^* . Let $\tilde{\Theta}^*$ be the precision matrix among the observed variables. From Theorem 3, we have that $\tilde{\Theta}^* = S^* - L^*$ where $S^* := \Theta_O^*$ is a sparse matrix and $L^* := \Theta_{OH}^*\Theta_H^{*-1}\Theta_{HO}^*$ is a low-rank matrix. Here, the support of S^* encodes the subgraph among the observed variables and the rank of L^* encodes the number of latent variables. We will propose a convex optimization procedure to estimate the matrices (S^*, L^*) from data.

3.3.1. Empirical extremal variogram matrix. An important ingredient of our procedure is an empirical estimate for the extremal variogram matrix Γ_O^* . To arrive at our estimate, define for any $m \in O$, the population extremal variogram matrix $\Gamma_O^{*,(m)}$ rooted at the node m ; see Definition 2. Suppose we have n independent and identically distributed samples $\{X_O^{(t)}\}_{t=1}^n \subseteq \mathbb{R}^p$ of the observed variables X_O . Then, a natural estimate $\hat{\Gamma}_O^{(m)}$ for $\Gamma_O^{*,(m)}$ is given by

$$\hat{\Gamma}_{ij}^{(m)} := \widehat{\text{Var}}\left(\log(1 - \hat{F}_i(X_i^{(t)})) - \log(1 - \hat{F}_j(X_j^{(t)})) : \hat{F}_m(X_m^{(t)}) \geq 1 - k/n\right), \quad i, j \in O.$$

Here, $\widehat{\text{Var}}$ denotes the sample variance, and k is the number of extreme samples considered in the conditioning event, which can be viewed as the *effective sample size*. Since in Section 2 we assumed that X has standard exponential margins, for $i \in O$, $t \in \{1, \dots, n\}$, inside the variance we normalize

the i -th entry of the t -th observation empirically by $-\log(1 - \hat{F}_i(X_i^{(t)}))$, where \hat{F}_i denotes the empirical distribution function of $X_i^{(1)}, \dots, X_i^{(n)}$. As (4) establishes that the empirical variogram matrix rooted at node m coincides with the true variogram matrix Γ_O^* for every m , a natural empirical estimator of this matrix is

$$(7) \quad \hat{\Gamma}_O := \frac{1}{p} \sum_{m=1}^p \hat{\Gamma}_O^{(m)}.$$

Under the assumption that $k \rightarrow \infty$ and $k/n \rightarrow 0$, and mild conditions on the underlying data generation, this estimator can be shown to be consistent for Γ_O^* (Engelke and Volgushev, 2022). Moreover, Engelke et al. (2022c) derive finite sample concentration bounds for $\hat{\Gamma}_O$ that can be used for high-dimensional consistency results. We refer to Appendix B for details on the assumptions and results.

3.3.2. Parameter estimation and structure learning. For structure learning in Hüsler–Reiss models, formulating optimization problems in the precision domain leads to computationally efficient procedures. Indeed, the precision matrix estimate obtained from plugging in the empirical extremal variogram $\hat{\Gamma}_O$ in place of Γ_O^* in the expression $\tilde{\Theta}^* = (\tilde{\Pi}(-\Gamma_O^*/2)\tilde{\Pi})^+$ is the minimizer of the following convex optimization problem:

$$(8) \quad \begin{aligned} \hat{\Theta} = \operatorname{argmin}_{\Theta \in \mathbb{S}^p} \quad & -\log \det(U^T \Theta U) - \frac{1}{2} \operatorname{tr}(\Theta \hat{\Gamma}_O), \\ \text{s.t. } \quad & \Theta \succeq 0, \quad \Theta \mathbf{1}_p = 0, \end{aligned}$$

where the matrix $U \in \mathbb{R}^{p \times (p-1)}$ consists of the first $p-1$ left singular vectors of $\tilde{\Pi}$ so that $UU^T = \tilde{\Pi}$; see Appendix D for a formal proof. The constraint $\succeq 0$ imposes positive semi-definiteness, \mathbb{S}^p denotes the space of symmetric $p \times p$ matrices, and the constraint $\Theta \mathbf{1}_p = 0$ ensures that Θ has zero row sum. The above optimization problem corresponds to the surrogate maximum likelihood estimator of the Hüsler–Reiss distribution; for more details on this justification we refer to Röttger et al. (2023b).

The formulation in terms of the precision matrix Θ opens the door to various regularized estimation methods. Röttger et al. (2023b) solve problem (8) under the additional constraint that $\Theta_{ij} \leq 0$ for all $i, j \in V$ to ensure a form of positive dependence. For a graph $\mathcal{G} = (V, E)$, in order to obtain a graph structured estimate of Γ , Hentschel et al. (2022) solve a matrix completion problem that corresponds to (8) under the constraint $\Theta_{ij} = 0$ for $(i, j) \notin E$. In the context of structure learning without latent variables, Engelke et al. (2022c) and Wan and Zhou (2023) consider adding an ℓ_1 penalty to the loss function akin to the graphical lasso.

In the setting with latent variables, we rely on the sparse plus low-rank decomposition described in Section 3.1. We, therefore, search over the space of precision matrices Θ that can be decomposed as $\Theta = S - L$ to identify a sparse matrix S and a low-rank matrix L , whose difference has zero row sum and yields a small surrogate negative likelihood. Motivated by the estimator for Gaussian latent variable graphical modeling (Chandrasekaran et al., 2012), we introduce the `eglatent` method that solves the following regularized *convex* likelihood problem for some $\lambda_n, \gamma \geq 0$:

$$(9) \quad \begin{aligned} (\hat{S}, \hat{L}) = \operatorname{argmin}_{S \in \mathbb{S}^p, L \in \mathbb{S}^p} \quad & -\log \det(U^T(S - L)U) - \operatorname{tr}((S - L)\hat{\Gamma}_O/2) + \lambda_n(\|S\|_1 + \gamma \operatorname{tr}(L)), \\ \text{s.t. } \quad & S - L \succeq 0, L \succeq 0, (S - L)\mathbf{1}_p = 0. \end{aligned}$$

Here, \hat{S} and \hat{L} are estimates for the population quantities S^* and L^* , respectively. The matrix $\hat{S} - \hat{L}$ represents an estimated precision matrix among the observed variables. By the constraints in (9) and the property of logdet functions, $\operatorname{span}(\mathbf{1}_p \mathbf{1}_p^\top)$ is the null space of $\hat{S} - \hat{L}$ and $\hat{S} - \hat{L}$ always specifies a valid Hüsler–Reiss model.

The function $\|\cdot\|_1$ denotes the ℓ_1 norm that promotes sparsity in the matrix S (Friedman et al., 2007). The role of the trace penalty on L is to promote low-rank structure (Fazel et al., 2004). The regularization parameter γ provides a trade-off between the graphical model component and the latent component. In particular, for very large values of γ , `eglatent` produces $\hat{L} = 0$ so that no latent variables are included in the model. As γ decreases, the number of latent variables increases and correspondingly the number of edges in the residual graphical structure decreases. The regularization parameter λ_n provides overall control of the trade-off between the fidelity of the model to the data and the complexity of the model, and thus naturally depends on the sample size. For $\lambda_n, \gamma \geq 0$, `eglatent` is a convex program that can be solved efficiently.

Remark 2. *A challenge with the optimization in (8), both theoretically and numerically, is the fact that the matrices range in the space of positive semi-definite matrices with zero row sum. This factor indeed seems to prohibit direct structure learning without latent variables (i.e., setting $L = 0$ in (9) to obtain a graphical lasso analog) where the estimated graphical structure can be rather different than the true graphical structure; see the discussion in Engelke et al. (2022c, Section 7). To circumvent this issue, Engelke et al. (2022c) and Wan and Zhou (2023) solve slightly different problems to obtain accurate graph estimation, although their estimated graphs do not always yield valid Hüsler–Reiss models. Remarkably, the addition of the low-rank component L in the `eglatent` estimator (9) solves these issues. Indeed, we will show that `eglatent` consistently recovers the subgraph among the observed variables and the number of latent variables, and matches the performance of existing procedures (Engelke et al., 2022c, Wan and Zhou, 2023) for learning an accurate model when no latent variables are present.*

4. CONSISTENCY GUARANTEES FOR EGLATENT

Recall from Section 3.3 that we denote by S^* the population matrix encoding the graphical structure among the observed variables conditioned on the latent variables, and by L^* the population matrix encoding the effect of a few latent variables on the observed variables. Further, $\tilde{\Theta}^* = S^* - L^*$ represents the marginal precision matrix in the Hüsler–Reiss model over the observed variables. In this section, we state a theorem to prove that the estimates of `eglatent` in (9) provide, with high probability, the correct graphical structure among the observed variables, the correct number of latent variables, and an accurate extremal model. Stated mathematically, we show with high probability that (i) the sign-pattern of \hat{S} is the same as that of S^* , i.e., $\text{sign}(\hat{S}) = \text{sign}(S^*)$, where $\text{sign}(0) = 0$; (ii) the rank of \hat{L} is the same as that of L^* , i.e., $\text{rank}(\hat{L}) = \text{rank}(L^*)$; and (iii) the estimated precision model $\hat{S} - \hat{L}$ closely approximates the true precision matrix $\tilde{\Theta}^*$, i.e., $\hat{S} - \hat{L} \approx \tilde{\Theta}^*$.

Our analysis requires assumptions on the population model so that the matrices S^* and L^* are identifiable from their sum, and that the number of effective samples k is of order $k \gtrsim p^2 \log(p)$.

4.1. Technical setup. As `eglatent` is solved in the precision matrix parameterization, the conditions for our theorems are naturally stated in terms of the precision matrix $S^* - L^*$. The assumptions are similar in spirit to convex relaxation methods for Gaussian latent-variable graphical model selection (Chandrasekaran et al., 2012), although some conditions are new due to the zero row and column sum structure of the observed precision matrix $S^* - L^*$.

To ensure correct graph recovery and correct number of latent variables, we seek an estimate (\hat{S}, \hat{L}) from `eglatent` such that $\text{support}(\hat{S}) = \text{support}(S^*)$ and $\text{rank}(\hat{L}) = \text{rank}(L^*)$. Building on both classical statistical estimation theory, as well as the recent literature on high-dimensional statistical inference, a natural set of conditions for accurate parameter estimation, is to assume that the curvature of $S^* - L^*$ is bounded in certain directions. The curvature is governed by the modified Hessian of the

surrogate log-likelihood loss at $S^* - L^*$:

$$\mathbb{I}^* := \left(S^* - L^* + \frac{1}{p} \mathbf{1}_p \mathbf{1}_p^\top \right)^{-1} \otimes \left(S^* - L^* + \frac{1}{p} \mathbf{1}_p \mathbf{1}_p^\top \right)^{-1},$$

where \otimes denotes a Kronecker product between matrices, and \mathbb{I}^* may be viewed as a map from \mathbb{S}^p to \mathbb{S}^p . The matrix \mathbb{I}^* modifies the Hessian of the surrogate log-likelihood loss $(S^* - L^*)^+ \otimes (S^* - L^*)^+$, where the addition of the term $\frac{1}{p} \mathbf{1}_p \mathbf{1}_p^\top$ (a dual parameter of the program (9)) helps to compactify the assumptions we place in our population model.

We impose conditions so that \mathbb{I}^* is well-behaved when applied to matrices of the form $S - S^* - (L - L^*)$ and $S - S^* - (L - L^* + t \mathbf{1}_p \mathbf{1}_p^\top)$. Here, S is in the neighborhood of S^* restricted to sparse matrices, L is in the neighborhood of L^* restricted to low-rank matrices, and $t \mathbf{1}_p \mathbf{1}_p^\top$ is a dual parameter for some $t \in \mathbb{R}$ due to the constraint $(S - L) \mathbf{1}_p = 0$ that appears in the analysis of (9). These local properties of \mathbb{I}^* around $S^* - L^*$ are conveniently stated in terms of tangent spaces to algebraic varieties of sparse and low-rank matrices. In particular, the tangent space of a matrix M with r non-zero entries with respect to the algebraic variety of $p \times p$ matrices with at most r non-zeros is given by

$$\Omega(M) := \{N \in \mathbb{R}^{p \times p} : \text{support}(N) \subseteq \text{support}(M)\}.$$

Moreover, the tangent space at a rank- r matrix M with respect to the algebraic variety of $p \times p$ matrices with rank less than or equal to r is given by:

$$T(M) := \{N_R + N_C : N_R, N_C \in \mathbb{R}^{p \times p}, \\ \text{row-space}(N_R) \subseteq \text{row-space}(M), \text{col-space}(N_C) \subseteq \text{col-space}(M)\}.$$

For more discussion on the tangent spaces of sparse and low-rank matrices, see Chandrasekaran et al. (2012). In the next section, we describe conditions on the population Hessian \mathbb{I}^* in terms of tangent spaces $\Omega(S^*)$ and $T(L^*)$. Under these conditions, we present a theorem in Section 4.3 showing that the convex program provides accurate estimates.

For notational simplicity, we let $\Omega^* := \Omega(S^*)$ and $T^* := T(L^*)$.

4.2. Identifiability of (S^*, L^*) and hessian conditions. Appealing to the previous literature on sparse-plus-low rank decompositions, the matrices S^* and L^* are identifiable from their sum if the row and columns of the matrix S^* are sufficiently sparse and the matrix L^* is sufficiently low-rank with most of its entries non-zero and similar in magnitude (Candès et al., 2011, Chandrasekaran et al., 2011, Recht et al., 2010). The structural constraint on L^* can be interpreted as the number of latent variables being small (as compared to the ambient dimension p) with their effects spread across all the observed variables. We measure the sparsity of S^* by the maximal number of non-zeros in any row/column (this amounts to the degree of the subgraph induced among the observed variables):

$$d^* := \max_i \sum_j \mathbb{I}[S_{ij}^* \neq 0].$$

Thus, we require d^* to be small so that no observed variable is directly connected to “many” other observed variables. To measure the “diffuseness” of the latent effects, we consider the following quantity for any linear subspace $Z \subseteq \mathbb{R}^p$ (Candès et al., 2011, Candès and Recht, 2012, Chandrasekaran et al., 2012, 2011):

$$\mu[Z] := \max_i \|\mathcal{P}_Z(\mathbf{e}_i)\|_2,$$

where \mathcal{P}_Z is the projection onto the subspace Z and \mathbf{e}_i is a standard coordinate basis. The quantity $\mu[Z]$ is also known as the “incoherence parameter” (Candès and Recht, 2012, Chandrasekaran et al., 2011). It measures how aligned the subspace Z is with respect to standard basis elements and is

lower-bounded by $\sqrt{\dim(Z)/p}$ and upper-bounded by one. In our setting, the relevant subspace is the row or column space of L^* and so we define:

$$\mu^* := \mu[\text{col-space}(L^*)].$$

Thus, a lower bound for μ^* is $\sqrt{h/p}$. A small value of μ^* ensures the matrix L^* has a small rank and its singular vectors are reasonably spread out – in other words, not sparse.

Finally, as described earlier, the zero row sum constraint in our estimator introduces a dual parameter $t\mathbf{1}_p\mathbf{1}_p^\top$ for some $t \in \mathbb{R}$. Our conditions will rely on how far $\text{span}(\mathbf{1}_p\mathbf{1}_p^\top)$ deviates from T^* , which is summarized in the parameter

$$\kappa^* := \|\mathcal{P}_{T^*\perp}(\mathbf{1}_p\mathbf{1}_p^\top/p)\|_2 \in [0, 1].$$

The smaller the quantity κ^* , the smaller the deviation of the subspace $\text{span}(\mathbf{1}_p\mathbf{1}_p^\top)$ from T^* . As a result, we do not want κ^* to be too small so that L^* and the dual parameter $t\mathbf{1}_p\mathbf{1}_p^\top$ can be distinguished from one another. We also do not want κ^* to be too large so that the size of t can be controlled.

In addition to the quantities (μ^*, d^*, κ^*) , we must control the behavior of the Hessian \mathbb{I}^* restricted to elements in the direct sums $\Omega^* \oplus T^*$ as well as $\Omega^* \oplus (T^* \oplus \text{span}(\mathbf{1}_p\mathbf{1}_p^\top))$. A more interpretable set of assumptions is to measure the behavior of \mathbb{I}^* restricted to the spaces Ω^* and T^* *separately* and use the bound on the quantities (μ^*, d^*, κ^*) to “couple” them to control the behavior of \mathbb{I}^* restricted to the combined spaces. We next present the decoupled conditions and describe in Appendix F how they combine.

Behavior of \mathbb{I}^ with respect to Ω^* .* We consider the following functions of \mathbb{I}^* with respect to Ω^* :

$$\begin{aligned} \alpha_\Omega &:= \min_{N \in \Omega^*, \|N\|_\infty=1} \|\mathcal{P}_{\Omega^*}\mathbb{I}^*\mathcal{P}_{\Omega^*}(N)\|_\infty, \\ \delta_{\Omega^\perp} &:= \max_{N \in \Omega^*, \|N\|_\infty=1} \|\mathcal{P}_{\Omega^*\perp}\mathbb{I}^*\mathcal{P}_{\Omega^*}(N)\|_\infty, \\ \beta_\Omega &:= \max_{N \in \Omega^*, \|N\|_2=1} \|\mathbb{I}^*(N)\|_2. \end{aligned}$$

Here, α_Ω quantifies the minimum gain of \mathbb{I}^* restricted to subspace Ω^* and with respect to the ℓ_∞ norm (the minimum gain of a matrix M restricted to subspace S and with respect to norm $\|\cdot\|$ is $\min_{x \in S, \|x\|=1} \|P_S M P_S(x)\|$); the quantity δ_{Ω^\perp} computes the inner-product between elements in Ω^* and $\Omega^{\star\perp}$ as quantified by the metric induced by \mathbb{I}^* ; and finally, β_Ω quantifies the behavior of \mathbb{I}^* restricted to Ω^* in spectral norm.

Behavior of \mathbb{I}^ with respect to T^* .* Similar to Ω^* , we control the behavior of \mathbb{I}^* associated with the subspace T^* . As discussed earlier, a complication that arises with tangent spaces to low-rank varieties is that they are locally smooth. To account for this curvature, we bound distances of nearby tangent spaces via the following induced norm:

$$\rho(T_1, T_2) := \max_{\|N\|_2 \leq 1} \|(\mathcal{P}_{T_1} - \mathcal{P}_{T_2})(N)\|_2.$$

The quantity $\rho(T_1, T_2)$ measures the sine of the largest angle between T_1 and T_2 . So we control the behavior of \mathbb{I}^* for tangent spaces T' close to the tangent space T^* . In particular, we consider the following functions:

$$\begin{aligned} \alpha_T &:= \min_{N \in T', \rho(T', T^*) \leq \mu^*/4, \|N\|_2=1} \|\mathcal{P}_{T'}\mathbb{I}^*\mathcal{P}_{T'}(N)\|_2, \\ \delta_{T^\perp} &:= \max \left\{ \max_{\substack{N \in T', \rho(T', T^*) \leq \mu^*/4, \\ \|N\|_2 \leq 1}} \|\mathcal{P}_{T'^\perp}\mathbb{I}^*\mathcal{P}_{T'}(N)\|_2, \max_{\substack{N \in T'^\perp, \rho(T', T^*) \leq \mu^*/4, \\ \|N\|_2 \leq 1}} \|\mathcal{P}_{T'}\mathbb{I}^*\mathcal{P}_{T'^\perp}(N)\|_2 \right\}, \\ \beta_T &:= \max_{N \in T', \rho(T', T^*) \leq \mu^*/4, \|N\|_\infty=1} \|\mathbb{I}^*(N)\|_\infty. \end{aligned}$$

Here, α_T quantifies the minimum gain of \mathbb{I}^* restricted to tangent spaces T' that are close to T^* with respect to the spectral norm; the quantify δ_T computes the inner-product between elements in T' and T'^{\perp} as quantified by the metric induced by \mathbb{I}^* ; and finally, β_T quantifies the behavior of \mathbb{I}^* restricted to T' in infinity norm.

With these above quantities defined, the main assumption is the following.

Assumption 1. *Define $\alpha = \min\{\alpha_{\Omega}, \alpha_T\}$, $\delta = \max\{\delta_{\Omega^{\perp}}, \delta_{T^{\perp}}\}$, and $\beta = \max\{\beta_{\Omega}, \beta_T\}$. Then, there exists $\nu_1 \in (0, \min\{1/2, 2\kappa^* + \mu^*/2\})$ and $\nu_2 \in \left(\frac{8\kappa^* + 4\mu^*}{\min\{1, \alpha\} + 2\kappa^* + \mu^*/2}, 1/2\right)$ such that $\delta/\alpha \leq 1 - 2\nu$ where $\nu = \min\{\nu_1, \nu_2\}$.*

Assumption 1 can be viewed as the generalization of the irrepresentability condition imposed on the covariance matrix or the Hessian. In particular, Assumption 1 is akin to the irrepresentability condition imposed in Meinshausen and Bühlmann (2006), Ravikumar et al. (2008), Wainwright (2009), Zhao and Yu (2006), which gives sufficient conditions for consistent recovery of graphical models using ℓ_1 -regularized maximum likelihood estimator. Similarly, Assumption 1 is akin to the irrepresentability condition imposed in Candès and Recht (2012), Chandrasekaran et al. (2012), which gives sufficient conditions for low-rank matrix recovery using nuclear norm regularization.

4.3. Theorem statement. We now describe the performance of `eglatent` under suitable conditions on the quantities described in the previous section. We state the theorem based on essential aspects of the conditions required for the success of our convex relaxation (i.e., the Hessian conditions) and omit complicated constants. We specify these constants in Appendix G. Our results depend on a second-order parameter $\xi > 0$ that determines the rate of convergence of the random vector X to its limiting Hüsler–Reiss distribution, with larger values being better (see Appendix B).

Theorem 3. *Let $\alpha, \beta, \delta, d^*, \mu^*, \kappa^*, \nu_1, \nu_2$ be defined as above with $\kappa^{*2} \geq \mu^*/2$ and $2\kappa^* + \mu^*/2 < 1$. Let $\nu = \min\{\nu_1, \nu_2\}$ and suppose Assumption 1 is satisfied. Suppose that:*

$$d^* \mu^* \leq \frac{\nu^2 \alpha^2}{(1 - 2\kappa^* - \mu^*) 18\beta^2 (2 - \nu)^2}.$$

Let the regularization γ be chosen in the interval $\gamma \in \left[\frac{2\beta d^ (2 - \nu)}{\nu \alpha}, \frac{\nu \alpha (1 - 2\kappa^* - \mu^*)}{36\beta \mu^* (2 - \nu)}\right]$. Let $m = \max\{1, 1/\gamma\}$ and $\bar{m} = \max\{1, \gamma\}$. Let the effective sample size k be chosen such that $k = n^{\xi/2(1+\xi)}$. Furthermore, suppose that:*

- (1) $k \gtrsim \frac{m^3 h d^{*2}}{\alpha^6 \nu^2} m^2 \nu^2 p^2 \log(p)$
- (2) $\lambda_n \sim \frac{m}{\nu} \sqrt{\frac{p^2 \log(p)}{k}}$
- (3) $\sigma_{\min}(L^*) \gtrsim \frac{m^4 \bar{m} h}{\nu \alpha^4} \sqrt{\frac{p^2 \log(p)}{k}}$
- (4) $|S_{ij}^*| \gtrsim \frac{m^3 \bar{m} \sqrt{h}}{\nu \alpha^2} \sqrt{\frac{p^2 \log(p)}{k}}$ for every (i, j) with $|S_{ij}^*| > 0$

Then, the estimate (\hat{S}, \hat{L}) defined as the unique minimizer of `eglatent` in (8) satisfies

$$\mathbb{P} \left(\text{sign}(\hat{S}) = \text{sign}(S^*), \text{rank}(\hat{L}) = \text{rank}(L^*), \|(\hat{S} - \hat{L}) - \tilde{\Theta}^*\|_2 \lesssim \frac{m^3 \sqrt{h}}{\nu \alpha^2} \sqrt{\frac{p^2 \log(p)}{k}} \right) \geq 1 - \frac{1}{p}.$$

We prove Theorem 3 in Appendix G. The theorem essentially states that if the minimum nonzero singular value of the low-rank term L^* and the minimum nonzero entry of the sparse piece S^* are bounded away from zero, then `eglatent` provides accurate estimates for the subgraph among the observed variables, the number of latent variables, and a marginal extremal model.

The quantities $(\alpha, \beta, \delta, d^*, \mu^*, \kappa^*, \nu)$ as well as the choices of the parameters λ_n and γ play a prominent role in the result. Larger values of α, ν and smaller values of μ^*, d^*, β lead to a better conditioned Hessian \mathbb{I}^* around the tangent spaces Ω^* and T^* . The better conditioning of the Hessian \mathbb{I}^* then results in less stringent requirements on the range of values for γ , sample complexity, the minimum nonzero singular value of L^* , and the magnitude of the minimum nonzero entry of S^* . Notice that the number of latent variables h appears explicitly in the bounds in Theorem 3. We also note the dependence on h is implicit in the dependence on μ^*, α, β and ν . Indeed, as larger h increases the dimension of the tangent space T^* , it results in smaller α, ν and larger values of β and μ^* .

Remark 3. *The sample size requirement in Theorem 3 is driven by how fast the empirical variogram matrix $\hat{\Gamma}_O$ converges in spectral norm to the true variogram matrix Γ_O^* . Engelke et al. (2022c) carried out extensive mathematical arguments to analyze the concentration of the empirical variogram matrix in ℓ_∞ norm. In our analysis, we use this result and the equivalence of norms to obtain a convergence rate in spectral norm. It is of interest to develop tighter convergence results, and we leave this as a topic for future research; see Section 6 for more discussion.*

5. EXPERIMENTAL DEMONSTRATIONS

In our numerical experiments, we use `eglatent` as a model selection procedure and perform a second refitting step on the selected model structure to estimate the model parameters; see Appendix H for details.

5.1. Synthetic simulations. We illustrate the utility of our method for recovering the subgraph among the observed variables and the number of latent variables on synthetic data. We compare the performance of our `eglatent` method to `eglearn` by Engelke et al. (2022c) for learning extremal graphical models. To evaluate the accuracy of the estimated graphs with edges \hat{E} relative to the true subgraph among the observed variables with edges $E = E_O$, we use the F -score

$$(10) \quad F = \frac{|E \cap \hat{E}|}{|E \cap \hat{E}| + \frac{1}{2}(|E^c \cap \hat{E}| + |E \cap \hat{E}^c|)}.$$

Larger F -scores thus indicate more accurate graph recovery.

5.1.1. Structure recovery. In order to evaluate the performance of our new method, we generate data from a random vector $X = (X_O, X_H)$ in the domain of attraction of a latent Hüsler–Reiss multivariate Pareto distribution Y with the precision matrix $\Theta^* \in \mathbb{R}^{p+h \times p+h}$, p observed variables $O = \{1, 2, \dots, p\}$ and h latent variables $H = \{p+1, \dots, p+h\}$. We choose to simulate X from the Hüsler–Reiss max-stable distribution with the same precision matrix Θ^* , which is well-known to be in the domain of attraction of Y ; see Resnick (2008) for details. The simulation can be done efficiently with the method in Dombry et al. (2016).

We specify the sub-graph $\mathcal{G}_0 = (E_O, O)$ among the observed variables to be a cycle graph and set Θ_{ij}^* to -2 for every $(i, j) \in E_O$ and zero otherwise. The latent variables are not connected in the joint graph so that $\Theta_{ij}^* = 0$ for every $i, j \in H, i \neq j$. We connect each latent variable node $i \in H$ to every $k \in O$ satisfying $k = i - (p+1) + \zeta h$ for some positive integer ζ (thus every latent variable is connected to a distinct set of observed variables in the graph). The corresponding entries Θ_{ik}^* in the precision matrix are chosen uniformly at random from the interval $[30/\sqrt{p+h}, 60/\sqrt{p+h}]$. Finally, we set the diagonal entries of Θ^* so that it has the all-ones vector in its null space. Appendix I shows results for a setting where the subgraph among the observed variables is generated according to an Erdős–Rényi graph.

We let $p = 30$, $h \in \{1, 2, 3\}$, and we set the number of marginal exceedances to $k = \lfloor n^{0.7} \rfloor$. We then generate n samples from the Hüsler–Reiss distribution parameterized by Θ^* so that we obtain

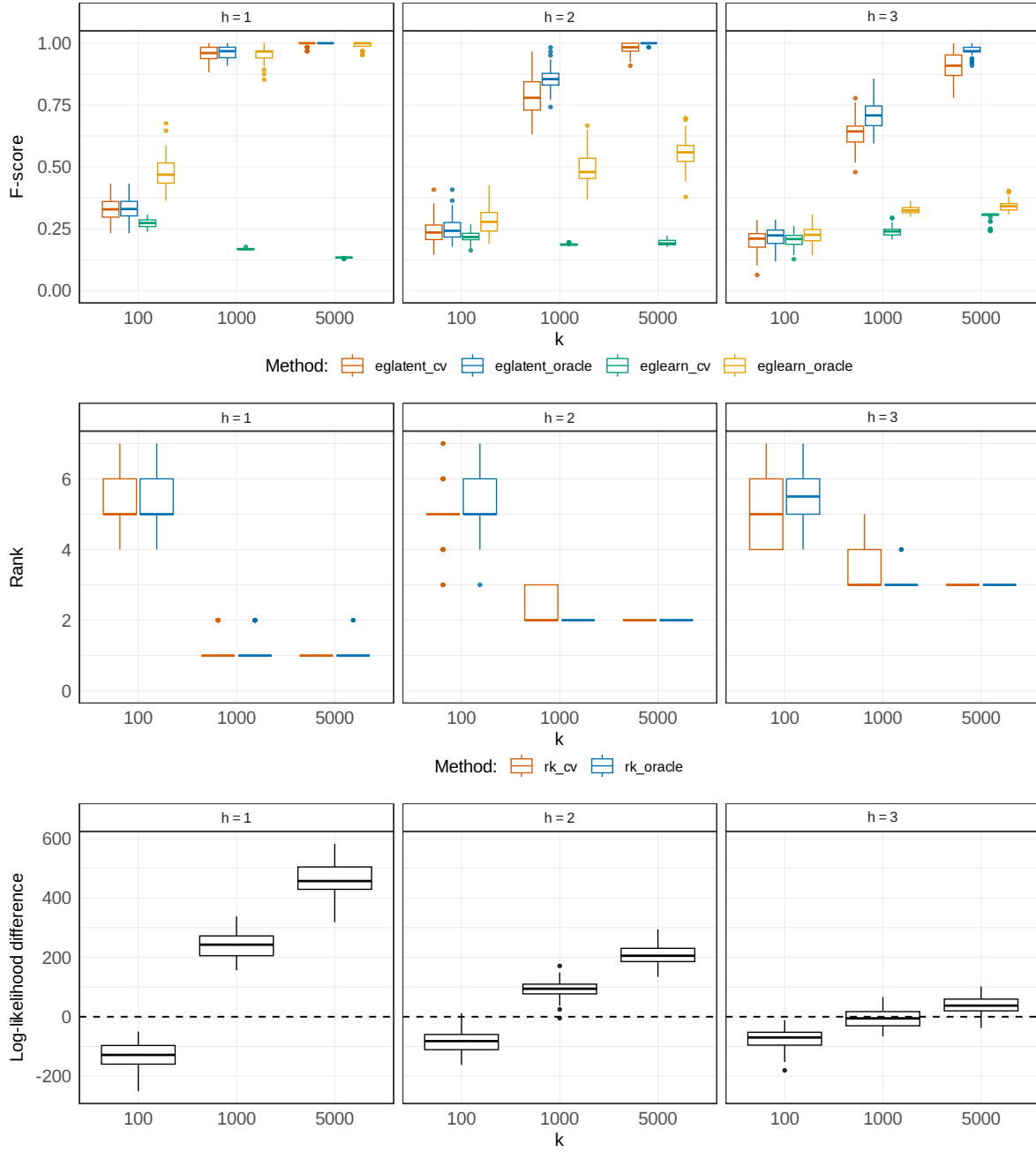


FIGURE 3. F -score (top row) and estimated number of latent variables (middle row) of `eglatent` method with the selection of the tuning parameter based on the oracle and validation on the F -score for the cycle graph with $h = 1, 2, 3$ latent variables and different effective sample sizes $k = 100, 1000, 5000$. The bottom row shows the difference between best `eglatent` and best `eglearn` log-likelihoods on the validation set.

$k \in \{100, 1000, 5000\}$ effective extreme samples. When deploying our **eglatent** estimator in (9), we fix $\gamma = 4$ to a reasonable default value. Concerning the regularization parameter λ_n , which also appears in the **eglearn** method, in both methods, it is chosen either by validation likelihood on a separate dataset of size n or by an oracle approach maximizing the F -score for the sub-graph among observed variables.

Figure 3 summarizes the performance of the methods on 50 independent trials for the different sample sizes and different numbers of latent variables. We observe that our proposed approach outperforms **eglearn** in several ways. Indeed, the top row shows that the graph learned by **eglearn** only poorly recovers the graphical structure among observed variables. This reveals a limitation of this method, namely that in the presence of latent variables, the marginal graph of observed variables is dense and sparsity cannot be well detected by methods that ignore this fact. Clearly, this problem becomes more pronounced with a larger number of latent variables. On the other hand, our new **eglatent** method exploits the latent structure for learning the sparse graph among the observed variables conditional on the latent variables. It recovers the graphical structure among the observed variables increasingly well with a growing sample size. In fact, the results for the tuning parameter λ_n chosen through validation likelihood are almost as good as those based on the oracle. The middle row of Figure 3 shows that **eglatent** is able to identify the correct number of latent variables, especially for larger sample sizes.

We can also compare the model in terms of their likelihood on the validation data. Again, our **eglatent** method generally attains a better validation likelihood and is thus more representative of the data. As an exception, we observe that if the effective sample size is small ($k = 100$), then **eglearn** performs better. The reason is that **eglatent** is a more flexible model with more parameters to learn, and it therefore benefits more from additional data.

5.1.2. Robustness to zero latent variables. We now evaluate the performance of **eglatent** when there are no latent variables present and compare its performance to **eglearn**. We first specify a graph structure using a Barabási–Albert model denoted by $BA(d, q)$, which is a preferential attachment model with d nodes and a degree parameter q (Albert and Barabási, 2001). We set $d = 20$ and $q = 2$. We then define a Hüsler–Reiss precision matrix $\Theta^* \in \mathbb{R}^{d \times d}$ with entries sampled uniformly at random from the interval $[-5, -2]$. The diagonal entries of Θ^* are chosen so that it has the all-ones vector in its null space. We generate n samples from the max-stable Hüsler–Reiss distribution parameterized by Θ^* such that there are $k = \lfloor n^{0.7} \rfloor = 2000$ effective marginal extreme samples. We also generate a separate dataset of size n for validation. For the method **eglatent**, for each value of the regularization parameter $\gamma = 1, 4, 8, 20$ the regularization parameter λ_n is chosen based on the validation set. The regularization parameter λ_n in **eglearn** is chosen similarly.

Figure 4 presents the F -scores and validation log-likelihood scores of **eglatent** as γ varies and for 50 independent trials. We also display the average numbers of edges and latent variables, as well as the performance of **eglearn**. As expected, larger values of γ lead to smaller estimates for the number of latent variables. We observe that when $\gamma = 4$, **eglatent** obtains an accurate graphical structure (F -score close to one) with a similar validation likelihood as **eglearn**. Here, **eglearn** yields a sparse graph since, unlike the previous settings, there are no unobserved confounding. Interestingly, the average number of estimated latent variables in this case is not close to zero. In particular, we observe that when γ is chosen so that **eglatent** yields nearly zero latent variables (i.e., $\hat{L} \approx 0$), the F -scores scores obtained by **eglatent** drop significantly. For such γ , our estimator (9) resembles the analog of the graphical lasso which is known to yield inaccurate models (Engelke et al., 2022c); see also Remark 2.

In summary, when the sample size is sufficiently large, **eglatent** yields a similar model fit and graph recovery as **eglearn** even when there are no latent variables. It is worth emphasizing that

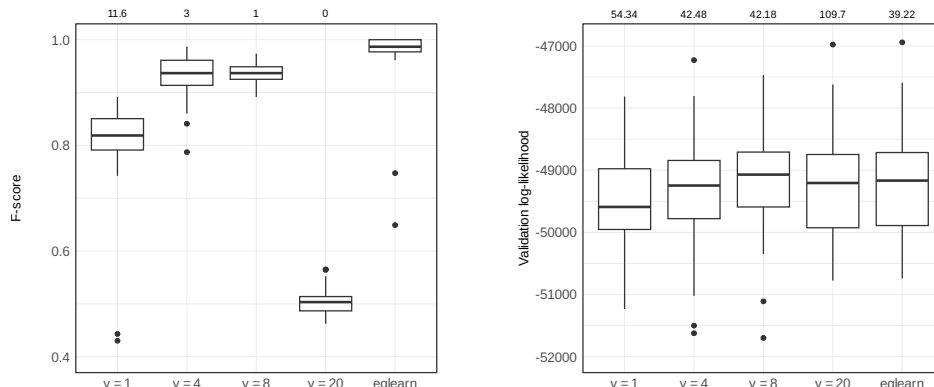


FIGURE 4. Left: F -score of **eglatent** for different regularization parameters $\gamma \in \{1, 4, 8, 20\}$ and **eglearn**; top axis shows the average number of estimated latent variables in **eglatent**. Right: the log-likelihood of the same methods evaluated on a validation data set; the top axis shows the average number of estimated edges in each model.

eglatent achieves this favorable performance by estimating some latent variables. This shows the robustness of our method to model misspecification.

5.2. Real data application. We apply our latent Hüsler–Reiss model to analyze large flight delays. We use a dataset from the R-package **graphicalExtremes** (Engelke et al., 2022a) with $p = 29$ airports in the southern U.S. shown in the left panel of Figure 5. Large flight delays cause huge financial losses and lead to congestion of critical airport infrastructure. Our method provides an improved model for the dependence of such excessive delays at different airports, and can eventually be used for stress testing of the system; see Hentschel et al. (2022) for details on this application. Unless otherwise noted, we fit the models on the whole dataset consisting of $n = 3603$ observations from 2005-01-01 to 2020-12-31. We compare our **eglatent** method for latent Hüsler–Reiss models with the **eglearn** algorithm by (Engelke and Volgushev, 2022) that estimates a graphical structure without latent variables. Throughout this application, we choose the exceedance threshold to be 0.85 (i.e., $1 - k/n = 0.85$) resulting in $k = 540$ marginal exceedances for the computation of the empirical variogram $\hat{\Gamma}_O$; see Section 3.3.1. The latter is the input for the different structure learning methods.

The left-hand side of Figure 6 shows the number of edges of **eglatent** and of **eglearn** as a function of the tuning parameter λ_n , where the parameter γ related to the latent variable selection in **eglatent** is fixed to $\gamma = 2$; different values of γ give similar results and are omitted here. We see that for both methods, larger values of λ_n result in sparser graphs. It is important to note that for **eglearn**, we count the edges of the usual estimated graph. For our **eglatent** method we count the edges of the residual graph among the observed variables. The latent graphs have generally fewer edges and are therefore more easily interpretable.

To compare the different model fits and to select the optimal value for the tuning parameter λ_n , we must compute the likelihood of the fitted models on an independent validation set. To this end, we split the data chronologically into five equally large folds and perform cross-validation by leaving one fold out (validation data) and fitting on the remaining four folds (training data). The results for model performance on the validation sets are then averaged. The right-hand side of Figure 6 shows the averaged log-likelihood values on the validation sets that were not used for model fitting. For both methods, we see that for too small values of λ_n , the graphs are too dense and overfit to the training data. In fact, for $\lambda_n = 0$, both models correspond to the fully connected graph whose

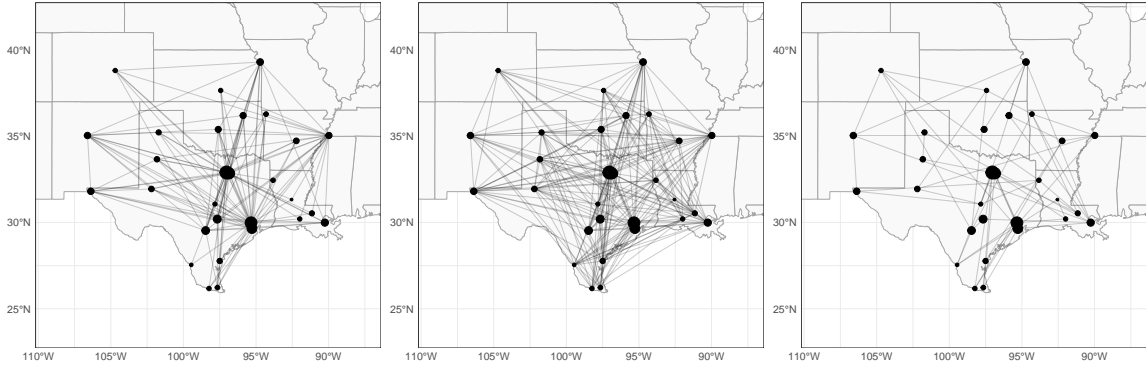


FIGURE 5. Airports in the Southern U.S. (dots) and flight connections, where the thickness of the nodes indicates the average number of daily flights at the airports. Left: flight connection graph with an edge between any pair of airports with daily flights. Center: estimated graph of optimal **eglearn** model. Right: estimated sub-graph corresponding to observed variables of optimal **eglatent** model.

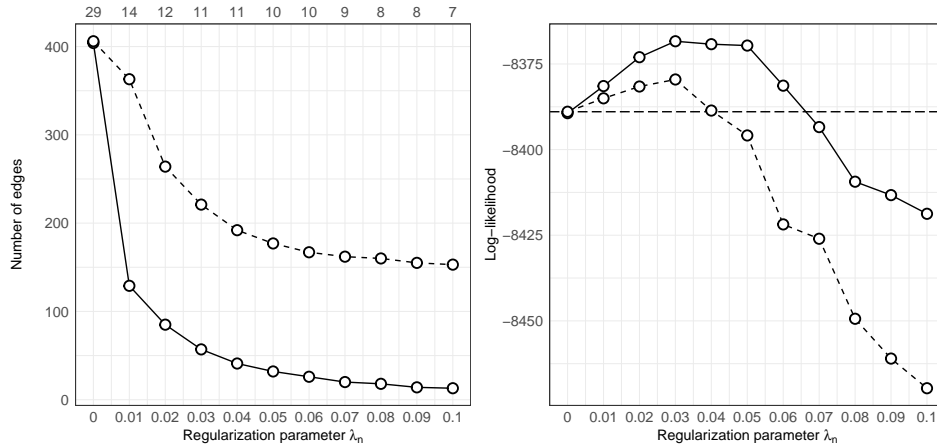


FIGURE 6. Left: number of edges of the estimated graph of **eglearn** (dashed line) and the estimated sub-graph of observed variables of **eglatent** (solid line) as functions of the regularization parameter ρ ; top axis shows the number of latent variables in **eglatent**. Right: corresponding log-likelihoods; horizontal line is the validation log-likelihood of the fully connected graph.

performance (horizontal line) is much worse than the models enforcing sparsity. For too large values of λ_n , the graph becomes too sparse and the model is not flexible enough. Clearly, the latent model outperforms **eglearn**, indicating that latent variables are present in this data set. In this particular application, they can be thought of as confounding factors such as meteorological variables or strikes in the aviation industry that affect many airports simultaneously.

Figure 5 compares the estimated graphs of **eglatent** (center) and **eglearn** (right) fitted on the whole data set, where the regularization parameter λ_n in both methods is chosen as the maximizers of the respective validation likelihoods. We observe that the latent graph is much sparser and therefore highlights more clearly certain features of the system. For instance, it seems that hubs, such as the Fort Worth International Airport in Dallas (the thickest point on the map), are more central in the graph since they have more connections than smaller airports.

6. FUTURE WORK

Our work on latent variables in the analysis of extremal dependence opens several future research directions. First, as described in Section 4.3, our sample size requirement is driven by a spectral norm concentration result on the empirical variogram matrix. This result was derived by translating the ℓ_∞ concentration result of Engelke et al. (2022c) to the spectral norm setting using equivalence of norms. To obtain tighter convergence results, one must obtain direct concentration bounds on the spectral norm; such a result would be of independent interest in the multivariate extremes literature. Second, solving `eglatent` can be challenging for large problems. Building on the work of Ma et al. (2012) in the Gaussian setting, faster solvers can be developed using alternating direction method of multipliers (Boyd et al., 2011). Moreover, we observed in Section 5.1.2 that `eglatent` estimates a few latent variables to accurately recover the underlying graphical structure when there are no latent variables present. It would be of interest to develop a theoretical justification for this phenomenon. Finally, additional structure on the dependency structures among the observed and latent variables, such as multivariate total positivity of order 2 (Röttger et al., 2023b) or colored graphs Röttger et al. (2023a), may be exploited to develop more powerful extremal graphical models with latent variables.

REFERENCES

- Albert, R., Barabási, A.L., 2001. Statistical mechanics of complex networks. ArXiv cond-mat/0106096. URL: <https://journals.aps.org/rmp/abstract/10.1103/RevModPhys.74.47>.
- Asadi, P., Davison, A.C., Engelke, S., 2015. Extremes on river networks. *Annals of Applied Statistics* 9, 2023–2050. URL: <https://www.jstor.org/stable/43826454>.
- Asenova, S., Mazo, G., Segers, J., 2021. Inference on extremal dependence in the domain of attraction of a structured Hüsler–Reiss distribution motivated by a Markov tree with latent variables. *Extremes* 24, 461–500. URL: <https://link.springer.com/article/10.1007/s10687-021-00407-5>.
- Asenova, S., Segers, J., 2023. Extremes of Markov random fields on block graphs: max-stable limits and structured Hüsler–Reiss distributions. *Extremes* 26, 433–468. URL: <https://link.springer.com/article/10.1007/s10687-023-00467-9>.
- Boyd, S.P., Parikh, N., Chu, E., Peleato, B., Eckstein, J., 2011. Distributed optimization and statistical learning via the alternating direction method of multipliers. *Foundational Trends of Machine Learning* 3, 1–122. URL: <https://dl.acm.org/doi/10.1561/22000000016>.
- Candès, E., Li, X., Ma, Y., Wright, J., 2011. Robust principal component analysis? *Journal of the ACM* 58, 1–37. URL: <https://dl.acm.org/doi/10.1145/1970392.1970395>.
- Candès, E., Recht, B., 2012. Exact matrix completion via convex optimization. *Foundations of Computational Mathematics* 55, 111–119. URL: <https://link.springer.com/article/10.1007/s10208-009-9045-5>.
- Chandrasekaran, V., Parrilo, P., Willsky, A., 2012. Latent variable graphical model selection via convex optimization. *Annals of Statistics* 40, 1935–1967. URL: <https://www.jstor.org/stable/41806519>.
- Chandrasekaran, V., Sanghavi, V., Parrilo, P., Willsky, A., 2011. Rank-sparsity incoherence for matrix decomposition. *SIAM Journal of Optimization* 21, 572–596. URL: <https://epubs.siam.org/doi/10.1137/090761793>.
- Chang, A., Allen, G.I., 2023. Subbotin graphical models for extreme value dependencies with applications to functional neuronal connectivity. *Ann. Appl. Stat.* 17, 2364–2386. URL: <https://doi.org/10.1214/22-aos1723>.
- Dombry, C., Engelke, S., Oesting, M., 2016. Exact simulation of max-stable processes. *Biometrika* 103, 303–317. URL: <https://academic.oup.com/biomet/article/103/2/303/1744000>, arXiv:1506.04430.

- Engelke, S., Hentschel, M., Lalancette, M., Röttger, F., 2024. Graphical models for multivariate extremes [arXiv:2402.02187](https://arxiv.org/abs/2402.02187).
- Engelke, S., Hitz, A.S., 2020. Graphical models for extremes (with discussion). *J. R. Stat. Soc. Ser. B Stat. Methodol* 82, 871–932. URL: <https://rss.onlinelibrary.wiley.com/doi/abs/10.1111/rssb.12355>.
- Engelke, S., Hitz, A.S., Gnecco, N., Hentschel, M., 2022a. graphicalExtremes: Statistical Methodology for Graphical Extreme Value Models. URL: <https://github.com/sebastian-engelke/graphicalExtremes>.
- Engelke, S., Ivanovs, J., 2021. Sparse structures for multivariate extremes. *Annu. Rev. Stat. Appl.* 8, 241–270. URL: <https://www.annualreviews.org/doi/abs/10.1146/annurev-statistics-040620-041554>.
- Engelke, S., Ivanovs, J., Strokorb, K., 2022b. Graphical models for infinite measures with applications to extremes and Lévy processes. URL: <https://arxiv.org/abs/2211.15769>, doi:10.48550/ARXIV.2211.15769.
- Engelke, S., Lalancette, M., Volgushev, S., 2022c. Learning extremal graphical structures in high dimensions. URL: <https://arxiv.org/abs/2111.00840>.
- Engelke, S., Opitz, T., Wadsworth, J., 2019. Extremal dependence of random scale constructions. *Extremes* 22, 623–666. URL: <https://link.springer.com/article/10.1007/s10687-019-00353-3>.
- Engelke, S., Volgushev, S., 2022. Structure learning for extremal tree models. *Journal of the Royal Statistical Society Series B: Statistical Methodology* 84, 2055–2087. URL: <https://doi.org/10.1111/rssb.12556>, doi:10.1111/rssb.12556.
- Fazel, M., Hindi, H.A., Boyd, S.P., 2004. Rank minimization and applications in system theory. *Proceedings of the 2004 American Control Conference* 4, 3273–3278 vol.4. URL: <https://ieeexplore.ieee.org/document/1384521>.
- Friedman, J., Hastie, T., Tibshirani, R., 2007. Sparse inverse covariance estimation with the graphical lasso. *Biostatistics* 9, 432–441. URL: <https://doi.org/10.1093/biostatistics/kxm045>.
- de Haan, L., Resnick, S., 1977. Limit theory for multivariate sample extremes. *Z. Wahrscheinlichkeitstheorie Verw. Gebiete* 40, 317–337. URL: <https://link.springer.com/article/10.1007/BF00533086>.
- Hentschel, M., Engelke, S., Segers, J., 2022. Statistical inference for Hüsler–Reiss graphical models through matrix completions. URL: <https://arxiv.org/abs/2210.14292>.
- Hu, S., Peng, Z., Segers, J., 2022. Modelling multivariate extreme value distributions via markov trees. URL: <https://arxiv.org/abs/2208.02627>, arXiv:2208.02627.
- Hüsler, J., Reiss, R.D., 1989. Maxima of normal random vectors: Between independence and complete dependence. *Statist. Prob. Letters* 7, 283–286. URL: <https://ideas.repec.org/a/eee/stapro/v7y1989i4p283-286.html>.
- Lauritzen, S.L., 1996. Graphical models. volume 17 of *Oxford statistical science series*. Clarendon Press, Oxford. URL: <https://www.tib.eu/de/suchen/id/TIBKAT%3A197598226>.
- Lederer, J., Oesting, M., 2023. Extremes in high dimensions: Methods and scalable algorithms. [arXiv:2303.04258](https://arxiv.org/abs/2303.04258).
- Ma, S., Xue, L., Zou, H., 2012. Alternating direction methods for latent variable gaussian graphical model selection. *Neural Computation* 25, 2172–2198. URL: <https://direct.mit.edu/neco/article/25/8/2172/7900/Alternating-Direction-Methods-for-Latent-Variable>.
- Meinshausen, N., Bühlmann, P., 2006. High-dimensional graphs and variable selection with the lasso. *Annals of Statistics* 34, 1436–1462. URL: <https://projecteuclid.org/journals/annals-of-statistics/volume-34/issue-3/High-dimensional-graphs-and-variable-selection-with-the-Lasso/10.1214/>

- 009053606000000281.full.
- Papastathopoulos, I., Storkorb, K., 2016. Conditional independence among max-stable laws. *Statistics & Probability Letters* 108, 9–15. URL: <https://www.sciencedirect.com/science/article/pii/S0167715215002874>.
- Ravikumar, P., Wainwright, M.J., Raskutti, G., Yu, B., 2008. High-dimensional covariance estimation by minimizing ℓ_1 -penalized log-determinant divergence. *Electronic Journal of Statistics* 5, 935–980. URL: <https://projecteuclid.org/journals/electronic-journal-of-statistics/volume-5/issue-none/High-dimensional-covariance-estimation-by-minimizing-%E2%84%931-penalized-log-determinant/10.1214/11-EJS631.full>.
- Recht, B., Fazel, M., Parrilo, P., 2010. Guaranteed minimum-rank solutions of linear matrix equations via nuclear norm minimization. *SIAM Review* 52, 471–501. URL: <https://epubs.siam.org/doi/10.1137/070697835>.
- Resnick, S.I., 2008. *Extreme Values, Regular Variation and Point Processes*. Springer, New York.
- Rootzén, H., Segers, J., Wadsworth, J.L., 2018. Multivariate generalized Pareto distributions: Parametrizations, representations, and properties. *J. Multivariate Anal.* 165, 117–131. URL: <https://www.sciencedirect.com/science/article/pii/S0047259X17303147>.
- Rootzén, H., Tajvidi, N., 2006. Multivariate generalized Pareto distributions. *Bernoulli* 12, 917–930. URL: <https://projecteuclid.org/journals/bernoulli/volume-12/issue-5/Multivariate-generalized-Pareto-distributions/10.3150/bj/1161614952.full>.
- Röttger, F., Coons, J.I., Grosdos, A., 2023a. Parametric and nonparametric symmetries in graphical models for extremes. *arXiv:2306.00703*.
- Röttger, F., Engelke, S., Zwiernik, P., 2023b. Total positivity in multivariate extremes. *The Annals of Statistics* 51, 962 – 1004. URL: <https://doi.org/10.1214/23-AOS2272>.
- Segers, J., 2020. One- versus multi-component regular variation and extremes of Markov trees. *Adv. in Appl. Probab.* 52, 855–878.
- Taeb, A., Chandrasekaran, V., 2016. Interpreting latent variables in factor models via convex optimization. *Mathematical Programming* 167, 129–154. URL: <https://link.springer.com/article/10.1007/s10107-017-1187-7>.
- Taeb, A., Reager, J.T., Turmon, M.J., Chandrasekaran, V., 2017. A statistical graphical model of the California reservoir system. *Water Resources Research* 53, 9721 – 9739. URL: <https://agupubs.onlinelibrary.wiley.com/doi/10.1002/2017WR020412>.
- Wainwright, M.J., 2009. Sharp thresholds for high-dimensional and noisy sparsity recovery using ℓ_1 -constrained quadratic programming (lasso). *IEEE Transactions on Information Theory* 55, 2183–2202. URL: <https://ieeexplore.ieee.org/document/4839045>.
- Wan, P., Zhou, C., 2023. Graphical lasso for extremes. *arXiv:2307.15004*.
- Zhao, P., Yu, B., 2006. On model selection consistency of lasso. *Journal of Machine Learning Research* 7, 2541–2563. URL: <https://www.jmlr.org/papers/volume7/zhao06a/zhao06a.pdf>.
- Zhou, C., 2009. Dependence structure of risk factors and diversification effects. *Risk and Insurance / Measures and Control* 2 URL: <https://api.semanticscholar.org/CorpusID:15682170>.
- Zscheischler, J., Seneviratne, S.I., 2017. Dependence of drivers affects risks associated with compound events. *Science Advances* 3. URL: <https://www.science.org/doi/10.1126/sciadv.1700263>.

SUPPLEMENTARY MATERIAL

APPENDIX A. NOTATIONS AND DEFINITIONS

We let $\mathbb{H}^* = \Omega^* \times T^*$ and $\mathbb{H}' = \Omega^* \times T'$ where T' is close to T^* . We denote $\mathbb{Q}' = \Omega^* \times (T' \oplus \text{span}(\mathbf{1}_p \mathbf{1}_p^\top))$. For $\omega \in (0, 1)$, we define in the following set:

$$U(\omega) := \{\Omega(S^*) \times T' : \rho(T(L^*), T') \leq \omega\}.$$

We denote the dual norm of the regularizer $\|S\|_{\ell_1} + \gamma\|L\|_*$ (here, we have replaced $\text{tr}(L)$ with $\|L\|_*$ since L is a positive definite matrix) in (9) by:

$$\Phi_\gamma(S, L) := \max \left\{ \|S\|_\infty, \frac{\|L\|_2}{\gamma} \right\}.$$

Further, we define the linear operators $\mathcal{J} : \mathbb{S}^p \times \mathbb{S}^p \rightarrow \mathbb{S}^p$ and $\mathcal{J}^+ : \mathbb{S}^p \rightarrow \mathbb{S}^p \times \mathbb{S}^p$ as:

$$\mathcal{J}(C, D) = C - D ; \mathcal{J}^+(C) = (C, C).$$

Finally, for any subspace H , the projection onto the subspace is denoted by \mathcal{P}_H .

Our analysis will depend on the following quantities for any pair of subspaces $\Omega, T \subseteq \mathbb{R}^{p \times p}$:

$$\theta(\Omega) := \max_{N \in \Omega, \|N\|_\infty=1} \|N\|_2 ; \xi(T) := \max_{N \in T, \|N\|_2=1} \|N\|_\infty.$$

When $\Omega = \Omega^*$ and $T = T^*$, these quantities are closely connected to the maximal degree d^* and the incoherence parameter μ^* (defined in Section 4.2). In particular, Chandrasekaran et al. (2012) showed that $\mu(\Omega^*) \in [0, d^*]$ and $\xi(T^*) \in [\mu^*, 2\mu^*]$.

APPENDIX B. FINITE SAMPLE CONVERGENCE GUARANTEES OF THE EMPIRICAL VARIOGRAM MATRIX

In addition to assumptions for identifiability, following Engelke et al. (2022c), we impose conditions to characterize the convergence rate of the empirical variogram matrix to the population variogram matrix. Throughout, we suppose that the random vector $X = (X_O, X_H)$ is in the domain of attraction of the multivariate Pareto distribution Y following a latent Hüsler–Reiss distribution with parameter matrix Γ ; for details see Section 2.1 and 3.1.

Assumption 2. *The marginal distribution functions F_i of X_i , $i \in O$, are continuous and there exists constants $\xi > 0$, $K < \infty$ such that for all triples of distinct indices $J = (i, j, m) \subset O$ and $q \in (0, 1]$,*

$$\sup_{x \in [0, q^{-1}]^2 \times [0, 1]} \left| q^{-1} \mathbb{P}(F_J(X_J) > 1 - qx) - \frac{\mathbb{P}(Y_J > 1/x)}{\mathbb{P}(Y_1 > 1)} \right| \leq Kq^\xi,$$

where $F_J(x) = (F_i(x_i), F_j(x_j), F_m(x_m))$.

Assumption 2 is a second-order condition that essentially controls the speed of convergence of the sample variogram matrix to the population variogram matrix.

Corollary 4. (Engelke et al., 2022c, Theorem 3) *Let Assumption 2 hold. Let $\ell \in (0, 1]$ be arbitrary. Suppose that $n^\ell \leq k \leq n/2$ where k is the effective sample size in computing the sample variogram matrix (see Section 3.3.1). Let $\vartheta \geq 0$ be any scalar satisfying $\vartheta \leq \sqrt{k}/(\log n)^4$. Then, there exists positive constants c_5, C_5, \tilde{C}_5 only depending on K, ξ, ℓ, ϵ , and $G(z)$ such that:*

$$\mathbb{P} \left(\|\hat{\Gamma}_O - \Gamma_O^*\|_\infty > C_5 \left\{ \left(\frac{k}{n} \right)^\xi (\log(n/k))^2 + \frac{1 + \vartheta}{\sqrt{k}} \right\} \right) \leq \tilde{C}_5 p^3 e^{-c_5 \vartheta^2}.$$

APPENDIX C. USEFUL LEMMAS

Our theoretical analysis relies on some lemmas.

Lemma 5. *Let $A \in \mathbb{S}^d$ and $B \in \mathbb{S}^d$ be two symmetric matrices with $A + B$ being nonsingular and row/column spaces of A and B being orthogonal to one another. Then, $(A + B)^{-1} = A^+ + B^+$.*

Proof of Lemma 5. Let $U_A D_A U_A^T$ and $U_B D_B U_B^T$ be the reduced SVD of A and B . Then, since $A + B$ is non-singular, and the subspaces spanned by the columns of U_A and U_B are orthogonal, we have that (U_A, U_B) forms an orthogonal matrix. Therefore,

$$(A + B) = (U_A \ U_B) \begin{pmatrix} D_A & 0 \\ 0 & D_B \end{pmatrix} (U_A \ U_B)^T,$$

and thus:

$$(A + B)^{-1} = U_A D_A^{-1} U_A^T + U_B D_B^{-1} U_B^T = A^+ + B^+.$$

□

Lemma 6. *Suppose that $U U^T M U U^T = M$. Then, $U(U^T M U)^{-1} U^T = M^+$.*

Proof of Lemma 6. Let $U D U^T$ be the reduced-SVD of M . Then, $U(U^T M U)^{-1} U^T = U D^{-1} U^T$, which is equivalent to M^+ . □

Lemma 7. *Let $\tilde{\Pi} = (I_p - \mathbf{1}_p \mathbf{1}_p^T / p)$. Let $\Theta = \begin{pmatrix} \Theta_O & \Theta_{OH} \\ \Theta_{HO} & \Theta_H \end{pmatrix} \in \mathbb{R}^{d \times d}$ with $\Theta_O \in \mathbb{R}^{p \times p}$, $\Theta_H \in \mathbb{R}^{h \times h}$ and $d = h + p$. Suppose Θ is a positive semi-definite matrix with its null-space being the span of the all-ones vector. Then:*

$$\tilde{\Pi}(\Theta_O - \Theta_{OH} \Theta_H^{-1} \Theta_{HO}) \tilde{\Pi} = \Theta_O - \Theta_{OH} \Theta_H^{-1} \Theta_{HO}.$$

Proof. Since $\Theta \mathbf{1}_d = 0$, we have

$$(11) \quad \Theta_O \mathbf{1}_p + \Theta_{OH} \mathbf{1}_h = 0$$

$$(12) \quad \Theta_{HO} \mathbf{1}_p + \Theta_H \mathbf{1}_h = 0$$

Consider $\Theta_O - \Theta_{OH} \Theta_H^{-1} \Theta_{HO}$, we have

$$\begin{aligned} (\Theta_O - \Theta_{OH} \Theta_H^{-1} \Theta_{HO}) \mathbf{1}_p &= \Theta_O \mathbf{1}_p - \Theta_{OH} \Theta_H^{-1} \Theta_{HO} \mathbf{1}_p \\ &\stackrel{\text{by (12)}}{=} \Theta_O \mathbf{1}_p + \Theta_{OH} \Theta_H^{-1} (\Theta_H \mathbf{1}_h) \\ &= \Theta_O \mathbf{1}_p + \Theta_{OH} \mathbf{1}_h \\ &\stackrel{\text{by (11)}}{=} 0 \end{aligned}$$

Thus, $\mathbf{1}_p \in \ker(\Theta_O - \Theta_{OH} \Theta_H^{-1} \Theta_{HO})$.

To complete the proof, we will show that $\dim(\ker(\Theta_O - \Theta_{OH} \Theta_H^{-1} \Theta_{HO})) = 1$. Suppose there exist non-zero vector $v \in \ker(\Theta_O - \Theta_{OH} \Theta_H^{-1} \Theta_{HO})$, and let $u = \Theta_H^{-1} \Theta_{HO} v$. Since $v \neq 0$, $u \neq 0$, and then it follows that

$$\Theta_O v - \Theta_{OH} u = 0$$

$$\Theta_{HO} v - \Theta_H u = 0$$

yielding

$$\Theta^* \begin{pmatrix} v \\ -u \end{pmatrix} = 0.$$

Since $\begin{pmatrix} v \\ -u \end{pmatrix} \in \ker(\Theta)$, $v = \alpha \mathbf{1}_p$ for some $\alpha \in R$, which implies that $\dim(\ker(\Theta_O - \Theta_{OH} \Theta_H^{-1} \Theta_{HO})) = 1$. \square

Lemma 8. *Let $\tilde{\Pi} = I_p - \mathbf{1}_p \mathbf{1}_p^\top / p$ and $\Pi = I_d - \mathbf{1}_d \mathbf{1}_d^\top / d$ with $d = p + h$. For any matrix $M \in \mathbb{R}^{d \times d}$, $\tilde{\Pi}(\Pi M \Pi)_{1:p, 1:p} \tilde{\Pi} = \tilde{\Pi} M_{1:p, 1:p} \tilde{\Pi}$*

Proof. Note that

$$(\Pi M \Pi)_{1:p, 1:p} = \begin{pmatrix} I_p & \mathbf{0} \end{pmatrix} \Pi M \Pi \begin{pmatrix} I_p \\ \mathbf{0} \end{pmatrix}$$

Then it follows that

$$\begin{aligned} \tilde{\Pi}(\Pi M \Pi)_{1:p, 1:p} \tilde{\Pi} &= \tilde{\Pi} \begin{pmatrix} I_p & \mathbf{0} \end{pmatrix} \Pi M \Pi \begin{pmatrix} I_p \\ \mathbf{0} \end{pmatrix} \tilde{\Pi} \\ (13) \quad &= \begin{pmatrix} \tilde{\Pi} & \mathbf{0} \end{pmatrix} \Pi M \Pi \begin{pmatrix} \tilde{\Pi} \\ \mathbf{0} \end{pmatrix}. \end{aligned}$$

Notice that:

$$\begin{aligned} (\tilde{\Pi} \ \mathbf{0}) \Pi &= ((I_p - \mathbf{1}_p \mathbf{1}_p^\top / p)(I_p - \mathbf{1}_p \mathbf{1}_p^\top / d) \ (I_p - \mathbf{1}_p \mathbf{1}_p^\top / p) \mathbf{1}_p / d) \\ (14) \quad &= ((I_p - \mathbf{1}_p \mathbf{1}_p^\top / p)(I_p - \mathbf{1}_p \mathbf{1}_p^\top / p + \mathbf{1}_p \mathbf{1}_p^\top / (p) - \mathbf{1}_p \mathbf{1}_p^\top / d) \ \mathbf{0}) \\ &= (\tilde{\Pi}(\tilde{\Pi} + \mathbf{1}_p \mathbf{1}_p^\top / (p) - \mathbf{1}_p \mathbf{1}_p^\top / d) \ \mathbf{0}) \\ &= (\tilde{\Pi} \ \mathbf{0}). \end{aligned}$$

Putting (13) and (14) together, we have the desired result. \square

Lemma 9 (Lemma 3.1 of Chandrasekaran et al. (2012)). *For any tangent spaces T_1, T_2 of same dimension with $\rho(T_1, T_2) < 1$, we have that: $\xi(T_2) \leq \frac{\xi(T_1) + \rho(T_1, T_2)}{1 - \rho(T_1, T_2)}$.*

Lemma 10. *Consider a tangent space T' of a symmetric matrix with $\rho(T^*, T') \leq \omega$ with $\omega < 1$. Let C' and C^* be the column spaces that form the tangent spaces T' and T^* respectively. Then, we have that: $\|\mathcal{P}_{C'} - \mathcal{P}_{C^*}\|_2 \leq \omega$.*

Proof of Lemma 10. Since $\omega < 1$, T^* and T' are of the same dimension. Let $\sigma_s(\cdot)$ be the s -th largest singular value of the input matrix. Notice that

$$\begin{aligned} \|\mathcal{P}_{C'} - \mathcal{P}_{C^*}\|_2 &= \|\mathcal{P}_{C'^\perp} - \mathcal{P}_{C^{*\perp}}\|_2 \\ &= \sqrt{1 - \sigma_{p-k}(\mathcal{P}_{C'^\perp} \mathcal{P}_{C^{*\perp}})^2} \\ &= \sqrt{1 - \sigma_{(p-k)^2}(\mathcal{P}_{T'^\perp} \mathcal{P}_{T^{*\perp}})} \\ &\leq \sqrt{1 - \sigma_{(p-k)^2}(\mathcal{P}_{T'^\perp} \mathcal{P}_{T^{*\perp}})^2} \\ &= \|\mathcal{P}_{T'^\perp} - \mathcal{P}_{T^{*\perp}}\|_2 \\ &= \|\mathcal{P}_{T'} - \mathcal{P}_{T^*}\|_2. \end{aligned}$$

\square

Lemma 11. *Let $\mathcal{C}_1, \mathcal{C}_2 \subseteq \mathbb{R}^p$ be a pair of subspaces. Then, for any $z \in \mathbb{R}^p$:*

$$\begin{aligned} \max_{v \in \mathcal{C}_1 \oplus \mathcal{C}_2, \|v\|_2=1} \langle z, v \rangle &\leq 2 \min \left\{ \max_{v \in \mathcal{C}_1, \|v\|_2=1} \langle z, v \rangle, \max_{v \in \mathcal{C}_2, \|v\|_2=1} \langle z, v \rangle \right\} \\ &\quad + \max \left\{ \max_{v \in \mathcal{C}_1, \|v\|_2=1} \langle z, v \rangle, \max_{v \in \mathcal{C}_2, \|v\|_2=1} \langle z, v \rangle \right\}. \end{aligned}$$

Proof of Lemma 11. Suppose without loss of generality that $\max_{u_1 \in \mathcal{C}_1, \|u_1\|_2=1} u_1^T z \leq \max_{u_2 \in \mathcal{C}_2, \|u_2\|_2=1} u_2^T z$.

$$\begin{aligned} \max_{v \in \mathcal{C}_1 \oplus \mathcal{C}_2, \|v\|_2=1} \langle z, v \rangle &= \max_{\substack{u_1 \in \mathcal{C}_1, u_2 \in \mathcal{C}_2, \|u_1\|_2=\|u_2\|_2=1 \\ v=c_1 u_1 + c_2 u_2}} |v^T z| / \|v\|_2 \\ &= \max_{\substack{u_1 \in \mathcal{C}_1, u_2 \in \mathcal{C}_2, \|u_1\|_2=\|u_2\|_2=1 \\ u_3=u_2 - (u_2^T u_1) u_1 \\ v=c_1 u_1 + c_2 u_3}} |v^T z| / \|v\|_2 \\ &\leq \max_{\substack{u_1 \in \mathcal{C}_1, u_2 \in \mathcal{C}_2, \|u_1\|_2=\|u_2\|_2=1 \\ u_3=u_2 - (u_2^T u_1) u_1 \\ v=c_1 u_1 + c_2 u_3}} \frac{|c_1|}{\sqrt{c_1^2 + c_2^2}} |u_1^T z| + \frac{|c_2|}{\sqrt{c_1^2 + c_2^2}} |u_3^T z| \\ &\leq \max_{u_1 \in \mathcal{C}_1, \|u_1\|_2=1} 2|u_1^T z| + \max_{u_2 \in \mathcal{C}_2, \|u_2\|_2=1} |u_2^T z| \end{aligned}$$

□

Lemma 12. *Let $Z \in T' \oplus \text{span}(\mathbf{1}_p \mathbf{1}_p^T)$ with $\rho(T', T^*) \leq \omega$ and $\|Z\|_2 = 1$. Then, $1 + 2(\kappa^* + \omega) \geq \|\mathcal{P}_{T'}(Z)\|_2 \geq 1 - 2(\kappa^* + \omega)$ and thus $\|\mathcal{P}_{T'^\perp}(Z)\|_2 \leq 2(\kappa^* + \omega)$.*

Proof of Lemma 10. Note that $\|Z\|_2 + \|\mathcal{P}_{T'^\perp}(Z)\|_2 \geq \|\mathcal{P}_{T'}(Z)\|_2 \geq \|Z\|_2 - \|\mathcal{P}_{T'^\perp}(Z)\|_2$. Let T' be a tangent space with associated row and column spaces \mathcal{C}' and \mathcal{R}' . Let $\tilde{\mathcal{C}} = \mathcal{C}' \oplus \text{span}(\mathbf{1}_p)$ and $\tilde{\mathcal{R}} = \mathcal{R}' \oplus \text{span}(\mathbf{1}_p)$. Since $Z \in T' \oplus \text{span}(\mathbf{1}_p)$, it is straightforward to show that $Z = \mathcal{P}_{\tilde{\mathcal{C}}} Z \mathcal{P}_{\tilde{\mathcal{R}}^\perp} + Z \mathcal{P}_{\tilde{\mathcal{R}}}$. Therefore, we have that $\mathcal{P}_{T'^\perp}(Z) = \mathcal{P}_{\mathcal{C}'^\perp} [\mathcal{P}_{\tilde{\mathcal{C}}} Z \mathcal{P}_{\tilde{\mathcal{R}}^\perp} + Z \mathcal{P}_{\tilde{\mathcal{R}}}] \mathcal{P}_{\mathcal{R}'^\perp}$. Thus, $\|\mathcal{P}_{T'^\perp}(Z)\|_2 \leq \|\mathcal{P}_{\mathcal{C}'^\perp} \mathcal{P}_{\tilde{\mathcal{C}}}\|_2 + \|\mathcal{P}_{\tilde{\mathcal{R}}} \mathcal{P}_{\mathcal{R}'^\perp}\|_2$. Letting $\mathcal{C}_1 = \mathcal{C}'$ and $\mathcal{C}_2 = \text{span}(\mathbf{1}_p)$, we appeal to Lemma 11 to conclude that:

$$\begin{aligned} \max_{v \in \tilde{\mathcal{C}}, \|v\|_2=1} \|\mathcal{P}_{\mathcal{C}'^\perp}(v)\|_2 &\leq \max_{\substack{z \in \mathcal{C}'^\perp \\ \|z\|_2=1}} \max_{u_1 \in \mathcal{C}', \|u_1\|_2=1} 2|\langle z, u_1 \rangle| + \max_{\substack{z \in \mathcal{C}'^\perp \\ \|z\|_2=1}} \max_{u_2 \in \text{span}(\mathbf{1}), \|u_2\|_2=1} |\langle z, u_2 \rangle| \\ &= \|\mathcal{P}_{\mathcal{C}'^\perp}(\mathbf{1}_p / \sqrt{p})\|_2. \end{aligned}$$

Again, appealing to Lemma 11,

$$\begin{aligned} \max_{v \in \mathcal{C}'^\perp, \|v\|_2=1} \|\mathcal{P}_{\tilde{\mathcal{C}}}(z)\|_2 &\leq \max_{\substack{z \in \mathcal{C}'^\perp \\ \|z\|_2=1}} \max_{u_1 \in \mathcal{C}', \|u_1\|_2=1} 2|\langle z, u_1 \rangle| + \max_{\substack{z \in \mathcal{C}'^\perp \\ \|z\|_2=1}} \max_{u_2 \in \text{span}(\mathbf{1}), \|u_2\|_2=1} |\langle z, u_2 \rangle| \\ &= \|\mathcal{P}_{\mathcal{C}'^\perp}(\mathbf{1}_p / \sqrt{p})\|_2. \end{aligned}$$

So we have concluded that $\|\mathcal{P}_{\mathcal{C}'^\perp} \mathcal{P}_{\tilde{\mathcal{C}}}\|_2 \leq \|\mathcal{P}_{\mathcal{C}'^\perp}(\mathbf{1}_p / \sqrt{p})\|_2$. Thus, appealing to Lemma 10, we conclude that: $\|\mathcal{P}_{\mathcal{C}'^\perp} \mathcal{P}_{\tilde{\mathcal{C}}}\|_2 \leq \kappa^* + \omega$. Similarly, we can conclude that: $\|\mathcal{P}_{\mathcal{R}'^\perp} \mathcal{P}_{\tilde{\mathcal{R}}}\|_2 \leq \|\mathcal{P}_{\mathcal{R}'^\perp}(\mathbf{1}_p / \sqrt{p})\|_2$ and thus $\|\mathcal{P}_{\mathcal{R}'^\perp} \mathcal{P}_{\tilde{\mathcal{R}}}\|_2 \leq \kappa^* + \omega$. Putting things together, we have the desired bound.

□

Lemma 13. *Let $T' \subseteq \mathbb{R}^{p \times p}$ be a tangent space to a low-rank variety. Then, $\|\mathcal{P}_{(T' \oplus \text{span}(\mathbf{1}_p \mathbf{1}_p^T))^\perp}(L)\|_2 \leq \|\mathcal{P}_{T'^\perp}(L)\|_2$ for any matrix $L \in \mathbb{R}^{p \times p}$*

Proof of Lemma 13. Let $\mathcal{R}', \mathcal{C}'$ be row/column space pair that form the tangent space T' . Let $\tilde{\mathcal{C}} = \text{span}(\mathcal{C}', \mathbf{1})$ and $\tilde{\mathcal{R}} = \text{span}(\mathcal{R}', \mathbf{1})$. Then, it is straightforward to see that $T' \oplus \text{span}(\mathbf{1}_p \mathbf{1}_p^\top)$ is itself a tangent space formed by column space $\tilde{\mathcal{C}}$ and row space $\tilde{\mathcal{R}}$. Thus, $\|\mathcal{P}_{(T' \oplus \text{span}(\mathbf{1}_p \mathbf{1}_p^\top))^\perp}(L^*)\|_2 = \|\mathcal{P}_{\tilde{\mathcal{C}}^\perp} L^* \mathcal{P}_{\tilde{\mathcal{R}}^\perp}\|_2$. Since $\mathcal{C}' \subseteq \tilde{\mathcal{C}}$, we have that: $\|\mathcal{P}_{\tilde{\mathcal{C}}^\perp} L \mathcal{P}_{\tilde{\mathcal{R}}^\perp}\|_2 \leq \|\mathcal{P}_{\mathcal{C}'^\perp} L \mathcal{P}_{\mathcal{R}'^\perp}\|_2 = \|\mathcal{P}_{T'^\perp}(L)\|_2$. \square

Lemma 14. *Suppose that $\kappa^* > \omega$. Then, $\text{span}(\mathbf{1}_p \mathbf{1}_p^\top) \cap (T' \oplus T^*) = \{0\}$ for every tangent space T' with $\rho(T', T^*) \leq \omega$.*

Proof of Lemma 14. It suffices to show that $\|\mathcal{P}_{(T' \oplus T^*)^\perp}(\mathbf{1}_p \mathbf{1}_p^\top / p)\|_2 > 0$. Let \mathcal{C}' be the column space associated with the tangent space T' at a symmetric matrix. Note that $T' \oplus T^*$ is another tangent space with column space $\mathcal{C}' \oplus \mathcal{C}^*$. Then, $\|\mathcal{P}_{(T' \oplus T^*)^\perp}(\mathbf{1}_p \mathbf{1}_p^\top / p)\|_2 = \|\mathcal{P}_{(\mathcal{C}' \oplus \mathcal{C}^*)^\perp}(\mathbf{1}/\sqrt{p})\|_2^2$. So it suffices to show that $\|\mathcal{P}_{\mathcal{C}' \oplus \mathcal{C}^*}(\mathbf{1}/\sqrt{p})\|_2 < 1$. Note that: $\|\mathcal{P}_{\mathcal{C}' \oplus \mathcal{C}^*}(\mathbf{1}/\sqrt{p})\|_2 \leq \|\mathcal{P}_{\mathcal{C}' \oplus \mathcal{C}^*} \mathcal{P}_{\mathcal{C}^*}(\mathbf{1}/\sqrt{p})\|_2 + \|\mathcal{P}_{\mathcal{C}' \oplus \mathcal{C}^*} \mathcal{P}_{\mathcal{C}^{\perp*}}(\mathbf{1}/\sqrt{p})\|_2 \leq \|\mathcal{P}_{\mathcal{C}^*}(\mathbf{1}/\sqrt{p})\|_2 + \|\mathcal{P}_{\mathcal{C}' \oplus \mathcal{C}^*} \mathcal{P}_{\mathcal{C}^{\perp*}}\|_2$. We have that: $\|\mathcal{P}_{\mathcal{C}^*}(\mathbf{1}/\sqrt{p})\|_2 = 1 - \kappa^*$. Using Lemma 11, it is straightforward to conclude that $\|\mathcal{P}_{\mathcal{C}' \oplus \mathcal{C}^*} \mathcal{P}_{\mathcal{C}^{\perp*}}\|_2 \leq \|\mathcal{P}_{\mathcal{C}'} \mathcal{P}_{\mathcal{C}^{\perp*}}\|_2 \leq \|\mathcal{P}_{\mathcal{C}'} - \mathcal{P}_{\mathcal{C}^*}\|_2$. Appealing to Lemma 10, and putting everything together, we conclude that: $\|\mathcal{P}_{\mathcal{C}' \oplus \mathcal{C}^*}(\mathbf{1}/\sqrt{p})\|_2 \leq (1 - \kappa^*) + \omega$. As $\kappa^* > \omega$, we have the desired result. \square

Lemma 15. *Let $Z = T' \oplus \text{span}(\mathbf{1}_p \mathbf{1}_p^\top)$ with $\|Z\|_2 = 1$ and $\rho(T', T^*) \leq \omega$. Then, assuming $\kappa^* > \sqrt{\omega}$, Z can be decomposed uniquely as follows $Z = Z_1 + Z_2$ where $Z_1 \in T'$, $Z_2 \in \text{span}(\mathbf{1}_p \mathbf{1}_p^\top)$ with $\max\{\|Z_1\|_2, \|Z_2\|_2\} \leq \frac{2\sqrt{5h}}{1 - \sqrt{1 - (\kappa^{*2} - \omega)^2}}$.*

Proof of Lemma 15. The unique decomposition follows from Lemma 14. Since $\omega < 1$, we have that T' and T^* have the same dimension. Since $Z_1 \in T' \oplus T^*$, then $\text{rank}(Z_1) \leq 4h$ (this follows from noting that every matrix inside T' or T^* has rank at most $2h$ and rank of a sum of matrices is less than the sum of the ranks). Further, $\text{rank}(Z_2) \leq 1$, so that $\text{rank}(Z) \leq 5h$. Therefore, $\|Z\|_F \leq \sqrt{5h}$. Notice that: $\|Z\|_F^2 = \|Z_1 + \mathcal{P}_{T'}(Z_2) + \mathcal{P}_{T'^\perp}(Z_2)\|_F^2 = \|Z_1 + \mathcal{P}_{T'}(Z_2)\|_F^2 + \|\mathcal{P}_{T'^\perp}(Z_2)\|_F^2$. Thus, $\|Z_1 + \mathcal{P}_{T'}(Z_2)\|_F \leq \sqrt{5h}$. Using reverse triangle inequality, we conclude that $\|Z_1\|_F \leq \sqrt{5h} + \|\mathcal{P}_{T'}(Z_2)\|_F$. Now notice that: $\|Z_2\|_F^2 = \|\mathcal{P}_{T'^\perp}(Z_2)\|_F^2 + \|\mathcal{P}_{T'}(Z_2)\|_F^2$, so that: $\sqrt{\|Z_2\|_F^2 - \|\mathcal{P}_{T'^\perp}(Z_2)\|_F^2} = \|\mathcal{P}_{T'}(Z_2)\|_F$. Since Z_2 is rank-1, we have then that: $\|\mathcal{P}_{T'}(Z_2)\|_F = \|Z_2\|_2 \sqrt{1 - \|\mathcal{P}_{T'^\perp}(\mathbf{1}_p \mathbf{1}_p^\top / p)\|_2^2}$. Combining things, we conclude that $\|Z_1\|_F \leq \sqrt{5h} + \|Z_2\|_2 \sqrt{1 - \|\mathcal{P}_{T'^\perp}(\mathbf{1}_p \mathbf{1}_p^\top / p)\|_2^2}$. Notice that $\|\mathcal{P}_{T'^\perp}(\mathbf{1}_p \mathbf{1}_p^\top / p)\|_2 \geq \|\mathcal{P}_{T^*\perp}(\mathbf{1}_p \mathbf{1}_p^\top / p)\|_2 - \omega = \kappa^{*2} - \omega$. Reverse triangle inequality also gives $\|Z_2\|_F \leq \|Z_1\|_F + \sqrt{5h}$. Putting the last bounds together, we have that: $\|Z_2\|_F \leq \frac{2\sqrt{5h}}{1 - \sqrt{1 - (\kappa^{*2} - \omega)^2}}$. Plugging this into a previous bound, we also find that $\|Z_1\|_F \leq \frac{2\sqrt{5h}}{1 - \sqrt{1 - (\kappa^{*2} - \omega)^2}}$. \square

Lemma 16. *Let $T' \subseteq \mathbb{R}^{p \times p}$ be a tangent space. We have that: $\max_{N \in T' \oplus \text{span}(\mathbf{1}_p \mathbf{1}_p^\top), \|N\|_2=1} \|N\|_\infty \leq 3\xi(T')$.*

Proof of Lemma 16. Let $(\mathcal{R}', \mathcal{C}')$ be the row/column space pair associated with T' . Let $\tilde{\mathcal{C}} = \mathcal{C}' \oplus \text{span}(\mathbf{1}_p)$ and $\tilde{\mathcal{R}} = \mathcal{R}' \oplus \text{span}(\mathbf{1}_p)$. Since $Z \in T' \oplus \text{span}(\mathbf{1})$, it is straightforward to show that $Z = \mathcal{P}_{\tilde{\mathcal{C}}} Z \mathcal{P}_{\tilde{\mathcal{R}}^\perp} + Z \mathcal{P}_{\tilde{\mathcal{R}}}$. Therefore, $\|Z\|_\infty \leq \max_i \|\mathcal{P}_{\tilde{\mathcal{C}}}(e_i)\|_2 + \max_i \|\mathcal{P}_{\tilde{\mathcal{R}}}(e_i)\|_2$. Letting $\mathcal{C}_1 = \mathcal{C}'$ and $\mathcal{C}_2 = \text{span}(\mathbf{1}_p)$, and appealing to Lemma 11, we have that:

$$\max_i \|\mathcal{P}_{\tilde{\mathcal{C}}}(e_i)\|_2 \leq 2 \max_i \max_{u_1 \in \text{span}(\mathbf{1}), \|u_1\|_2=1} |2u_1^T e_i| + \max_i \max_{u_2 \in \mathcal{C}', \|u_2\|_2=1} |u_2^T e_i| \leq 2/\sqrt{p} + \mu[\mathcal{C}'].$$

Analogously, letting $\mathcal{C}_1 = \mathcal{R}'$ and $\mathcal{C}_2 = \text{span}(\mathbf{1})$, and appealing to Lemma 11, we have that:

$$\max_i \|\mathcal{P}_{\tilde{\mathcal{R}}}(e_i)\|_2 \leq 2/\sqrt{p} + \mu[\mathcal{R}'].$$

Since $\xi(T') \geq \max\{\mu[C'], \mu[\mathcal{R}']\}$ and $2\xi(T') \geq \frac{2}{\sqrt{p}}$, we conclude the desired result. \square

APPENDIX D. ARRIVING AT ESTIMATOR (9)

Recall that $\tilde{\Theta}^* = (\tilde{\Pi}(-\Gamma_{\mathcal{O}}^*/2)\tilde{\Pi})^+$, where $\tilde{\Pi} = UU^T$. Furthermore, the null-space of $\tilde{\Theta}^*$ is the subspace $\text{span}(\mathbf{1}_p \mathbf{1}_p^T)$. In other words, $UU^T \tilde{\Theta}^* UU^T = \tilde{\Theta}^*$. We arrive at our estimator by noting that $\hat{\Theta}^*$ is the unique minimizer of the convex program:

$$(15) \quad \begin{aligned} \hat{\Theta} = \operatorname{argmin}_{\Theta \in \mathbb{S}^p} & -\log \det(U^T \Theta U) - \frac{1}{2} \operatorname{tr}(\Theta \Gamma_{\mathcal{O}}^*), \\ \text{s.t } & \Theta \succeq 0, \Theta \mathbf{1}_p = 0. \end{aligned}$$

To see why that is, first note that the constraint $\Theta \succeq 0$ can be removed since the log-det function forces $U^T \Theta U$ to be positive definite and together with the constraint $\Theta \mathbf{1}_p$ forces $\Theta \succeq 0$ and additionally $UU^T \Theta UU^T = \Theta$. Note that $\operatorname{tr}(\Theta \Gamma_{\mathcal{O}}^*) = \operatorname{tr}(UU^T \Theta UU^T \Gamma_{\mathcal{O}}^*) = \operatorname{tr}(\Theta UU^T \Gamma_{\mathcal{O}}^* UU^T)$. Thus, an equivalent optimization to (15) is

$$(16) \quad \begin{aligned} \hat{\Theta} = \operatorname{argmin}_{\Theta \in \mathbb{S}^p} & -\log \det(U^T \Theta U) - \frac{1}{2} \operatorname{tr}(\Theta UU^T \Gamma_{\mathcal{O}}^* UU^T), \\ \text{s.t } & \Theta \in \text{span}(\mathbf{1}_p \mathbf{1}_p^T)^\perp. \end{aligned}$$

Using Lagrangian duality theory, we have that $\hat{\Theta}$ must satisfy for some $t \in \mathbb{R}$

$$-U(U^T \hat{\Theta} U^{-1})U^T - \frac{1}{2} UU^T \Gamma_{\mathcal{O}}^* UU^T + t \mathbf{1}_p \mathbf{1}_p^T = 0.$$

Note that $t = 0$ since the first two terms live in the space spanned by the columns of U and the last term lies in the orthogonal subspace. Similarly, $-U(U^T \hat{\Theta} U^{-1})U^T - \frac{1}{2} UU^T \Gamma_{\mathcal{O}}^* UU^T = 0$. Since $UU^T \hat{\Theta} UU^T = \hat{\Theta}$, we appeal to Lemma 6 to conclude that $\hat{\Theta}^+ = -\frac{1}{2} \frac{1}{2} UU^T \Gamma_{\mathcal{O}}^* UU^T$. Some simple manipulations allow us to conclude that $\hat{\Theta} = \tilde{\Theta}^*$.

APPENDIX E. PROOF OF THEOREM 2

Proof of Theorem 2. For notational simplicity, we let $M = -\Gamma^*/2$. Let $\Pi = I_d - \mathbf{1}_d \mathbf{1}_d^T/d$. We have from Hentschel et al. (2022) that $(\Pi M \Pi)^+ = \Theta^*$ or equivalently $\Pi M \Pi = (\Theta^*)^+$. Since Θ^* has zero row/column sums and thus its row/column spaces are orthogonal to the all-ones vector, we have by Lemma 5 that for any $t > 0$, $(\Theta^* + t \mathbf{1}_d \mathbf{1}_d^T)^{-1} = \Theta^{*+} + (t \mathbf{1}_d \mathbf{1}_d^T)^+ = \Theta^{*+} + \frac{1}{td^2} (\mathbf{1}_d \mathbf{1}_d^T)$. As $\Pi \mathbf{1}_d \mathbf{1}_d^T \Pi = 0$, we have that:

$$\Pi M \Pi = \Pi (\Theta^* + t \mathbf{1}_d \mathbf{1}_d^T)^{-1} \Pi.$$

The equation above implies

$$\tilde{\Pi} [\Pi M \Pi]_{1:p, 1:p} \tilde{\Pi} = \tilde{\Pi} [\Pi (\Theta^* + t \mathbf{1}_d \mathbf{1}_d^T)^{-1} \Pi]_{1:p, 1:p} \tilde{\Pi}.$$

Using Lemma 8, we have that:

$$(17) \quad \tilde{\Pi} M_{1:p, 1:p} \tilde{\Pi} = \tilde{\Pi} [(\Theta^* + t \mathbf{1}_d \mathbf{1}_d^T)^{-1}]_{1:p, 1:p} \tilde{\Pi}.$$

We will now analyze the term $[(\Theta^* + t \mathbf{1}_d \mathbf{1}_d^T)^{-1}]_{1:p, 1:p}$ inside (17). From Schur's complement, we have that:

$$(18) \quad \begin{aligned} & [(\Theta^* + t \mathbf{1}_d \mathbf{1}_d^T)^{-1}]_{1:p, 1:p} = \\ & [\Theta_{\mathcal{O}}^* + t \mathbf{1}_p \mathbf{1}_p^T - (\Theta_{\mathcal{O}H}^* + t \mathbf{1}_p \mathbf{1}_h^T) (\Theta_H^* + t \mathbf{1}_h \mathbf{1}_h^T)^{-1} (\Theta_{HO}^* + t \mathbf{1}_h \mathbf{1}_p^T)]^{-1}. \end{aligned}$$

By the Woodbury inversion lemma, we have that:

$$(19) \quad (\Theta_H^* + t\mathbf{1}_h\mathbf{1}_h^T)^{-1} = (\Theta_H^*)^{-1} - (\Theta_H^*)^{-1}\mathbf{1}_h \left(\frac{1}{t} + \mathbf{1}_h^T(\Theta_H^*)^{-1}\mathbf{1}_h \right)^{-1} \mathbf{1}_h^T(\Theta_H^*)^{-1}.$$

Plugging the result of (19) into (18), we have that:

$$\begin{aligned} & [(\Theta^* + t\mathbf{1}_d\mathbf{1}_d^T)^{-1}]_{1:p,1:p} \\ &= \Theta_O^* + t\mathbf{1}_p\mathbf{1}_p^T - (\Theta_{OH}^* + t\mathbf{1}_p\mathbf{1}_h^T)(\Theta_H^* + t\mathbf{1}_h\mathbf{1}_h^T)^{-1}(\Theta_{HO}^* + t\mathbf{1}_h\mathbf{1}_p^T) \\ &= A + B + C \end{aligned}$$

where

$$\begin{aligned} A &= \Theta_O^* - \Theta_{OH}^*(\Theta_H^*)^{-1}\Theta_{HO}^*, \\ B &= t\mathbf{1}_p\mathbf{1}_p^T + t^2\mathbf{1}_p\mathbf{1}_p^T(\Theta_H^* + t\mathbf{1}_h\mathbf{1}_h^T)^{-1}\mathbf{1}_h\mathbf{1}_p^T, \\ C &= t\mathbf{1}_p\mathbf{1}_h^T(\Theta_H^* + t\mathbf{1}_h\mathbf{1}_h^T)^{-1}\Theta_{HO}^* + t\Theta_{OH}^*(\Theta_H^* + t\mathbf{1}_h\mathbf{1}_h^T)^{-1}\mathbf{1}_h\mathbf{1}_p^T \\ &\quad + \Theta_{OH}^*(\Theta_H^*)^{-1}\mathbf{1}_h \left(\frac{1}{t} + \mathbf{1}_h^T(\Theta_H^*)^{-1}\mathbf{1}_h \right)^{-1} \mathbf{1}_h^T(\Theta_H^*)^{-1}\Theta_{HO}^*. \end{aligned}$$

From Lemma 7, we have that: $\tilde{\Pi}A\tilde{\Pi} = A$. Furthermore, notice that B lies in the all-ones subspace, i.e. $\tilde{\Pi}B\tilde{\Pi} = 0$ and is a positive semi-definite matrix for $t > 0$. Thus, the matrix $A + B$ is invertible. Notice

$$\lim_{t \rightarrow 0} t\mathbf{1}_p\mathbf{1}_h^T(\Theta_H^* + t\mathbf{1}_h\mathbf{1}_h^T)^{-1}\Theta_{HO}^* = \lim_{t \rightarrow 0} t\mathbf{1}_p\mathbf{1}_h^T(\Theta_H^*)^{-1}\Theta_{HO}^* = 0,$$

$$\lim_{t \rightarrow 0} t\Theta_{OH}^*(\Theta_H^* + t\mathbf{1}_h\mathbf{1}_h^T)^{-1}\mathbf{1}_h\mathbf{1}_p^T = \lim_{t \rightarrow 0} t\Theta_{OH}^*(\Theta_H^*)^{-1}\mathbf{1}_h\mathbf{1}_p^T = 0,$$

$$\lim_{t \rightarrow 0} \Theta_{OH}^*(\Theta_H^*)^{-1}\mathbf{1}_h \left(\frac{1}{t} + \mathbf{1}_h^T(\Theta_H^*)^{-1}\mathbf{1}_h \right)^{-1} \mathbf{1}_h^T(\Theta_H^*)^{-1}\Theta_{HO}^* = \lim_{t \rightarrow 0} t\Theta_{OH}^*(\Theta_H^*)^{-1}\mathbf{1}_h(\Theta_H^*)^{-1}\Theta_{HO}^* = 0,$$

so that $\lim_{t \rightarrow 0} C = 0$. Notice on the other hand that $\lim_{t \rightarrow 0} A + B \neq 0$. By the Woodbury inversion lemma, we have that: $(A + B + C)^{-1} = (A + B)^{-1} - (A + B)^{-1}C(I + (A + B)^{-1}C)^{-1}(A + B)^{-1}$. Thus:

$$\lim_{t \rightarrow 0} \tilde{\Pi}(A + B + C)^{-1}\tilde{\Pi} = \tilde{\Pi} \lim_{t \rightarrow 0} (A + B)^{-1}\tilde{\Pi} - \lim_{t \rightarrow 0} \tilde{\Pi}(A + B)^{-1}C(I + A^{-1}C)^{-1}A^{-1}\tilde{\Pi}.$$

Since $\lim_{t \rightarrow 0} C = 0$, we have that:

$$\lim_{t \rightarrow \infty} \tilde{\Pi}[(\Theta^* + t\mathbf{1}_d\mathbf{1}_d^T)^{-1}]_{1:p,1:p}\tilde{\Pi} = \lim_{t \rightarrow 0} \tilde{\Pi}(A + B + C)^{-1}\tilde{\Pi} = \lim_{t \rightarrow 0} \tilde{\Pi}(A + B)^{-1}\tilde{\Pi} = \tilde{\Pi}A^+\tilde{\Pi} = A^+.$$

Here, the second equality follows from noting that the row/column spaces of A and B are orthogonal to one another and so by Lemma 5, $(A + B)^{-1} = A^+ + B^+$. Furthermore, since B is a multiple of all-ones matrix, $\tilde{\Gamma}B^+\tilde{\Gamma} = 0$. The last equality follows from Lemma 7. Noting that $M_{1:p,1:p} = -\Gamma_O^*/2$ and plugging in A^+ for $\tilde{\Pi}[(\Theta^* + t\mathbf{1}_d\mathbf{1}_d^T)^{-1}]_{1:p,1:p}\tilde{\Pi}$ in (17), we conclude that:

$$(\tilde{\Pi}(-\Gamma_O^*/2)\tilde{\Pi})^+ = \Theta_O^* - \Theta_{OH}^*(\Theta_H^*)^{-1}\Theta_{HO}^*.$$

Taking pseudo-inverses of both sides, we have the desired result. In Lemma 7, we also showed that:

$$\Theta_O^* - \Theta_{OH}^*(\Theta_H^*)^{-1}\Theta_{HO}^* = \tilde{\Pi}(\Theta_O^* - \Theta_{OH}^*(\Theta_H^*)^{-1}\Theta_{HO}^*)\tilde{\Pi},$$

as desired. \square

APPENDIX F. COUPLED HESSIAN CONDITIONS IMPLIED BY ASSUMPTION 1 AND THE CHOICE γ

Consider the following quantities measuring the behavior of the Hessian for some $\omega \in (0, 1)$

$$\begin{aligned}\chi &= \min_{\mathbb{H}' \in U(\omega)} \min_{Z \in \mathbb{H}', \|Z\|_{\Phi_\gamma} = 1} \|\mathcal{P}_{\mathbb{H}} \mathcal{J}^+ \mathbb{I}^* \mathcal{J} \mathcal{P}_{\mathbb{H}}(Z)\|_{\Phi_\gamma}, \\ \varepsilon &= \max_{\mathbb{H}' \in U(\omega)} \max \left\{ \max_{Z \in \mathbb{H}, \|Z\|_{\mathbb{H}} = 1} \|\mathcal{P}_{\mathbb{H}^\perp} \mathcal{J}^+ \mathbb{I}^* \mathcal{J} \mathcal{P}_{\mathbb{H}}(Z)\|_{\Phi_\gamma}, \max_{Z \in \mathbb{H}^\perp, \|Z\|_{\Phi_\gamma} = 1} \|\mathcal{P}_{\mathbb{H}} \mathcal{J}^+ \mathbb{I}^* \mathcal{J} \mathcal{P}_{\mathbb{H}^\perp}(Z)\|_{\Phi_\gamma} \right\}, \\ \chi_+ &= \min_{\mathbb{H}' \in U(\omega)} \min_{Z \in \mathbb{Q}', \Phi_\gamma(Z) = 1} \|\mathcal{P}_{\mathbb{H}'} \mathcal{J}^+ \mathbb{I}^* \mathcal{J} \mathcal{P}_{\mathbb{Q}'}(Z)\|_{\Phi_\gamma}, \\ \varepsilon_+ &= \max_{\mathbb{H}' \in U(\omega)} \max_{Z \in \mathbb{H}, \|Z\|_{\Phi_\gamma} = 1} \|\mathcal{P}_{\mathbb{H}^\perp} \mathcal{J}^+ \mathbb{I}^* \mathcal{J} \mathcal{P}_{\mathbb{Q}'}(Z)\|_{\Phi_\gamma}.\end{aligned}$$

The notations for the quantities $U(\omega)$, Φ_γ , \mathbb{H}' , \mathbb{Q}' are defined in Section A. The quantity χ being large ensures that the Hessian \mathbb{I}^* is well-conditioned restricted to the image $\mathcal{J}\mathbb{H}' \subseteq \mathbb{S}^p$ for all \mathbb{H}' close to \mathbb{H}^* ; the quantity ε being small implies that any element of $\mathcal{J}\mathbb{H}'$ and any element of $\mathcal{J}\mathbb{H}'^\perp$ have a small inner-product for all \mathbb{H}' close to \mathbb{H}^* . Finally, χ_+ and ε_+ are analogs of χ and ε , accounting for the dual parameter that lies in the subspace $\text{span}(\mathbf{1}_p \mathbf{1}_p^\top)$.

The quantities $\chi, \varepsilon, \chi_+, \varepsilon_+$ represent coupled Hessian quantities. We next show that the uncoupled conditions assumed in Theorem 3 imply control on these quantities.

Proposition 17. *Suppose the conditions of Theorem 3 are satisfied. Then, the following properties are satisfied:*

$$\begin{aligned}P1 \quad &\chi \geq \alpha, \\ P2 \quad &\frac{\varepsilon}{\xi} \leq 1 - \frac{2}{\zeta_1} \\ P3 \quad &\frac{\varepsilon_+}{\xi_+} \leq 1 - \frac{2}{\zeta_2}\end{aligned}$$

where $\omega = \mu^*/4$, $\alpha = \alpha$, $\zeta_1 = 2/\nu_1$ and $\zeta_2 = \frac{2}{1 - \frac{1+2\kappa^* + \mu^*/2}{1-2\kappa^* - \mu^*/2}(1-\nu_2)}$.

Proof of Proposition 17. Throughout, we will use the notation $\theta(\Omega^*)$ and $\xi(T^*)$ defined in Section A, as well as the bounds $\theta(\Omega^*) \leq d^*$ and $\xi(T^*) \in [\mu^*, 2\mu^*]$. Recall that γ is in the range defined in Theorem 3.

We begin by proving that Property *P1* holds under the conditions of Proposition 17. Let $Z = (Z_1, Z_2)$. Suppose that $\|Z_1\|_\infty = 1$. Then, we have using Lemma 9 with $\omega = \mu^*/4$ to conclude that:

$$\begin{aligned}\|\mathcal{P}_{\Omega^*} \mathbb{I}^* \mathcal{J} \mathcal{P}_{\mathbb{H}}(Z)\|_\infty &\geq \|\mathcal{P}_{\Omega^*} \mathbb{I}^* \mathcal{P}_{\Omega^*}(Z_1)\|_\infty - \|\mathcal{P}_{\Omega^*} \mathbb{I}^*(Z_2)\|_\infty \\ &\geq \alpha - \|\mathbb{I}^*(Z_2)\|_\infty \geq \alpha - 3\gamma\beta\xi(T^*) \geq \alpha/2.\end{aligned}$$

Suppose that $\|Z_2\|_2 = \gamma$. Then, we have that:

$$\begin{aligned}\|\mathcal{P}_{T'} \mathbb{I}^* \mathcal{J} \mathcal{P}_{\mathbb{H}}(Z)\|_2 &\geq \|\mathcal{P}_{T'} \mathbb{I}^* \mathcal{P}_{T'}(Z_1)\|_2 - \|\mathcal{P}_{T'} \mathbb{I}^*(Z_2)\|_2 \\ &\geq \alpha - 2\|\mathbb{I}^*(Z_2)\|_2 \geq \alpha\gamma - 2\beta\theta(\Omega^*) \geq \alpha\gamma/2.\end{aligned}$$

Putting together the last two inequalities proves that Property *P1* holds. We next prove that Property *P2* holds. Note that for $Z = (Z_1, Z_2) \in \mathbb{H}'$ with $\|Z_1\|_\infty = 1$, we have

$$\|\mathcal{P}_{\Omega^*} \mathbb{I}^* \mathcal{J} \mathcal{P}_{\mathbb{H}}(Z)\|_\infty \leq \|\mathcal{P}_{\Omega^*} \mathbb{I}^*(Z_1)\|_\infty + \|\mathcal{P}_{\Omega^*} \mathbb{I}^*(Z_2)\|_\infty \leq \delta + 3\xi(T^*)\beta\gamma.$$

Similarly, suppose that $\|Z_2\|_2 = \gamma$. We have that:

$$\|\mathcal{P}_{T'} \mathbb{I}^* \mathcal{J} \mathcal{P}_{\mathbb{H}}(Z)\|_2 \leq \|\mathcal{P}_{T'} \mathbb{I}^*(Z_2)\|_2 + \|\mathcal{P}_{T'} \mathbb{I}^*(Z_1)\|_2 \leq \delta\gamma + \beta\mu(\Omega^*).$$

Combining these last two bounds with the bounds from the first part, we have that:

$$\frac{\varepsilon}{\chi} \leq \frac{\delta + \beta \max\{3\xi(T^*)\gamma, 2\theta(\Omega^*)/\gamma\}}{\alpha - \beta \max\{3\xi(T^*)\gamma, 2\theta(\Omega^*)/\gamma\}} \leq \frac{\delta + \nu_1\alpha/(2 - \nu_1)}{\alpha - \nu_1\alpha/(2 - \nu_1)} \leq 1 - \nu_1 = 1 - \frac{2}{\zeta_1}.$$

Here, we have used the bound for γ and Assumption 1.

Next, we will show that Property *P3* holds. Specifically, we consider the quantity $\min_{Z \in \mathbb{Q}', \Phi_\gamma(Z)=1} \|\mathcal{P}_{\mathbb{H}'} \mathcal{J}^+ \mathbb{I}^* \mathcal{J} \mathcal{P}_{\mathbb{Q}'}(Z)\|_{\Phi_\gamma}$. Let $Z = (Z_1, Z_2)$ where $\|Z\|_{\Phi_\gamma} = 1$, $Z \in \mathbb{Q}'$. Suppose $\|Z_1\|_\infty = 1$. Then using Lemmas 9 and 16, we have that:

$$\begin{aligned} \|\mathcal{P}_{\Omega^*} \mathcal{J}^+ \mathbb{I}^* \mathcal{J}(Z)\|_\infty &\geq \|\mathcal{P}_{\Omega^*} \mathbb{I}^* \mathcal{P}_{\Omega^*}(Z_1)\|_\infty - \|\mathcal{P}_{\Omega^*} \mathbb{I}^*(Z_2)\|_\infty \\ &\geq \alpha - \|\mathbb{I}^*(Z_2)\|_\infty \geq \alpha - \gamma\beta\xi(T' \oplus \text{span}(\mathbf{1}_p \mathbf{1}_p^\top)) \geq \alpha - 3\gamma\beta\xi(T') \geq \alpha - 9\xi(T^*)\beta\gamma. \end{aligned}$$

Now suppose that $\|Z_2\|_2 = \gamma$. Then, we have using Lemma 12 that:

$$\begin{aligned} \|\mathcal{P}_{T'} \mathbb{I}^* \mathcal{J}(Z)\|_2 &\geq \|\mathcal{P}_{T'} \mathbb{I}^* \mathcal{P}_{T'}(Z_2)\|_2 - \|\mathcal{P}_{T'} \mathbb{I}^* \mathcal{P}_{T'^\perp}(Z_2)\|_2 - \|\mathcal{P}_{T'} \mathbb{I}^*(Z_1)\|_2 \\ &\geq \alpha\gamma(1 - 2\kappa^* - \mu^*/2) - \delta\gamma(2\kappa^* + \mu^*/2) - \beta\theta(\Omega^*). \end{aligned}$$

Combining the above inequality, we have that:

$$(20) \quad \min_{Z \in \mathbb{Q}', \Phi_\gamma(Z)=1} \|\mathcal{P}_{\mathbb{H}'} \mathcal{J}^+ \mathbb{I}^* \mathcal{J} \mathcal{P}_{\mathbb{Q}'}(Z)\|_{\Phi_\gamma} \geq \alpha(1 - 2\kappa^* - \mu^*/2) - \delta(2\kappa^* + \mu^*/2) - \max\{9\xi(T^*)\beta\gamma, \beta\theta(\Omega^*)\}.$$

Now we consider the quantity $\max_{Z \in \mathbb{Q}', \Phi_\gamma(Z)=1} \|\mathcal{P}_{\mathbb{H}'^\perp} \mathcal{J}^+ \mathbb{I}^* \mathcal{J} \mathcal{P}_{\mathbb{Q}'}(Z)\|_{\Phi_\gamma}$. Let $Z = (Z_1, Z_2)$ where $\|Z\|_{\Phi_\gamma} = 1$, $Z \in \mathbb{Q}'$. Suppose $\|Z_1\|_\infty = 1$.

$$\begin{aligned} \|\mathcal{P}_{\Omega^{*\perp}} \mathcal{J}^+ \mathbb{I}^* \mathcal{J}(Z)\|_\infty &\leq \|\mathcal{P}_{\Omega^{*\perp}} \mathbb{I}^* \mathcal{P}_{\Omega^*}(Z_1)\|_\infty + \|\mathcal{P}_{\Omega^{*\perp}} \mathbb{I}^*(Z_2)\|_\infty \\ &\leq \delta + \|\mathbb{I}^*(Z_2)\|_\infty \leq \delta + 9\xi(T^*)\beta\gamma. \end{aligned}$$

Now suppose that $\|Z_2\|_2 = \gamma$. Then, we have using Lemma 12:

$$\begin{aligned} \|\mathcal{P}_{T'^\perp} \mathbb{I}^* \mathcal{J}(Z)\|_2 &\leq \|\mathcal{P}_{T'^\perp} \mathbb{I}^* \mathcal{P}_{T'}(Z_2)\|_2 + \|\mathcal{P}_{T'^\perp} \mathbb{I}^* \mathcal{P}_{T'^\perp}(Z_2)\|_2 + \|\mathcal{P}_{T'^\perp} \mathbb{I}^*(Z_1)\|_2 \\ &\leq \delta\gamma(1 + 2\kappa^* + \mu^*/2) + \gamma(2\kappa^* + \mu^*/2) + \beta\theta(\Omega^*). \end{aligned}$$

Combining the above inequality, we have that:

$$(21) \quad \min_{Z \in \mathbb{Q}', \Phi_\gamma(Z)=1} \|\mathcal{P}_{\mathbb{H}'^\perp} \mathcal{J}^+ \mathbb{I}^* \mathcal{J} \mathcal{P}_{\mathbb{Q}'}(Z)\|_{\Phi_\gamma} \leq \delta(1 + 2\kappa^* + \mu^*/2) + 2\kappa^* + \mu^*/2 + \max\{9\xi(T^*)\beta\gamma, \beta\theta(\Omega^*)\}.$$

Putting the bounds (20) and (21) together, we have:

$$\begin{aligned} \frac{\varepsilon_+}{\chi_+} &\leq \frac{\delta(1 + 2\kappa^* + \mu^*/2) + 2\kappa^* + \mu^*/2 + \beta \max\{9\xi(T^*)\gamma, \theta(\Omega^*)\}}{\alpha(1 - 2\kappa^* - \mu^*/2) - \delta(2\kappa^* + \mu^*/2) - \beta \max\{9\xi(T^*)\gamma, \theta(\Omega^*)\}} \\ &= \frac{1 + 2\kappa^* + \mu^*/2}{1 - 2\kappa^* - \mu^*/2} \frac{\delta + \frac{2\kappa^* + \mu^*/2}{1 + 2\kappa^* + \mu^*/2} + \frac{\beta}{1 + 2\kappa^* + \mu^*/2} \max\{9\xi(T^*)\gamma, \theta(\Omega^*)\}}{\alpha - \delta \frac{2\kappa^* + \mu^*/2}{1 - 2\kappa^* - \mu^*/2} - \frac{\beta}{1 - 2\kappa^* - \mu^*/2} \max\{9\xi(T^*)\gamma, \theta(\Omega^*)\}} \\ &\leq \frac{1 + 2\kappa^* + \mu^*/2}{1 - 2\kappa^* - \mu^*/2} \frac{\delta + \frac{\nu_2\alpha}{2 - \nu_2}}{\alpha - \frac{\nu_2\alpha}{2 - \nu_2}} \\ &= \frac{1 + 2\kappa^* + \mu^*/2}{1 - 2\kappa^* - \mu^*/2} (1 - \nu_2) = 1 - \frac{2}{\zeta_2}. \end{aligned}$$

□

APPENDIX G. PROOF OF THEOREM 3

G.1. Full theoretical statement. Let $\alpha, \beta, \delta, d^*, \mu^*, \kappa^*, \nu_1, \nu_2$ be the quantities in Theorem 3. Let $\omega = \mu^*/4$, and $\zeta_1 = 2/\nu_1$ and $\zeta_2 = \frac{2}{1 - \frac{1+2\kappa^*+\mu^*/2}{1-2\kappa^*-\mu^*/2}(1-\nu_2)}$ (see Proposition 17. Let c_5, C_5, \tilde{C}_5 be constants

that ensure Corollary 4 is satisfied. Let $\psi = \max\{1, \|(S^* - L^*)^+\|_2\}$, $C_0 = 8 + \frac{32\sqrt{5h}}{\alpha(1 - \sqrt{1 - (\kappa^* - \omega)^2})(\frac{2}{\zeta_1} - 2(\kappa^* + \omega))} \left[1 + \frac{1}{3\zeta_2}\right]$, $C_1 = \psi(m + d^*)$, and $C_2 = m \max\left\{\left(\frac{4C_0}{\alpha} + \frac{1}{\psi}\right), 1\right\}$. We also define,

$$C_4 = \min \left\{ \min \left\{ \frac{8\alpha}{C_1}, \frac{\min\{\alpha, 1\}(\frac{2}{\zeta_1} - 2(\kappa^* + \omega))}{16m\psi C_2^2} \right\}, \frac{\alpha(\frac{2}{\zeta_1} - 2(\kappa^* + \omega))}{4(1 + \frac{1}{3\zeta_2})} \right. \\ \left. , \frac{\alpha(\frac{2}{\zeta_1} - 2(\kappa^* + \omega))}{64C_1(1 + \frac{1}{3\zeta_2})}, \frac{\alpha^2(\frac{2}{\zeta_1} - 2(\kappa^* + \omega))^2}{6144\zeta_2(1 + \frac{1}{3\zeta_2})^2} \right\}.$$

Theorem 18. Suppose $\kappa^{*2} \geq \mu^*/2$ and $2\kappa^* + \mu^*/2 < 1$. Let $\nu = \min\{\nu_1, \nu_2\}$ and suppose Assumption 1 is satisfied. Suppose that:

$$d^* \mu^* \leq \frac{\nu^2 \alpha^2}{(1 - 2\kappa^* - \mu^*)18\beta^2(2 - \nu)^2}.$$

Let the regularization γ be chosen in the interval $\gamma \in \left[\frac{2\beta d^*(2-\nu)}{\nu\alpha}, \frac{\nu\alpha(1-2\kappa^*-\mu^*)}{36\beta\mu^*(2-\nu)}\right]$. Let $m = \max\{1, \frac{1}{\gamma}\}$ and $\bar{m} = \max\{1, \gamma\}$. Let the effect sample size k be chosen as $(n/2)^{\xi/2(1+\xi)} \leq k \leq (n/2)^{\xi/(1+\xi)}$. Furthermore, suppose that:

$$k \geq \max \left\{ \frac{C_5^2 1152 m^2 \zeta_2^2 p^2 \log(\tilde{C}_5 p)}{C_4^2 c_5^2} + \frac{72 m^2 \zeta_2^2}{C_4^2}, \frac{262144(1 + \xi)^{16} \log(\tilde{C}_5 p)}{c_5 \xi^{16}}, \right. \\ \left. \left(\frac{2 - \xi}{\xi}\right)^{16/7 + \xi} \left(\frac{2\sqrt{\log(\tilde{C}_5 p)}}{\sqrt{c_5}}\right)^{-8/7 - \xi/2} \right\}$$

and

- (1) $\lambda_n = C_5 \left[\frac{24m\zeta_2}{\sqrt{c_5}} \sqrt{\frac{p^2 \log(\tilde{C}_5 p)}{k}} + \frac{6m\zeta_2}{\sqrt{k}} \right]$,
- (2) $\sigma_{\min}(L^*) \geq \max \left\{ 16m\bar{m} \frac{\lambda_n C_2}{\omega}, \frac{2\psi C_2^2 \lambda_n}{C_0}, \left(mC_2 + \frac{\alpha(\frac{2}{\zeta_1} - 2(\kappa^* + \omega))}{4[1 + \frac{1}{3\zeta_2}]} \right) \lambda_n \right\}$,
- (3) $|S_{ij}^*| \geq 12m\bar{m}\lambda_n C_2$ whenever $|S_{ij}^*| > 0$.

Then, the estimate (\hat{S}, \hat{L}) is the unique minimizer of (9) with

$$\mathbb{P} \left(\text{sign}(\hat{S}) = \text{sign}(S^*), \text{rank}(\hat{L}) = \text{rank}(L^*), \|\hat{S} - \hat{L} - \tilde{\Theta}^*\|_2 \leq 2mC_2\lambda_n \right) \geq 1 - \frac{1}{p}.$$

To arrive at the scalings provided in Theorem 3, note that, $\zeta_1 = \mathcal{O}(1/\nu)$, $\zeta_2 = \mathcal{O}(1/\nu)$, $C_0 = \mathcal{O}(\sqrt{h\nu}/\alpha)$, $C_1 = \mathcal{O}(md^*)$, $C_2 = \mathcal{O}(m\sqrt{h}/\alpha^2)$, $C_4 = \mathcal{O}(\alpha^3\nu/(d^*m^3\sqrt{h}))$. This scaling allows us to conclude that: $k \gtrsim \frac{m^3 h d^{*2}}{\alpha^6 \nu^2} m \nu p \log(p)$, $\lambda_n = \frac{m}{\nu} \sqrt{\frac{p^2 \log(p)}{k}}$, $\sigma_{\min}(L^*) \gtrsim \frac{m^4 h \bar{m}}{\nu \alpha^4} \sqrt{\frac{p^2 \log(p)}{k}}$, $S_{ij}^* \gtrsim \frac{m^3 \bar{m} \sqrt{h}}{\nu \alpha^2} \sqrt{\frac{p^2 \log(p)}{k}}$, and finally $\|(\hat{S} - \hat{L}) - \tilde{\Theta}^*\|_2 \lesssim \frac{m^3 \sqrt{h}}{\nu \alpha^2} \sqrt{\frac{p^2 \log(p)}{k}}$.

G.2. Proof strategy. The high-level proof strategy is similar in spirit to the proofs of consistency results for sparse graphical model recovery and latent variable graphical model recovery (Chandrasekaran et al., 2012), although our convex program and the conditions required for its success are different from these previous results. Consider the following convex program

$$(22) \quad \begin{aligned} (\hat{S}, \hat{L}) = \arg \min_{S, L \in \mathbb{S}^p} & -\log \det(U^T(S-L)U) - \text{tr}((S-L)\hat{\Gamma}_O/2) + \lambda_n(\|S\|_1 + \gamma\|L\|_\star) \\ & \text{subject-to } S-L \in \text{span}(\mathbf{1}_p \mathbf{1}_p^\top) \end{aligned}$$

Comparing (22) with the convex program (9), the differences are: i) we have removed the positive-definite constraints, ii) we have replaced $\text{tr}(L)$ with $\|L\|_\star$ which is valid for positive semi-definite L , iii) we have replaced the constraint $(S-L)\mathbf{1}_p = 0$ with $S-L \in \text{span}(\mathbf{1}_p \mathbf{1}_p^\top)$ which is equivalent since the matrices S, L are symmetric. Regarding item i), the positive definiteness of $\hat{S} - \hat{L}$ is automatically met due to the log-det term. We show with high probability that $\hat{L} \succeq 0$.

Note that due to the log-det term, we have that $UU^T(S-L)UU^T = S-L$. Appealing to Lemma 6, we conclude that $U(U^T(S-L)U)^{-1}U^T$, which is the gradient of the negative log-determinate term with respect to S is equivalent to $(S-L)^+$. Similarly, since $\text{tr}((S-L)\hat{\Gamma}_O/2) = \text{tr}(UU^T(S-L)UU^T\hat{\Gamma}_O/2) = \text{tr}((S-L)UU^T\hat{\Gamma}_O/2UU^T)$, the gradient of the trace term in the objective with respect to S is given by $UU^T\hat{\Gamma}_O/2UU^T$. Standard convex analysis states that (\hat{S}, \hat{L}) is the solution of the convex program (22) if there exists a dual variable $t \in \mathbb{R}$ with the following conditions being satisfied:

$$(23) \quad \begin{aligned} -UU^T(\hat{\Gamma}_O/2)UU^T - (\hat{S} - \hat{L})^+ + t\mathbf{1}_p \mathbf{1}_p^\top &= -\lambda \partial \|\hat{S}\|_1 \\ UU^T(\hat{\Gamma}_O/2)UU^T + (\hat{S} - \hat{L})^+ - t\mathbf{1}_p \mathbf{1}_p^\top &= -\lambda \gamma \partial \|\hat{L}\|_\star \\ \hat{S} - \hat{L} &\in \text{span}(\mathbf{1}_p \mathbf{1}_p^\top). \end{aligned}$$

Recall that elements of the subdifferential with respect to nuclear norm at a matrix M have the key property that they decompose with respect to the tangent space $T(M)$. Specifically, the subdifferential with respect to the nuclear norm at a matrix M with (reduced) SVD given by $M = U_l Q U_r^T$ is as follows:

$$N \in \partial \|M\|_\star \Leftrightarrow \mathcal{P}_{T(M)}(N) = U_l V_r^T, \|\mathcal{P}_{T(M)^\perp}(N)\|_2 \leq 1,$$

where \mathcal{P} denotes a projection operator. Similarly, we have the following for the subdifferential of ℓ_1 norm:

$$N \in \partial \|M\|_1 \Leftrightarrow \mathcal{P}_{\Omega(M)}(N) = \text{sign}(N), \|\mathcal{P}_{\Omega(M)^\perp}(N)\|_\infty \leq 1.$$

Let SVD of \hat{L} be $\hat{U}\hat{D}\hat{V}^T$ and let $Z = (-\lambda \text{sign}(\hat{S}), -\lambda \gamma \hat{U}\hat{V}^T)$. Then, letting $\mathbb{H} = \Omega(\hat{S}) \times T(\hat{L})$ the optimality conditions of (22) reduce to:

$$(24) \quad \begin{aligned} \mathcal{P}_{\mathbb{H}} \mathcal{J}^+(-UU^T\hat{\Gamma}_O/2UU^T - (\hat{S} - \hat{L})^+ - t\mathbf{1}_p \mathbf{1}_p^\top) &= Z, \\ \Phi_\gamma(\mathcal{P}_{\mathbb{H}^\perp} \mathcal{J}^+(-UU^T\hat{\Gamma}_O/2UU^T - (\hat{S} - \hat{L})^+ - t\mathbf{1}_p \mathbf{1}_p^\top)) &\leq \lambda_n, \\ \hat{S} - \hat{L} &\in \text{span}(\mathbf{1}_p \mathbf{1}_p^\top). \end{aligned}$$

To ensure that the estimates (\hat{S}, \hat{L}) are close to their respective population parameters, the quantity $\Delta_S = \hat{S} - S^*$ and $\Delta_L = \hat{L} - L^*$ must be small. Since the optimality conditions of (22) are stated in terms of $(\hat{S} - \hat{L})^+$, we bound the deviation between $(\hat{S} - \hat{L})^+$ and $(S^* - L^*)^+$. Specifically, the Taylor Series expansion of $(\hat{S} - \hat{L})^+$ around $(S^* - L^*)^+$ is given by:

$$(\hat{S} - \hat{L})^+ = (S^* - L^* + \mathcal{J}(\Delta_S, \Delta_L))^+ = (S^* - L^*)^+ + (S^* - L^*)^+ \mathcal{J}(\Delta_S, \Delta_L)(S^* - L^*)^+ + \mathcal{R}_{\Gamma_0^*} \mathcal{J}(\Delta_S, \Delta_L).$$

where some algebra yields the following representation for the remainder term $\mathcal{R}_{\Gamma_0^*}(\mathcal{J}(\Delta_S, \Delta_L))$:

$$(25) \quad \mathcal{R}_{\Gamma_0^*}(\mathcal{J}(\Delta_S, \Delta_L)) = U(S^* - L^* + \mathbf{1}_p \mathbf{1}_p^\top / p)^{-1} \left[\sum_{k=2}^{\infty} (-\mathcal{J}(\Delta_S, \Delta_L)(S^* - L^* + \mathbf{1}_p \mathbf{1}_p^\top / p)^{-1})^k \right] U^T.$$

From Theorem 2, we have that $(S - L)^+ = UU^T(-\Gamma^*/2)UU^T$. Since $UU^T(S^* - L^*)UU^T = S^* - L^*$, we appeal to Lemma 6 to conclude that $(U^T(S^* - L^*)U)^{-1} = U^T(-\Gamma_0^*)U$. Let $E_n := UU^T(\hat{\Gamma}_O - \Gamma^*)/2UU^T$. Then, we have the following equivalent characterization of the optimality conditions (23):

$$(26) \quad \begin{aligned} & \mathcal{P}_{\mathbb{H}} \mathcal{J}^+((S^* - L^*)^+ \mathcal{J}(\Delta_S, \Delta_L)(S^* - L^*)^+ + \mathcal{R}_{\Gamma_0^*} \mathcal{J}(\Delta_S, \Delta_L) + E_n + t \mathbf{1}_p \mathbf{1}_p^\top) = Z, \\ & \Phi_\gamma(\mathcal{P}_{\mathbb{H}^\perp} \mathcal{J}^+((S^* - L^*)^+ \mathcal{J}(\Delta_S, \Delta_L)(S^* - L^*)^+ + \mathcal{R}_{\Gamma_0^*} \mathcal{J}(\Delta_S, \Delta_L) + E_n + t \mathbf{1}_p \mathbf{1}_p^\top)) \leq \lambda_n, \\ & \hat{S} - \hat{L} \in \text{span}(\mathbf{1}_p \mathbf{1}_p^\top). \end{aligned}$$

Finally, Since $(S^* - L^*) \mathbf{1}_p \mathbf{1}_p^\top = 0$ and $\mathcal{J}(\Delta_S, \Delta_L) \mathbf{1}_p \mathbf{1}_p^\top = 0$, we have the following formulation of the optimality condition (26) in terms of the matrix \mathbb{I}^*

$$(27) \quad \begin{aligned} & \mathcal{P}_{\mathbb{H}} \mathcal{J}^+(\mathbb{I}^*(\mathcal{J}(\Delta_S, \Delta_L + t \mathbf{1}_p \mathbf{1}_p^\top)) + \mathcal{R}_{\Gamma_0^*} \mathcal{J}(\Delta_S, \Delta_L + t \mathbf{1}_p \mathbf{1}_p^\top) + E_n) = Z, \\ & \Phi_\gamma(\mathcal{P}_{\mathbb{H}^\perp} \mathcal{J}^+(\mathbb{I}^*(\mathcal{J}(\Delta_S, \Delta_L + t \mathbf{1}_p \mathbf{1}_p^\top)) + \mathcal{R}_{\Gamma_0^*} \mathcal{J}(\Delta_S, \Delta_L + t \mathbf{1}_p \mathbf{1}_p^\top) + E_n)) \leq \lambda_n, \\ & \hat{S} - \hat{L} \in \text{span}(\mathbf{1}_p \mathbf{1}_p^\top). \end{aligned}$$

It is straightforward to show that if for some (\hat{S}, \hat{L}) , the second condition in (27) is satisfied with strict inequality, that is:

$$\Phi_\gamma(\mathcal{P}_{\mathbb{H}^\perp} \mathcal{J}^+(\mathbb{I}^*(\mathcal{J}(\Delta_S, \Delta_L + t \mathbf{1}_p \mathbf{1}_p^\top)) + \mathcal{R}_{\Gamma_0^*} \mathcal{J}(\Delta_S, \Delta_L + t \mathbf{1}_p \mathbf{1}_p^\top) + E_n)) < \lambda_n.$$

G.3. Constrained optimization problem. We consider the following non-convex optimization problem:

$$(28) \quad \begin{aligned} & \underset{S \in \mathbb{S}^p, L \in \mathbb{S}^p}{\text{argmin}} \quad -\log \det(U^T(S - L)U) - \text{tr}((S - L)\hat{\Gamma}_O/2) + \lambda_n(\|S\|_1 + \gamma\|L\|_*), \\ & \text{subject-to } S - L \in \text{span}(\mathbf{1}_p \mathbf{1}_p^\top); (S, L) \in \mathcal{M} \end{aligned}$$

where:

$$\mathcal{M} = \left\{ S, L \in \mathbb{S}^p : S \in \Omega^*, \text{rank}(L) \leq \text{rank}(L^*) \right. \\ \left. \|\mathcal{P}_{T^{\star\perp}}(L - L^*)\|_2 \leq \frac{C_0 \lambda_n}{\psi}; \Phi_\gamma(\mathcal{J}^+ \mathbb{I}^* \mathcal{J}(S - S^*, L - L^*)) \leq C_0 \lambda_n \right\},$$

with $C_0 = 10 + \frac{32\sqrt{5}h}{\alpha(1 - \sqrt{1 - (\kappa^* - \omega)^2})(\frac{2}{\xi_1} - 2(\kappa^* + \omega))} \left[1 + \frac{1}{3\xi_2} \right]$. The optimization program (28) is non-convex due to the rank constraint $\text{rank}(L) \leq \text{rank}(L^*)$ in the set \mathcal{M} . These constraints ensure that the matrix L belongs to an appropriate variety. The constraints in \mathcal{M} along $T^{\star\perp}$ ensure that the tangent space $T(L)$ is close to T^* . Finally, the last condition roughly controls the error. We begin by proving the following useful proposition:

Proposition 19. *Let (S, L) be a set of feasible variables of (28). Let $\Delta = (S - S^*, L - L^*)$. Then, $\Phi_\gamma(\Delta) \leq C_2 \lambda_n$ where $C_2 = m \max\left\{\left(\frac{4C_0}{\alpha} + \frac{1}{\psi}\right), 1\right\}$.*

Proof of Proposition 19. Let $\mathbb{H}^* = \Omega^* \times T^*$. Then:

$$\begin{aligned} \Phi_\gamma[\mathcal{J}^+\mathbb{I}^*\mathcal{J}\mathcal{P}_{\mathbb{H}^*}(\Delta)] &\leq \Phi_\gamma[\mathcal{J}^+\mathbb{I}^*\mathcal{J}(\Delta)] + \Phi_\gamma[\mathcal{J}^+\mathbb{I}^*\mathcal{J}\mathcal{P}_{\mathbb{H}^*\perp}(\Delta)] \\ &\leq C_0\lambda_n + mC_0\lambda_n \leq 2mC_0\lambda_n. \end{aligned}$$

Since $\Phi_\gamma[\mathcal{P}_{\mathbb{H}^*}(\cdot)] \leq 2\Phi_\gamma[\cdot]$, we have that: $\Phi_\gamma[\mathcal{P}_{\mathbb{H}^*}\mathcal{J}^+\mathbb{I}^*\mathcal{J}\mathcal{P}_{\mathbb{H}^*}(\Delta)] \leq 4mC_0\lambda_n$. Then, appealing to Property *P1*, we have that: $\Phi_\gamma[\mathcal{P}_{\mathbb{H}^*}(\Delta)] \leq \frac{4C_0\lambda_n}{\alpha}$. Moreover, $\Phi_\gamma(\Delta) \leq \Phi_\gamma[\mathcal{P}_{\mathbb{H}^*}(\Delta)] + \Phi_\gamma[\mathcal{P}_{\mathbb{H}^*\perp}(\Delta)] \leq \lambda_n m \left(\frac{4C_0}{\alpha} + \frac{1}{\psi} \right)$. \square

Proposition 19 leads to powerful implications. In particular, under additional conditions on the minimum nonzero singular values of L^* , any feasible set of variables (S, L) of (28) has two key properties: (a) The variables (S, L) are smooth points of their underlying varieties with $L \succeq 0$ and $S - L \succeq 0$, and (b) The constraints in \mathcal{M} along $T^{*\perp}$ are locally inactive at L . These properties, among others, are proved in the following corollary.

Corollary 20. *Consider any feasible variables (S, L) of (28). Let $T' = T(L)$. Let σ be the smallest nonzero singular value of L^* and s be the smallest in magnitude nonzero value of S^* . Let $\mathbb{H}' = \Omega^* \times T'$, $C_{T'} = \mathcal{P}_{T'\perp}(L^*)$ and $C_{T' \oplus \text{span}(\mathbf{1}_p \mathbf{1}_p^\top)} = \mathcal{P}_{(T' \oplus \text{span}(\mathbf{1}_p \mathbf{1}_p^\top))^\perp}(L^*)$. Suppose that the following inequalities are met: $\sigma \geq \max \left\{ 16m\bar{m} \frac{\lambda_n C_2}{\omega}, \frac{2\psi C_2^2 \lambda_n}{C_0}, \left(mC_2 + \frac{\alpha(\frac{2}{\zeta_1} - 2(\kappa^* + \omega))}{4[1 + \frac{1}{3\zeta_2}]} \right) \lambda_n \right\}$ and $s \geq 12m\bar{m}\lambda_n C_2$. Then,*

- (1) L and S are smooth points of their underlying varieties so that $\text{support}(\hat{S}) = \text{support}(S^*)$ and $\text{rank}(\hat{L}) = \text{rank}(L^*)$. Furthermore, $L \succeq 0$, and $S - L \succeq 0$
- (2) $\|\mathcal{P}_{T'^\perp}(\hat{L} - L^*)\|_2 \leq \frac{C_0\lambda_n}{2\psi}$,
- (3) $\rho(T', T^*) \leq \omega$,
- (4) $\max\{\Phi_\gamma(\mathcal{J}^+\mathbb{I}^*C_{T'}), \Phi_\gamma(\mathcal{J}^+\mathbb{I}^*C_{T' \oplus \mathbf{1}_p \mathbf{1}_p^\top})\} \leq \frac{\lambda_n}{6\zeta_2}$,
- (5) $\Phi_\gamma[\mathcal{J}^+C_{T'}] \leq \frac{4\lambda_n}{\alpha(\frac{2}{\zeta_1} - 2(\kappa^* + \omega))} \left[1 + \frac{1}{3\zeta_2} \right]$.

Proof of Corollary 20. We appeal to the results regarding the perturbation analysis of the low-rank matrix variety.

- (1) Based on assumptions regarding the minimum nonzero singular value of L^* and minimum nonzero entry in magnitude of S^* , one can check that since $\omega \leq 1$

$$\begin{aligned} \sigma &\geq 12m\bar{m} \frac{\lambda_n C_2}{\omega} \geq 12m\bar{m}\lambda_n C_2 \geq 8\|L - L^*\|_2, \\ s &\geq 12m\bar{m}\lambda_n C_2 \geq 12m\bar{m}\lambda_n C_2 \geq 2\|S - S^*\|_2. \end{aligned}$$

Combining these results, we conclude that S, L are smooth points of their varieties, namely that $\text{rank}(L) = \text{rank}(L^*)$ and $\text{support}(S) = \text{support}(S^*)$. The fact that $L \succeq 0$ follows from $\sigma \geq 2\|L - L^*\|_2$. Furthermore, to check that $S - L \succeq 0$, first note that $\sigma_{\min}(S^* - L^*) \geq \frac{1}{\sqrt{\psi}}$. Then, $\|S - L - (S^* - L^*)\|_2 \leq 2mC_2\lambda_n$. From the choice of λ_n and the condition on the sample size, we have that $4mC_2\lambda_n < \frac{1}{\sqrt{\psi}}$. Thus, $S - L \succeq 0$.

- (2) Since $\sigma \geq 8\|L - L^*\|_2$, we can appeal to Proposition 2.2 of Chandrasekaran et al. (2012) to conclude that the constraint in \mathcal{M} along $\mathcal{P}_{T'^\perp}$ is strictly feasible:

$$\|\mathcal{P}_{T'^\perp}(L - L^*)\|_2 \leq \frac{\|L - L^*\|_2^2}{\sigma} \leq \frac{C_2^2 \lambda_n^2}{\sigma} < \frac{C_0 \lambda_n}{\psi}.$$

- (3) Appealing to Proposition 2.1 of Chandrasekaran et al. (2012), we prove that the tangent space T' is close to T^* :

$$\rho(T', T^*) \leq \frac{2\|L - L^*\|_2}{\sigma} \leq \frac{2m\bar{m}\lambda_n C_2 \omega}{12m\bar{m}\lambda_n C_2} \leq \omega.$$

- (4) Letting σ' be the minimum nonzero singular value of L . One can check that:

$$\sigma' \geq \sigma - \|L - L^*\|_2 \geq \sigma - mC_2\lambda_n \geq 10mC_2\lambda_n \geq 8\|L - L^*\|_2.$$

One can also obtain the following lower bounds for σ' :

$$\begin{aligned} \sigma' &\geq \sigma - \|L - L^*\|_2 \geq \sigma - mC_2\lambda_n \geq 6\zeta_2 mC_2^2 \psi \lambda_n - mC_2\lambda_n \geq 6\zeta_2 m\psi C_2^2 \lambda_n \\ \sigma' &\geq \sigma - \|L - L^*\|_2 \geq \sigma - mC_2\lambda_n \geq \frac{\alpha(\frac{2}{\zeta_1} - 2(\kappa^* + \omega))\lambda_n}{4\left[1 + \frac{1}{3\zeta_2}\right]} \end{aligned}$$

where we have used $C_2\psi \geq 1$. Once again appealing to Proposition 2.2 of Chandrasekaran et al. (2012) and simple algebra, we have:

$$\Phi_\gamma[\mathcal{J}^+ \mathbb{I}^* C_{T'}] \leq m\psi \|C_{T'}\|_2 \leq m\psi \frac{\|L - L^*\|_2^2}{\sigma'} \leq m\psi \frac{C_2^2 \lambda_n^2}{6\zeta_2 m\psi C_2^2 \lambda_n} \leq \frac{\lambda_n}{6\zeta_2}.$$

From Lemma 13, we have that $\|C_{T' \oplus \mathbf{1}_p \mathbf{1}_p^\top}\|_2 \leq \|C_{T'}\|_2$. Following the same logic as above, we can then show that: $\Phi_\gamma[\mathcal{J}^+ \mathbb{I}^* C_{T' \oplus \mathbf{1}_p \mathbf{1}_p^\top}] \leq \frac{\lambda_n}{6\zeta_2}$.

- (5) Finally, we show that:

$$\Phi_\gamma[C_{T'}] \leq m\|\mathcal{P}_{T'^\perp}(L - L^*)\|_2 \leq m \frac{\|L - L^*\|_2^2}{\sigma'} \leq \frac{mC_2^2 \lambda_n^2}{\sigma'} \leq \frac{4\lambda_n}{\alpha(\frac{2}{\zeta_1} - 2(\kappa^* + \omega))} \left[1 + \frac{1}{3\zeta_2}\right].$$

□

Consider any optimal solution $(\hat{S}^{\mathcal{M}}, \hat{L}^{\mathcal{M}})$ of (28). We will show that $(\hat{S}^{\mathcal{M}}, \hat{L}^{\mathcal{M}})$ is the unique solution of the nonconvex program (28), as well as the unique solution of (22).

G.4. Variety constrained program to tangent space constrained program. Let $(\hat{S}^{\mathcal{M}}, \hat{L}^{\mathcal{M}})$ be any optimal solution of (28). In Corollary 20, we conclude that the variables $(\hat{S}^{\mathcal{M}}, \hat{L}^{\mathcal{M}})$ are smooth points of their respective varieties. As a result, the rank constraint $\text{rank}(L) \leq \text{rank}(L^*)$ can be linearized to $L \in T(\hat{L}^{\mathcal{M}})$. Since all the remaining constraints are convex, the optimum of the linearized program is also the optimum of (28). Moreover, we once more appeal to Corollary 20 to conclude that the constraints in \mathcal{M} along $T^{\star\perp}$ are strictly feasible at $\hat{L}^{\mathcal{M}}$. As a result, these constraints are inactive and can be removed in this “linearized program”. We now argue that the constraint $\Phi_\gamma[\mathcal{J}^+ \mathbb{I}^* \mathcal{J}(\hat{S}^{\mathcal{M}} - S^*, \hat{L}^{\mathcal{M}} - L^*)]$ is inactive. For notational simplicity, we let $T' = T(\hat{L}^{\mathcal{M}})$ and $\mathbb{H}' = \Omega^* \times T'$, we consider the following optimization problem:

$$(29) \quad \begin{aligned} (\tilde{S}, \tilde{L}) &= \underset{S \in \mathbb{S}^p, L \in \mathbb{S}^p}{\text{argmin}} \quad -\log \det(U^T(S - L)U) - \text{tr}((S - L)\hat{\Gamma}_O/2) + \lambda_n(\|S\|_1 + \gamma\|L\|_\star) \\ &\text{subject-to } (S, L) \in \mathbb{H}', S - L \in \text{span}(\mathbf{1}_p \mathbf{1}_p^\top). \end{aligned}$$

We prove that under conditions imposed on the regularization parameter λ_n , the pair of variables $(\hat{S}^{\mathcal{M}}, \hat{L}^{\mathcal{M}})$ is the unique optimum of (29). First, note that the optimum of (29) is unique since it is a strictly convex program convex because the negative log-likelihood terms have a strictly positive-definite Hessian due to Property P1. To show that $(\hat{S}^{\mathcal{M}}, \hat{L}^{\mathcal{M}})$ is the optimum of (29), it suffices to show strict feasibility of the constraint, that is: $\Phi_\gamma[\mathcal{J}^+ \mathbb{I}^* \mathcal{J}(\tilde{S} - S^*, \tilde{L} - L^*)] < C_0 \lambda_n$.

The optimality conditions of (29) states that there exists $Q_\Omega \in \Omega^{\star\perp}$, $Q_T \in T^{\prime\perp}$, $t \in \mathbb{R}$ such that:

$$(30) \quad \begin{aligned} -\hat{\Gamma}_O/2 - (\tilde{S} - \tilde{L})^+ + t\mathbf{1}_p\mathbf{1}_p^\top + Q_\Omega &= -\lambda\partial\|\tilde{S}\|_1, \\ \hat{\Gamma}_O/2 + (\tilde{S} - \tilde{L})^+ - t\mathbf{1}_p\mathbf{1}_p^\top + Q_T &= -\lambda\gamma\partial\|\tilde{L}\|_\star, \\ \tilde{S} - \tilde{L} &\in \text{span}(\mathbf{1}_p\mathbf{1}_p^\top). \end{aligned}$$

Let the reduced SVD of \tilde{L} be given by $\tilde{L} = \bar{U}\bar{D}\bar{V}^T$ and $Z = (\lambda\text{sign}(\tilde{S}), \lambda\gamma\bar{U}\bar{V}^T)$. Following a similar logic as in Section G.2 and restricting the optimality conditions to the space of \mathbb{H} , we have the following equivalent characterization of the optimality conditions:

$$(31) \quad \begin{aligned} \mathcal{P}_{\mathbb{H}'}\mathcal{J}^+(\mathbb{I}^*(\mathcal{J}(\Delta_S, \Delta_L + t\mathbf{1}_p\mathbf{1}_p^\top)) + \mathcal{R}_{\Gamma_0^*}\mathcal{J}(\Delta_S, \Delta_L + t\mathbf{1}_p\mathbf{1}_p^\top) + E_n) &= Z, \\ \tilde{S} - \tilde{L} &\in \text{span}(\mathbf{1}_p\mathbf{1}_p^\top). \end{aligned}$$

Here, $\Delta_S = \tilde{S} - S^*$, $\Delta_L = \tilde{L} - L^*$. In the remaining, we will denote $\Delta_{L+} = \tilde{L} - L^* + t\mathbf{1}_p\mathbf{1}_p^\top$. Our result relies on the following propositions to control the remainder term.

Proposition 21. *Suppose $\Phi_\gamma(\Delta_S, \Delta_{L+}) \leq \frac{1}{2C_1}$ for $C_1 = \psi(m + d^*)$ and any $\Delta_S \in \Omega^*$. Then, $\Phi_\gamma[\mathcal{J}^+\mathcal{R}_{\Gamma_0^*}(\mathcal{J}(\Delta_S, \Delta_{L+}))] \leq 2m\psi C_1^2 \Phi_\gamma(\Delta_S, \Delta_{L+})^2$.*

Proof of Proposition 21. We have that:

$$\begin{aligned} \|\mathcal{J}(\Delta_S, \Delta_{L+})\|_2 &\leq \|\Delta_S\|_2 + \|\Delta_{L+}\|_2 \leq \theta(\Omega^*)\|\Delta_S\|_\infty + \gamma\frac{\|\Delta_{L+}\|_2}{\gamma} \leq (\gamma + \theta(\Omega^*))\Phi_\gamma(\Delta_S, \Delta_{L+}) \\ &\leq (m + d^*)\Phi_\gamma(\Delta_S, \Delta_{L+}) \leq \frac{1}{2\psi}. \end{aligned}$$

Therefore,

$$\begin{aligned} \|\mathcal{R}_{\Gamma_0^*}(\mathcal{J}(\Delta_S, \Delta_{L+}))\|_2 &\leq \psi \sum_{k=2}^{\infty} (\|\Delta_S + \Delta_{L+}\|_2 \psi)^k \leq \psi^3 \|\Delta_S + \Delta_{L+}\|_2^2 \frac{1}{1 - \|\Delta_S + \Delta_{L+}\|_2 \psi} \\ &\leq 2\psi^3 \left(1 + \frac{\alpha}{6\zeta_2}\right)^2 \Phi_\gamma(\Delta_S, \Delta_{L+})^2 = 2\psi C_2^2 \Phi_\gamma(\Delta_S, \Delta_{L+})^2. \end{aligned}$$

Putting everything together, we have the desired result. \square

Notice that the bound on the remainder term is dependent on the error term $\Phi_\gamma(\Delta_S, \Delta_{L+})$. In the following proposition, we bound this error so we can control the remainder term.

Proposition 22. *Let \tilde{S}, \tilde{L} be the solution of convex program (29). Define*

$$r = \max \left\{ \frac{4}{\alpha(\frac{2}{\zeta_1} - 2(\kappa^* + \omega))} [\Phi_\gamma(\mathcal{J}^+E_n) + \Phi_\gamma(\mathcal{J}^+\mathbb{I}^*C_{T'}) + \lambda_n], \Phi_\gamma[(0, C_{T'})] \right\}.$$

If we have that $r \leq \min \left\{ \frac{8\alpha}{C_1}, \frac{\min\{\alpha, 1\}(\frac{2}{\zeta_1} - 2(\kappa^ + \omega))}{16m\psi C_2^2} \right\}$, then $\Phi_\gamma(\Delta_S, \Delta_L) \leq \frac{4r\sqrt{5h}}{1 - \sqrt{1 - (\kappa^* + \omega)^2}}$*

and $\Phi_\gamma(0, t\mathbf{1}_p\mathbf{1}_p^\top) \leq \frac{4r\sqrt{5h}}{1 - \sqrt{1 - (\kappa^ + \omega)^2}}$.*

The proof of the proposition relies on the following lemma which we state and prove first.

Lemma 23. *Consider the following optimization:*

$$(32) \quad \begin{aligned} \underset{S \in \mathbb{S}^p, L \in \mathbb{S}^p}{\text{argmin}} \quad & -\log \det(U^T(S - L)U) - \text{tr}((S - L)\hat{\Gamma}_O/2) + \text{trace}(t\mathbf{1}_p\mathbf{1}_p^\top(S - L)) + \lambda_n(\|S\|_1 + \gamma\|L\|_\star). \\ \text{subject-to} \quad & (S, L) \in \mathbb{H}' \end{aligned}$$

Then, the solution of (32) is unique and is equal to \tilde{S}, \tilde{L} (i.e. the solution of (29)).

Proof of Lemma 23. Note that by Property P1, the estimator (32) is strictly convex. We will denote the optimal solution of (32) by (\tilde{S}, \tilde{L}) . We are using the same notation as the optimal solution of (29) as we will show momentarily that these optimal solutions are identical. Specifically, define Z as is done before Proposition 21. Let $\Delta_S = \tilde{S} - S^*$ and $\Delta_L = \tilde{L} - L^*$. The optimality condition of (32) is given by:

$$(33) \quad \mathcal{P}_{\mathbb{H}'} \mathcal{J}^+(\mathbb{I}^* \mathcal{J}(\Delta_S, \Delta_L + t\mathbf{1}_p \mathbf{1}_p^\top) + \mathcal{R}_{\Gamma_0^*} \mathcal{J}(\Delta_S, \Delta_L + t\mathbf{1}_p \mathbf{1}_p^\top) + E_n) = Z.$$

Notice that the optimality condition (33) is identical to the first condition in (31). Since (32) has a unique solution, then, the optimal solutions of (29) and (32) coincide. \square

Proof of Proposition 22. Since T' is a tangent space such that $\rho(T', T^*) \leq \omega$, we have from Property P1 that the operator $\mathcal{B} = (\mathcal{P}_{\mathbb{H}'} \mathcal{J}^+ \mathbb{I}^* \mathcal{J} \mathcal{P}_{\mathbb{H}'})^{-1}$ is bijective and is well-defined. Consider the following function taking as input $(\delta_S, \delta_{L+}) \in \mathcal{Q}'$ where $\mathcal{Q}' = \Omega^* \times (T' \oplus t\mathbf{1}_p \mathbf{1}_p^\top)$:

$$F(\delta_S, \delta_{L+}) = (\delta_S, \delta_{L+}) - \mathcal{B} \{ \mathcal{P}_{\mathbb{H}'} \mathcal{J}^+ [\mathbb{I}^* \mathcal{J}(\delta_S, \delta_{L+}) + \mathcal{R}_{\Gamma_0^*} (\mathcal{J}(\delta_S, \delta_{L+} + C_{T'}) + \mathbb{I}^* C_{T'} + E_n - Z)] \}.$$

Here, $C_{T'} = \mathcal{P}_{T'^\perp}(L^*)$. Now a point (δ_S, δ_{L+}) is a fixed point of F if and only if $\mathcal{P}_{\mathbb{H}'} \mathcal{J}^+ [\mathbb{I}^* \mathcal{J}(\delta_S, \delta_{L+}) + \mathcal{R}_{\Gamma_0^*} (\mathcal{J}(\delta_S, \delta_{L+} + C_{T'}) + \mathbb{I}^* C_{T'} + E_n)] = Z$. Further, a fixed point (δ_S, δ_{L+}) provides certificates of optimality for (32). Specifically, let $\tilde{S} = S^* + \delta_S$. By Lemma 14, find a unique decomposition of $\delta_{L+} = L + t\mathbf{1}_p \mathbf{1}_p^\top$ where $L \in T'$. Then, let $\tilde{L} = \mathcal{P}_{T'}(L^*) + L$. By construction, the parameters (\tilde{S}, \tilde{L}) then satisfy the optimality condition for (33) and thus also the optimality condition of (31) after appealing to Lemma 23. In other words, the fixed point of the function F is $\mathcal{P}_{\mathbb{H}'}(\Delta_S, \Delta_L) + (0, t\mathbf{1}_p \mathbf{1}_p^\top)$.

Next, using Brouwer's fixed point theorem, we show that F has a fixed point that lies in the ball $\mathbb{B}_r = \{(\delta_S, \delta_{L+}) \in \mathcal{Q}' \mid \Phi_\gamma(\delta_S, \delta_{L+}) \leq r\}$. Specifically, note that F can be equivalently expressed as:

$$F(\delta_S, \delta_{L+}) = \mathcal{P}_{\mathbb{H}'^\perp}(\delta_S, \delta_{L+}) - \mathcal{B} \{ \mathcal{P}_{\mathbb{H}'} \mathcal{J}^+ [\mathcal{R}_{\Gamma_0^*} (\mathcal{J}(\delta_S, \delta_{L+} + C_{T'}) + \mathbb{I}^* [C_{T'} + \mathcal{J} \mathcal{P}_{\mathbb{H}'^\perp}(\delta_S, \delta_{L+})] + E_n - Z)] \}.$$

First, note that by appealing to Lemma 12, we have that:

$$\Phi_\gamma [\mathcal{P}_{\mathbb{H}'^\perp}(\delta_S, \delta_{L+})] \leq 2r(\kappa^* + \omega).$$

Similarly, we have from Property P2 that:

$$\Phi_\gamma [\mathcal{B} \{ \mathcal{P}_{\mathbb{H}'} \mathcal{J}^+ \mathcal{I} \mathcal{J} \mathcal{P}_{\mathbb{H}'^\perp}(\delta_S, \delta_{L+}) \}] \leq r \left(1 - \frac{2}{\zeta_1} \right).$$

Finally, we note that:

$$\begin{aligned} & \Phi_\gamma [\mathcal{B} \{ \mathcal{P}_{\mathbb{H}'} \mathcal{J}^+ [\mathcal{R}_{\Gamma_0^*} (\mathcal{J}(\delta_S, \delta_{L+} + C_{T'}) + \mathbb{I}^* C_{T'} + E_n - Z)] \}] \\ & \leq \frac{2}{\alpha} (\Phi_\gamma [\mathcal{J}^+ \mathcal{R}_{\Gamma_0^*} (\mathcal{J}(\delta_S, \delta_{L+} + C_{T'}))] + \Phi_\gamma [\mathbb{I}^* C_{T'}] + \Phi_\gamma [E_n] + \lambda_n) \\ & \leq \frac{r(\frac{2}{\zeta_1} - 2(\kappa^* - \omega))}{2} + \frac{2}{\alpha} (\Phi_\gamma [\mathcal{J}^+ \mathcal{R}_{\Gamma_0^*} (\mathcal{J}(\delta_S, \delta_{L+} + C_{T'}))]) \end{aligned}$$

where the last inequality is by the definition of r . By the assumption on r , we have that $\Phi_\gamma((\delta_S, \delta_{L+}) + (0, C_{T'})) \leq \frac{1}{2\zeta_1}$. And so we can appeal to Proposition 21 to conclude that:

$$\frac{2}{\alpha} \Phi_\gamma [\mathcal{J}^+ \mathcal{R}_{\Gamma_0^*} (\mathcal{J}((\delta_S, \delta_{L+} + C_{T'})))] \leq \frac{8m\psi C_1^2 r^2}{\alpha} \leq \frac{16m\psi C_2^2 r}{\alpha(\frac{2}{\zeta_1} - 2(\kappa^* + \omega))} \frac{r(\frac{2}{\zeta_1} - 2(\kappa^* + \omega))}{2} \leq r/2,$$

where the last inequality uses the bound on r .

So by Brouwer's fixed point theorem, we conclude that: $\Phi_\gamma[\mathcal{P}_{\mathbb{H}'}(\Delta_S, \Delta_L) + (0, t\mathbf{1}_p\mathbf{1}_p^\top)] \leq r$. Finally, note that: $\Phi_\gamma[\mathcal{P}_{\mathbb{H}'^\perp}(\Delta_S, \Delta_L)] \leq r$. Thus, $\Phi_\gamma[(\Delta_S, \Delta_L) + (0, t\mathbf{1}_p\mathbf{1}_p^\top)] \leq 2r$. Finally, appealing to Lemma 15 and some manipulations, we have the bound $\max\{\Phi_\gamma(\Delta_S, \Delta_L), t\mathbf{1}_p\mathbf{1}_p^\top\} \leq \frac{4r\sqrt{5h}}{1-\sqrt{1-(\kappa^{*2}-\omega)^2}}$. \square

We are now ready to state the following proposition.

Proposition 24. *Suppose that $\Phi_\gamma[\mathcal{J}^+E_n] \leq \frac{\lambda_n}{6\zeta_2}$ and suppose that:*

$$\lambda_n \leq \min \left\{ \min \left\{ \frac{8\alpha}{C_1}, \frac{\min\{\alpha, 1\}(\frac{2}{\zeta_1} - 2(\kappa^* + \omega))}{16m\psi C_2^2} \right\}, \frac{\alpha(\frac{2}{\zeta_1} - 2(\kappa^* + \omega))}{4(1 + \frac{1}{3\zeta_2})}, \frac{\alpha(\frac{2}{\zeta_1} - 2(\kappa^* + \omega))}{64C_1(1 + \frac{1}{3\zeta_2})}, \frac{\alpha^2(\frac{2}{\zeta_1} - 2(\kappa^* + \omega))^2}{6144\zeta_2(1 + \frac{1}{3\zeta_2})^2} \right\}.$$

Then, we have that: $\tilde{S} = \hat{S}^{\mathcal{M}}$, $\tilde{L} = \hat{L}^{\mathcal{M}}$.

Proof. From Corollary 20, we have that $\Phi_\gamma[\mathcal{J}^+\mathbb{I}^*C_{T'}] \leq \frac{\lambda_n}{6\zeta_2}$. We then have that:

$$\begin{aligned} & \frac{4}{\alpha(\frac{2}{\zeta_1} - 2(\kappa^* + \omega))} [\Phi_\gamma(\mathcal{J}^+E_n) + \Phi_\gamma(\mathcal{J}^+\mathbb{I}^*C_{T'}) + \lambda_n] \\ & \leq \frac{4\lambda_n}{\alpha(\frac{2}{\zeta_1} - 2(\kappa^* + \omega))} \left[1 + \frac{1}{3\zeta_2} \right] \leq \min \left\{ \frac{8\alpha}{C_1}, \frac{\min\{\alpha, 1\}(\frac{2}{\zeta_1} - 2(\kappa^* + \omega))}{16m\psi C_2^2} \right\}. \end{aligned}$$

We also have from Corollary 20 that $\Phi_\gamma\mathcal{J}^+C_{T'} \leq \frac{4\lambda_n}{\alpha(\frac{2}{\zeta_1} - 2(\kappa^* + \omega))} \left[1 + \frac{1}{3\zeta_2} \right]$. Let $r = \frac{4\lambda_n}{\alpha(\frac{2}{\zeta_1} - 2(\kappa^* + \omega))} \left[1 + \frac{1}{3\zeta_2} \right]$. We can appeal to Proposition 22 to conclude that:

$$\Phi_\gamma[\Delta_S, \Delta_L] \leq \frac{16\lambda_n\sqrt{5h}}{\alpha(1 - \sqrt{1 - (\kappa^{*2} - \omega)^2})(\frac{2}{\zeta_1} - 2(\kappa^* + \omega))} \left[1 + \frac{1}{3\zeta_2} \right].$$

From the bound on λ_n , we have that: $\Phi_\gamma[\Delta_S, \Delta_L] \leq \frac{1}{2C_1}$. So we can appeal to Proposition 21 to conclude that:

$$(34) \quad \Phi_\gamma[\mathcal{J}^+\mathcal{R}_{\Gamma_o^*}\mathcal{J}(\Delta_S, \Delta_L)] \leq 2m\psi C_1^2 \Phi_\gamma[\Delta_S, \Delta_L]^2 \leq \frac{\lambda_n}{6\zeta_2},$$

where here again we use the bound on λ_n . Note that $\Delta_{L+} = \Delta_L + t\mathbf{1}_p\mathbf{1}_p^\top$. We have from Corollary 20 that $\Phi_\gamma[\mathcal{J}^+\mathbb{I}^*C_{T'}] \leq \frac{\lambda_n}{6\zeta_2}$. From the optimality conditions of (29), we have that:

$$\begin{aligned} \Phi_\gamma(\mathcal{P}_{\mathbb{H}'}\mathcal{J}^+\mathbb{I}^*\mathcal{J}\mathcal{P}_{\mathbb{H}'}(\Delta_S, \Delta_L)) & \leq 2\lambda_n + 2\Phi_\gamma(0, t\mathbf{1}_p\mathbf{1}_p^\top) + \Phi_\gamma[\mathcal{J}^+\mathcal{R}_{\Gamma_o^*}\mathcal{J}(\Delta_S, \Delta_L)] \\ & \quad + \Phi_\gamma[\mathcal{P}_{\mathbb{H}'}\mathcal{J}^+\mathbb{I}^*C_{T'}] + \Phi_\gamma[\mathcal{J}^+E_n], \\ & \leq 2\lambda_n + \frac{\lambda_n}{2\zeta_2} + \frac{16\lambda_n\sqrt{5h}}{\alpha(1 - \sqrt{1 - (\kappa^{*2} - \omega)^2})(\frac{2}{\zeta_1} - 2(\kappa^* + \omega))} \left[1 + \frac{1}{3\zeta_2} \right], \end{aligned}$$

where the second inequality follows from bound on $\Phi_\gamma((0, t\mathbf{1}_p\mathbf{1}_p^\top))$ in Proposition 22. Appealing to Property *P2*, we have that: $\Phi_\gamma(\mathcal{P}_{\mathbb{H}^\perp}\mathcal{J}^+\mathbb{I}^*\mathcal{J}\mathcal{P}_{\mathbb{H}'}(\Delta_S, \Delta_L)) \leq \Phi_\gamma(\mathcal{P}_{\mathbb{H}^\perp}\mathcal{J}^+\mathbb{I}^*\mathcal{J}\mathcal{P}_{\mathbb{H}'}(\Delta_S, \Delta_L))$. Therefore:

$$\begin{aligned} \Phi_\gamma(\mathcal{J}^+\mathbb{I}^*\mathcal{J}(\Delta_S, \Delta_L)) &\leq \Phi_\gamma(\mathcal{P}_{\mathbb{H}'}\mathcal{J}^+\mathbb{I}^*\mathcal{J}\mathcal{P}_{\mathbb{H}'}(\Delta_S, \Delta_L)) + \Phi_\gamma(\mathcal{P}_{\mathbb{H}^\perp}\mathcal{J}^+\mathbb{I}^*\mathcal{J}\mathcal{P}_{\mathbb{H}'}(\Delta_S, \Delta_L)) \\ &\quad + \Phi_\gamma[\mathcal{J}^+\mathbb{I}^*C_{T'}] \leq 8\lambda_n + \frac{32\lambda_n\sqrt{5h}}{\alpha(1-\sqrt{1-(\kappa^{*2}-\omega)^2})(\frac{2}{\zeta_1}-2(\kappa^*+\omega))} \left[1 + \frac{1}{3\zeta_2}\right] \\ &< C_0\lambda_n. \end{aligned}$$

□

G.5. Removing the tangent space constraint. It remains to connect the estimator (29) with (9). In particular, we check that $\tilde{S} = \hat{S}$ and $\tilde{L} = \hat{L}$ where (\tilde{S}, \tilde{L}) is the solution of (29) and (\hat{S}, \hat{L}) is the solution of (9). We formalize this in the following proposition.

Proposition 25. *Suppose that $\Phi_\gamma[\mathcal{J}^+E_n] \leq \frac{\lambda_n}{6\zeta_2}$. Then, $\tilde{S} = \hat{S}$ and $\tilde{L} = \hat{L}$.*

Proof of Proposition 25. We must show that (\tilde{S}, \tilde{L}) satisfy the optimality conditions of (22) in (27), namely that there exists a dual variable t such that

$$\begin{aligned} (35) \quad &\mathcal{P}_{\mathbb{H}}\mathcal{J}^+(\mathbb{I}^*(\mathcal{J}(\Delta_S, \Delta_L + t\mathbf{1}_p\mathbf{1}_p^\top)) + \mathcal{R}_{\Gamma_0^*}\mathcal{J}(\Delta_S, \Delta_L) + E_n) = Z, \\ &\Phi_\gamma(\mathcal{P}_{\mathbb{H}^\perp}\mathcal{J}^+(\mathbb{I}^*(\mathcal{J}(\Delta_S, \Delta_L + t\mathbf{1}_p\mathbf{1}_p^\top)) + \mathcal{R}_{\Gamma_0^*}\mathcal{J}(\Delta_S, \Delta_L) + E_n)) < 1, \\ &\tilde{S} - \tilde{L} \in \text{span}(\mathbf{1}_p\mathbf{1}_p^\top), \end{aligned}$$

where $\Delta_S = \tilde{S} - S^*$ and $\Delta_L = \tilde{L} - L^*$. Notice that the first and third optimality conditions are the same as (31). It remains to show the second inequality where the strict inequality is to ensure that (\tilde{S}, \tilde{L}) is the unique solution. It suffices to show that:

$$(36) \quad \begin{aligned} &\Phi_\gamma(\mathcal{P}_{\mathbb{H}^\perp}\mathcal{J}^+(\mathbb{I}^*\mathcal{P}_{\mathbb{Q}'}(\mathcal{J}(\Delta_S, \Delta_L + t\mathbf{1}_p\mathbf{1}_p^\top))) \\ &< \lambda_n - \Phi_\gamma[\mathcal{R}_{\Gamma_0^*}\mathcal{J}(\Delta_S, \Delta_L)] - \Phi_\gamma[\mathcal{J}^+\mathbb{I}^*C_{T' \oplus \mathbf{1}_p\mathbf{1}_p^\top}] - \Phi_\gamma[\mathcal{J}^+E_n]. \end{aligned}$$

Manipulating the first optimality condition, we have that:

$$\begin{aligned} \Phi_\gamma(\mathcal{P}_{\mathbb{H}}\mathcal{J}^+(\mathbb{I}^*\mathcal{P}_{\mathbb{Q}'}(\mathcal{J}(\Delta_S, \Delta_L + t\mathbf{1}_p\mathbf{1}_p^\top))) &\leq \lambda_n + 2(\Phi_\gamma[\mathcal{R}_{\Gamma_0^*}\mathcal{J}(\Delta_S, \Delta_L)] + \Phi_\gamma[\mathcal{J}^+\mathbb{I}^*C_{T' \oplus \mathbf{1}_p\mathbf{1}_p^\top}] + \Phi_\gamma[\mathcal{J}^+E_n]) \\ &\leq \lambda_n + \frac{\lambda_n}{\zeta_2} = \lambda_n \left(1 + \frac{1}{\zeta_2}\right), \end{aligned}$$

where we have here used the bound $\Phi_\gamma[\mathcal{J}^+\mathbb{I}^*C_{T' \oplus \mathbf{1}_p\mathbf{1}_p^\top}] \leq \frac{\lambda_n}{6\zeta_2}$ from Corollary 20 and the bounds $\Phi_\gamma[\mathcal{R}_{\Gamma_0^*}\mathcal{J}(\Delta_S, \Delta_L)] \leq \frac{\lambda_n}{6\zeta_2}$ from (34) and $\Phi_\gamma[\mathcal{J}^+E_n] \leq \frac{\lambda_n}{6\zeta_2}$ from proposition statement. Appealing to Property *P3*, we then have that:

$$\Phi_\gamma(\mathcal{P}_{\mathbb{H}^\perp}\mathcal{J}^+(\mathbb{I}^*\mathcal{P}_{\mathbb{Q}'}(\mathcal{J}(\Delta_S, \Delta_L + t\mathbf{1}_p\mathbf{1}_p^\top))) \leq \lambda_n \left(1 + \frac{1}{\zeta_2}\right) \left(1 - \frac{1}{\zeta_2}\right) = \lambda_n \left(1 - \frac{1}{\zeta_2^2}\right) < \lambda_n \left(1 - \frac{1}{2\zeta_2}\right).$$

Since $\Phi_\gamma[\mathcal{R}_{\Gamma_0^*}\mathcal{J}(\Delta_S, \Delta_L)] + \Phi_\gamma[\mathcal{J}^+\mathbb{I}^*C_{T' \oplus \mathbf{1}_p\mathbf{1}_p^\top}] + \Phi_\gamma[\mathcal{J}^+E_n] \leq \frac{\lambda_n}{2\zeta_2}$, we have shown that (36) holds. □

G.6. Bounding the error term $\Phi_\gamma[\mathcal{J}^+E_n]$. Let $\lambda_n = C_5 \left[\frac{24m\zeta_2}{\sqrt{c_5}} \sqrt{\frac{p^2 \log(\tilde{C}_5 p)}{k}} + \frac{6m\zeta_2}{\sqrt{k}} \right]$ where c_5, C_5, \tilde{C}_5 are defined in Corollary 4.

Lemma 26. *Under the conditions of Theorem 3, we have:*

$$\mathbb{P}\left(\Phi_\gamma[\mathcal{J}^+ E_n] \leq \frac{\lambda_n}{6\zeta_2}\right) \geq 1 - p^{-1}.$$

Proof. Note that $\Phi_\gamma[\mathcal{J}^+ E_n] \leq m\|\Gamma_O^* - \hat{\Gamma}_O\|_2 \leq pm\|\Gamma_O^* - \hat{\Gamma}_O\|_\infty$. To show that, $\Phi_\gamma[\mathcal{J}^+ E_n] \leq \frac{\lambda_n}{6\zeta_2}$, it suffices to show that

$$(37) \quad \|\Gamma_O^* - \hat{\Gamma}_O\|_\infty \leq \frac{4C_5}{\sqrt{c_5}} \sqrt{\frac{\log(\tilde{C}_5 p)}{k}} + \frac{C_5}{\sqrt{k}}.$$

Based on the condition on k , it is straightforward to show that:

$$C_5 \left\{ \left(\frac{k}{n}\right)^\xi (\log(n/k))^2 + \frac{1+\vartheta}{\sqrt{k}} \right\} \leq \frac{4C_5}{\sqrt{c_5}} \sqrt{\frac{\log(\tilde{C}_5 p)}{k}} + \frac{C_5}{\sqrt{k}}.$$

for $\vartheta = 2\sqrt{\log(\tilde{C}_5 p)/\sqrt{c_5}}$. Note that $\vartheta \leq \sqrt{k}/\log(n)^4$. Furthermore, since $(n/2)^{\xi/(1+\xi)} \geq k$, $k \leq n/2$. Appealing to Corollary 4, we have that with probability greater than $1 - \tilde{C}_5 p^3 e^{-c_5 \vartheta^2} = 1 - p^{-1}$ that the bound in (37) is satisfied. \square

G.7. Summary and putting things together. Combining Propositions 24 and 25, we conclude that under the conditions of Theorem 3, with probability greater than $1 - 1/p$, the optimal solution (\hat{S}, \hat{L}) of (22) is unique and equal to an optimal solution $(\hat{S}^{\mathcal{M}}, \hat{L}^{\mathcal{M}})$ of (28). From Corollary 20, we have that $\hat{S} - \hat{L} \succeq 0$, $\hat{L} \succeq 0$. Thus, $(\hat{S}, \hat{L}) = (\hat{S}^{\mathcal{M}}, \hat{L}^{\mathcal{M}})$ is also the unique minimizer of (9). The guarantees on the closeness of (\hat{S}, \hat{L}) to the population parameters (S^*, L^*) then follows from Corollary 20 and Proposition 19.

APPENDIX H. REFITTING FOR EGLTENT

Suppose (\hat{S}, \hat{L}) is the solution of (9) in the first step. We then obtain refitted parameters (\tilde{S}, \tilde{L}) as the second step by solving the following convex optimization program:

$$\begin{aligned} (\tilde{S}, \tilde{L}) = \operatorname{argmin}_{S \in \mathbb{S}^p, L \in \mathbb{S}^p} & -\log \det(U^T (S - L) U) - \operatorname{tr}((S - L)\hat{\Gamma}_O/2), \\ \text{s.t. } & S - L \succeq 0, L \succeq 0, (S - L)\mathbf{1}_p = 0, \\ & \operatorname{support}(S) \subseteq \operatorname{support}(\hat{S}), \operatorname{col-space}(L) \subseteq \operatorname{col-space}(\hat{L}). \end{aligned}$$

Here, the constraint $\operatorname{support}(S) \subseteq \operatorname{support}(\hat{S})$ restricts the graph structure of our refitted solution to be contained in the graph estimated in the first step. Similarly, the constraint $\operatorname{col-space}(L) \subseteq \operatorname{col-space}(\hat{L})$ restricts the row/column space of the refitted low-rank term to be contained in the row/column space estimated in the first step.

APPENDIX I. ADDITIONAL EXPERIMENTAL RESULTS

We consider the exact same setup as in the simulation study in Section 5.1.1. The only difference is that we specify the sub-graph $\mathcal{G}_0 = (E_O, O)$ among the observed variables to be an Erdős–Rényi with edge probability 0.08 and set Θ_{ij}^* to -2 for every $(i, j) \in E_O$ and zero otherwise. The latent variables are not connected in the joint graph so that $\Theta_{ij}^* = 0$ for every $i, j \in H, i \neq j$. We connect each latent variable node $i \in H$ to every $k \in O$ where $k = i + \zeta h$ for some positive integer ζ . The corresponding entries Θ_{ik}^* in the precision matrix are chosen uniformly at random from the interval $[30/\sqrt{p+h}, 60/\sqrt{p+h}]$. Finally, we set the diagonal entries of Θ^* so that it has the all-ones vector in its null space.

The rest of the simulation study is carried out as described in Section 5.1.1. Figure 7 summarizes the performance of all the methods on 50 independent results. We again observe that our approach outperforms `eglearn`, and accurately recovers the graphical structure among the observed variables as well as the number of latent variables. In terms of validation likelihood, `eglatent` is a bit weaker than in the simulation with the cycle graph.

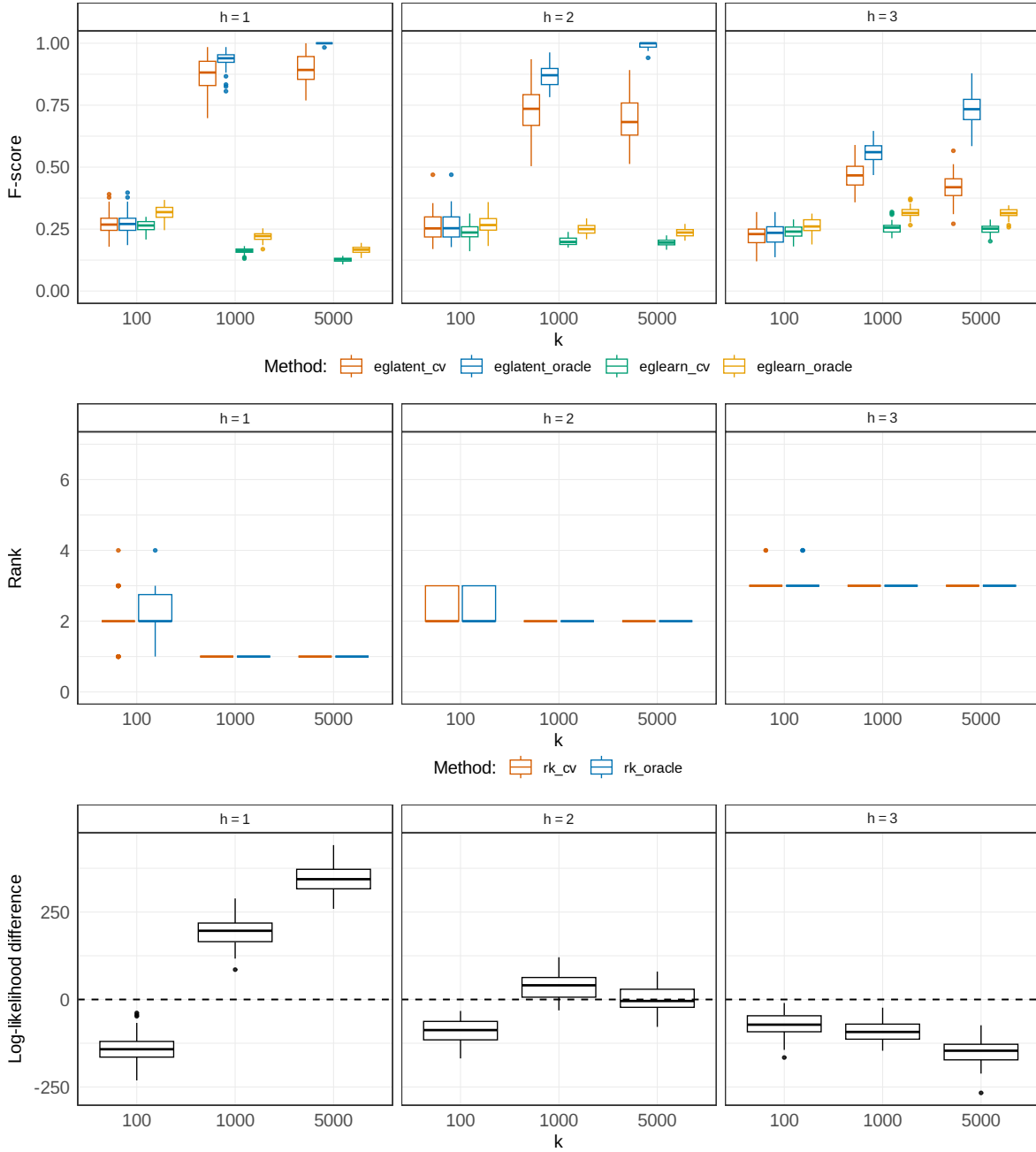


FIGURE 7. F -score (top row) and estimated number of latent variables (middle row) of `eglatent` method with the selection of the tuning parameter based on the oracle and cross-validation on the F -score for the random graph with $h = 1, 2, 3$ latent variables and different effective sample sizes $k = 100, 1000, 5000$. The bottom row shows the difference between best `eglatent` and best `eglearn` log-likelihoods on the validation set.